GELATIN METHACRYLATE HYDROGEL MICROPARTICLE-BASED 3D PLATFORM FOR ELASTICITY-DRIVEN MULTI-LINEAGE DIFFERENTIATION OF HUMAN MESENCHYMAL STEM CELLS

Francesco Pappalardo



First Supervisor: Prof Felicity Rose

Second Supervisor: Prof Morgan Alexander

The University of Nottingham

School of Pharmacy

Year of study 2016/2020

ABSTRACT

Understanding the mechanisms of the fate of stem cells is one of the major cornerstones of regenerative medicine research. Mesenchymal stem cells (MSCs) are multipotent cells that can differentiate into muscle, cartilage, bone, fat and nerve cells, and the complex mechanisms that they undergo are still not fully understood. Advances in cell signalling and developmental biology provided rudimentary pathways to differentiate MSCs in 2D culture to the aforementioned cell types, but the cellular microenvironment contains not just chemical signals but also those that are mechanical in nature. Previous research showed that matrix stiffness plays a significant role in MSC differentiation and that substrates can be tuned in their mechanical properties to tailor MSC lineage determination. However, most of the research performed in this area are in a 2D format, where it does not capture the 3D interaction effects of cells in culture and other physical aspects of the biomaterials such as curvature. Transitioning into a 3D platform can enable us to determine more accurately the physiological nature of stem cell behaviour.

In this thesis, a 3D culture platform has been produced using hydrogel microparticles made from methacrylated gelatin (GelMA). GelMA was selected as a material due to its biocompatibility, interactions with cellular integrins, and more importantly its tuneability of matrix stiffness. The latter property is essential to translate the 2D culture methods of varying matrix stiffness into a 3D format, where MSCs can be observed upon adhesion to these GelMA microparticles. Several ultra-porous microparticles of different sizes (170-760 μm) and modulus (0.23-130 kPa) were produced by tuning the dispersed and continuous phases of the co-flow microfluidic system used for their fabrication. An operability range of 5-13% w/v GelMA concentration in the dispersed phase, along with mineral oil in the continuous phase containing 1% w/v Span 80 as a surfactant was used. GelMA solution flow rates of 1-5 mL/h and 50-200 mL/h of mineral oil were also seen as viable process factors that produced acceptable, nearly monodispersed microparticles. Beyond these concentrations and flow rates, either highly heterogeneously sized microparticles were fabricated or the needle was blocked disabling the production of microparticles. Using these microparticles, MSCs were seeded and cultured for 7 days without any exogenous differentiation factors

supplemented with the media. With only matrix stiffness therefore as a differentiation stimulus, the differentiation of MSCs could be tuned based on the surface modulus of the microparticle: 0.2-1.5 kPa for neurogenic, ~6 kPa for adipogenic, ~18 kPa for myogenic, and ~44 kPa for osteogenic lineages in preliminary studies. These data have been confirmed through immunocytochemical methods by staining for relevant markers of differentiation.

With this result, a successful platform could be used in performing 3D culture of MSCs in a stiffness-controlled manner where differentiation is directed through the matrix modulus alone. Such significant results could provide a new 3D biomaterial for MSC culture and differentiation, and these GelMA hydrogel microparticles could be utilised in suspension culture of MSCs with the aforementioned material as a carrier. This would have application in clinically relevant production of MSCs for regenerative medicine use.

ACKNOWLEDGMENT

I would like to thank my supervisors Prof Felicity Rose and Prof Morgan Alexander for the guidance and invaluable support they have provided me and for the opportunity to join the innovative EPSRC program in Next Generation Biomaterials Discovery. I acknowledge the University of Nottingham for funding my PhD project.

I also must express special thanks to Dr Marta Alvarez Paino and especially Dr Mahetab Amer, whom I am honoured to consider my mentor throughout this PhD, giving me precious advice and human and professional support.

I would also like to thank Prof Xinyong Chen who trained me in the use of Atomic force microscopy, providing his knowledge to me with patience and great professionalism. Likewise, thanks to Nicola Weston who performed the study on environmental Scanning Electron Microscope and ion residuals via Energy-Dispersive X-ray spectroscopy.

I would like to thank my family in Italy and all the friends I made here in Nottingham that stayed close to me during these hard times of pandemics, that continued to bear with me with patience and cheer for me. In particular, I would like to thank Inchirah Adala, Francesco Catrambone, Joshua Jones and Elisa Tarsitano for their presence, advice, and laughter together as we struggled during our PhD years.

Lastly, I wish to express my greatest thanks to Dr Jopeth Ramis, whose help and vicinity really made the difference both in professional and personal life, helping me in giving direction to this project and purpose to every adventure that we have had and to whatever else still awaits on the horizon.

Per aspera sic itur ad astra

TABLE OF CONTENTS

ABSTRACT I

ACKNOWLEDGMENT III

TABLE OF CONTENTS IV

LIST OF TABLES VIII

LIST OF FIGURES VIII

LIST OF ABBREVIATIONS XIII

LIST OF PRESENTATIONS IN CONFERENCES XV

1. INTRODUCTION 1

1.1 Regenerative Medicine 1

1.1.1 Background and Scope of Regenerative Medicine 1

1.1.2 2D versus 3D influence on cell function 2

1.2 How mechanobiology influences Mesenchymal Stem Cells 4

1.2.1 Mesenchymal Stem Cell Fundamentals for Tissue Engineering applications 4

1.2.2 Mechanobiology of Bone Marrow-derived Mesenchymal stem cell 5

1.2.3 Mechanotransduction signalling in Bone Marrow-derived Mesenchymal stem cell inducing lineage differentiation 8

1.3 Biomaterials for Tissue Engineering 13

1.3.1 Biomaterials to influence Mesenchymal stem cell behaviour 13

1.3.2 Natural and Synthetic Polymers 16

1.3.3 Hydrogels and gelatin-derived composites 19

1.4 Polymeric microparticles for Tissue Engineering 21

1.4.1 The Microparticle-based approach *21*

1.4.2 Applications of polymeric microparticles in Tissue Engineering *21*

1.4.3 Polymeric microparticle production *23*

1.4.4 Microfluidic-based fabrication of microparticles *24*

1.5 Aims of the Thesis and Research question 27

2. METHODS 29

2.1 Consumables and Materials used 29

2.2 GelMA synthesis via precipitation method 29

2.3 Characterisation of GelMA degree of substitution via 2,4,6-trinitrobenzene sulfonic acid assay 30

2.4 GelMA 2D discs generation 30

2.5 GelMA microparticles production using co-current flow microfluidic system 30

2.6 Design of Experiment 32

2.7 Co-current flow microfluidic simulation 34

2.8 GelMA microparticle size characterisation 36

2.9 Characterisation of GelMA microparticle morphology via environmental Scanning Electron Microscope and ion residuals via energy-dispersive x-ray spectroscopy 37

2.10 Cell culture of mesenchymal stem cells 38

2.11 Cryopreservation and resuscitation of cells 39

2.12 Live&Dead assay 39

2.13 Differentiation test of immortalised hMSCs grown on GelMA microparticles by visualisation of ALP and Vinculin expression 40

2.14 Screening of early lineage markers of primary hMSCs on GelMA flat discs and microparticles 40

2.15 Atomic force microscopy 41

2.16 Atomic force microscopy: Young's modulus calculation with the Derjaguin-Muller-Toporov model 43

2.17 Atomic force microscopy sample preparation and analysis 45

2.18 Image analysis via Ilastik and CellProfiler 46

2.19 Statistical Analysis 47

3. PRODUCTION, MECHANICAL CHARACTERISATION AND BIOCOMPATIBILITY OF GELATIN METHACRYLATE MICROPARTICLES FABRICATED VIA A CO-CURRENT FLOW CAPILLARY SYSTEM 48

3.1 Introduction 48

3.2 Results and Discussion 51

3.2.1 Simulation of co-current flow production of GelMA microparticles 51

3.2.2 GelMA microparticle size characterisation 53

3.2.3 GelMA microparticle structure characterisation 56

3.2.4 GelMA microparticle surface modulus characterisation 59

3.2.5 Cell viability 61

3.3 Summary and Conclusion 64

4. GELATIN METHACRYLATE MICROPARTICLES INFLUENCE ON MESENCHYMAL STEM CELLS MULTI-LINEAGE DIFFERENTIATION 67

4.1 Introduction 67

4.2 Results and Discussion 69

4.2.1 GelMA flat discs and microparticles elasticity characterisation 69

4.2.2 Alkaline Phosphatase and Vinculin expression of ihMSCs cultured on GelMA discs and microparticles 70

4.2.3 Primary hMSCs lineage marker screening *72*

4.3 Summary and Conclusion 76

5. CONCLUSIONS 79

5.1 Key Findings 79

5.2 Overall Discussion in Context of the Wider Literature 81

5.3 Current limitations 83

5.4 Conclusion 83

5.5 Future work 84

LIST OF REFERENCES 86

APPENDICES 101

LIST OF TABLES

TABLE 1.1 Examples of natural polymers

TABLE 1.2 Examples of synthetic polymers and their uses

TABLE 2.1 Experimental Runs using Central Composite Design for assessment of disperse and continuous flow rates in determining size and surface modulus of GelMA microparticles.

TABLE 2.2 Values of the parameters used in co-flow simulation

TABLE 3.1 Data obtained from the experimental runs examining the effect of flow rates in determining the responses of diameter, surface modulus, Span and CV% of GelMA microparticles.

TABLE 4.1 Young's modulus of GelMA discs as obtained by AFM measurements.

LIST OF FIGURES

FIGURE 1.1 Schematic diagram of 2D monolayer cell culture (A) and the three main examples of 3D cell culture system, that is cell spheroids/aggregates grown on matrix (B), cells embedded within a matrix (C), or scaffold-free cell spheroids in suspension (D).

FIGURE 1.2 Schematic diagram of a focal adhesion. Focal adhesions comprise hundreds of proteins classified on the basis of their contribution to four fundamental processes: receptor/matrix binding, actin cytoskeleton binding, intracellular signal transduction and actin polymerisation. By adjusting to the intracellular and extracellular contractile forces, the collective action of the mechanosensitive components forms the mechanoresponsive network of the cell.

FIGURE 1.3 (A) Several signalling molecules help regulating the commitment and differentiation of MSCs towards diverse lineages. The molecules shown and lineages affected are based upon references. (B) Signalling pathways triggered by mechanical stimuli applied to a cell. The presence of external forces that increase tension on the cytoskeleton activating integrins and/or induce matrix-bound factors release which activate mechanosensory proteins such as G-protein coupled receptors (GPCR), ion channels and growth factor receptors (GFRs), allow the cell to detect

mechanical loading and activate a variety of downstream signalling pathways, promoting gene expression and/or cytoskeleton reorganisation.

FIGURE 1.4 Schematic representation of a cell inside a 3D ECM. In this context, cellular traction forces are evenly distributed and propagated along ECM fibres, causing both ECM and cytoskeleton remodelling and cell reshaping.

FIGURE 1.5 Schematic of (A) GelMA synthesis from gelatin and methacrylic anhydride and (B) formation of hydrogels via UV-catalysed crosslinking. Image reproduced from Dong et al., 2019.

FIGURE 1.6 Schematic representation of the applications of polymeric microparticles in tissue engineering. Briefly, these include: (A) Incorporation in hydrogels, matrices or porous scaffolds as an added factor for modifying their porosity and viscoelastic properties, or as delivery systems for macromolecules; (B) Injectable delivery systems for controlled-release of bioactive molecules; (C) Scaffolds obtained by (a) cell agglomeration, (b) chemical agglomeration or sintering; (Cc) Microcarriers for cell expansion; (D) Hydrogel particles with encapsulated cells for organ printing and mesoscale self-assembly.

FIGURE 1.7 Most common designs used in droplet microfluidics: T-junction system (A); flow-focusing system (B); Co-flow system (C).

FIGURE 2.1 Model geometry (left) and the meshed configuration (right), where a free triangular mesh was used. Total degrees of freedom solved for was 25874 (plus 23901 internal DOFs).

FIGURE 2.2 (A) Silicon nitride MLCT cantilevers, of which the cantilever C was used; (B-C) Rotated (pyramidal) tip of cantilever C. (D) 20μm diameter polystyrene microparticle attached to MLCT-C tip. Images were taken via SEM.

FIGURE 2.3 DMT model contact mechanics in AFM. The applied force (F) causes an indentation (d) that develops on the substrate in response to a non-deformable sphere with a contact area (a) closely related to the sphere radius. Figure adapted from (Quantitative Imaging of Living Biological Samples Using PeakForce QNM, 2012).

FIGURE 2.4 Pipeline of the image analysis of hMSCs showing positive signal to the marker screening. The Raw image as taken by the microscope is first pre-processed with ImageJ for clearing up the image of background, then rendered through Ilastik machine learning training to recognise eligible pixels and batch process to extract probability masks showing the signal of interest. The probability mask is then listed in CellProfiler software for images segmentation and counting of positives to evaluate the percentage of marker positive cells.

FIGURE 3.1 Velocity plots of the microfluidic system with 5% w/v (a) and 13% w/v (d) GelMA solution. The 2D plots are accompanied by 1D plot which is obtained from the solutions in a cut line at (5.5, 0) and (5.5, 1.4), where time-dependent velocity profiles are shown as a function of arc length. Qd1 = 1.5 mL/h, Qd2 = 3 mL/h, and Qc = 100 mL/h.

FIGURE 3.2 Droplet formation regime of 5% w/v and 13% w/v GelMA solutions. Plot shows tailing (A) and (B) regime and a steady, consistent droplet formation (C) and (D). 1D plot of arc length vs volume fraction (E) and (F) show inconsistent volume fractions at predefined arc length (measured at (3.5, 0.7) and (4.5, 0.7) of the 2D plot), indicative of tailing flow regime.

FIGURE 3.3 (A) Microparticles imaged under optical microscope; (B) Surface plot of the diameter response with respect to the disperse phase (DP) and continuous phase (CP) flow rates. The graph shows the direct proportionality between DP flow rate and diameter and the inverse proportionality between CP flow rate and diameter.

FIGURE 3.4 (A) eSEM imaging of GelMA microparticles at small, medium and large diameter ranges. The porous surface structure is revealed after water sublimation at low pressure. Scale bar, left column = 500 μm; right column = 40 μm. (B) Representative eSEM micrograph of GelMA microparticles, showing an internal porous structure. Alignment is seen on the wall pores tangent to the surface, indicating a vertical alignment from core to the surface. Scale bar, left column = 200 μm; right column = 40 μm.

FIGURE 3.5 eDX spectra of GelMA microparticle spectra (image is a representative of three samples taken).

FIGURE 3.6 (A) F-D curves of representative experimental runs (R), showing the different degree of deformation for small, medium and large microparticle diameter; (B) Scatter plot of Microparticle diameter versus Young's modulus. The graph shows the inverse correlation equation between the two responses. (C) Histogram plot of Young's modulus values for each experimental run. Error bars indicate the standard deviation of the mean, calculated on 100 points per each sample. Statistical significance calculated via two-way ANOVA at 5% significance level (**: $p<0.01$, ***: $p<0.001$).

FIGURE 3.7 Surface plots of surface Young's modulus response with respect to the disperse phase (DP) and continuous phase (CP) flow rates. Considering the inverse proportionality between surface Young's modulus and the microparticle size, the effect of the DP flow rate is inversely proportional and the effect of CP flow rate is directly proportional.

FIGURE 3.8 Histogram plot of cell viability for small (≤300 μm), medium (>300 μm; ≤600 μm) and large (>600 μm) microparticles on days 1, 4 and 7. Error bars indicate the standard deviation of the mean, calculated from 6 images per each condition, evaluating the number of live cells divided by the total number of cells. Statistical significance calculated via two-way ANOVA at 5% significance level (**: $p<0.01$)

FIGURE 3.9 Bright field (top) and Fluorescence (bottom) images of the experimental conditions, as displayed. Live cells were stained with Calcein-AM (green), whilst dead cells with Ethidium homodimer (red). Scale bar =100 μm.

FIGURE 4.1 Box plot graphs of Young's modulus of GelMA flat discs (A) and microparticles (B) stiffness change in respect to different degrees of methacrylation and concentration. Values have been calculated on 3 different samples, measuring 3 force maps of 100 spots per each condition.

FIGURE 4.2 (A) Frequency distribution of GelMA microparticles diameters, calculated on a total of 100 microparticles; (B) Microparticles imaged under optical microscope. Scale bar = 200 μm.

FIGURE 4.3 Bright field (left) and Fluorescence (right) images of the experimental conditions, as displayed. Cells were stained for Alkaline Phosphatase (green), Vinculin (red) and DAPI. The peak

of expression of ALP at 7d and its decrease at 14d, correlated with a stronger signal of vinculin at the 14d rather than at 7d, suggest that both the GelMA disc and GelMA MPs are able to induce the variation of marker expression in ihMSCs. Scale bar = 100 μm.

FIGURE 4.4 (A) Fluorescence images of MSCs cultured in GelMA Flat Discs and (B) Quantification of % positive samples based on total cell count. Standard deviations for % calculated values are as follows: MAP2b (1.5 kPa) = 7.1; PPARγ (1.5 kPa) = 0.2, (6 kPa) = 7.6, (44 kPa) = 2.7; Myogenin (18 kPa) = 6.3, (44 kPa) = 0.1; Osterix (18 kPa) = 1.9, (44 kPa) = 5.8; all at n=2 technical replicates and N=3 donors.

FIGURE 4.5 (A) Fluorescence images of MSCs cultured in GelMA MPs and (B) Quantification of % positive samples based on total cell count. Standard deviations for % calculated values are as follows: MAP2b (1.5 kPa) = 8.9; PPARγ (6 kPa) = 8.6, (44 kPa) = 1.4; Myogenin (18 kPa) = 6.8; Osterix (18 kPa) = 2.9, (44 kPa) = 4.8; all at n=2 technical replicates and N=3 donors.

FIGURE 4.6 (A) Fluorescence images of MSCs cultured in Tissue Culture Plates (Controls) (B) Quantification of % positive samples based on total cell count. Standard deviations for % calculated values are as follows: PPARγ (+Adipo) = 1.8, (+Osteo) = 1.5; Osterix (-Control) = 0.3, (+Osteo) = 4.1; all at n=2 technical replicates and N=3 donors.

FIGURE 5.1 Schematic of the project workflow towards scalable production of differentiated MSCs.

LIST OF ABBREVIATIONS

AFM	Atomic force microscopy
ANOVA	Analysis of variance
BSA	Bovine serum albumin
DMEM	Dulbecco's modified eagle medium
DMSO	Dimethyl sulfoxide
DNA	Deoxyribonucleic acid
DS	Degree of substitution
ECM	Extra-cellular matrix
EDTA	Ethylenediaminetetraacetic acid
eSEM	Environmental scanning electron microscope
FBS	Foetal bovine serum
GelMA	Gelatin methacryloyl
hMSCs	Human mesenchymal stem cells
ihMSCs	Immortalised human mesenchymal stem cells
MAP2b	Microtubule-associated protein 2b
MP	Microparticle
MSCs	Mesenchymal stem cells
Pa	Pascals, N/m2
PBS	Phosphate buffered solution
PCL	Polycaprolactone
PLGA	Poly Lactic-co-Glycolic Acid
PPARγ	Peroxisome proliferator-activated receptor gamma
RM	Regenerative medicine
SD	Standard deviation
TE	Tissue engineering

TGF-β1	Transforming growth factor-β1
TNBS	2,4,6-Trinitrobenzene-sulfonic acid

LIST OF PRESENTATIONS IN CONFERENCES

Poster Presentations:

Surface modulus and topography characterisation of morphological diverse microbeads, Francesco Pappalardo, Mahetab Amer, Marta Alvarez-Paino, Kevin Shakesheff, Morgan Alexander and Felicity Rose, Next Generation Biodiscovery Workshop, University of Nottingham, January 2018

Co-flow microfluidic system for the production of tuneable elastic Gelatin Methacryloyl microparticles, Francesco Pappalardo, Jopeth Ramis, Marta Alvarez-Paino, Kevin Shakesheff, Morgan Alexander and Felicity Rose. TCES-UKSB Joint Conference, June 2019; also presented at Tissue Engineering and Regenerative Medicine International Society Conference – Americas, December 2019

1. INTRODUCTION

1.1 Regenerative Medicine

1.1.1 Background and Scope of Regenerative Medicine

Regenerative medicine (RM) is a field of translational science involving tissue engineering (TE) and mammalian cell biology, aimed at restoring tissue and organ-related medical needs by recreating or enhancing original biological function after deterioration or injury (Mason and Dunnill, 2007). The concept applies to the use of living cells to restore different tissues and organs by activating and supporting the body's self-repair processes, and to the concept of tissue replacement approaches. By developing and re-implanting tissue in the body, the need for additional donor-derived tissues and organs can be resolved in line with the original vision of RM. This practice could help satisfy the needs arising from the shortage of transplantation organs, which is often inaccessible due to a lack of suitable or compatible donors.

Current methods for tissue replacement can be classified based on the type and source of the implant, namely autografts, allografts, metallic and non-metallic (ceramics, polymers) devices (Laurencin and Nair, 2014). These methods have a range of limitations, including postoperative complications such as infection, poor donor integration effectiveness, activation of an immune response or the need for immune suppression, and donor site morbidity. RM seeks to solve these challenges through a targeted, customized and cost-effective approach. Several methods under the RM definition include the use of stem cell therapy, biomaterial scaffolding, drug-based techniques to deliver biologically active molecules, and transplantation of *in vitro* developed organs or tissues, usually referred to as TE (Langer and Vacanti, 1993). These organs or tissues are then used in a broad variety of applications and techniques to reconstruct or rebuild portions of the human body, which are intended to reproduce the *in vivo* cues and yield tissue-like replacements. In particular, a temporary scaffold could effectively direct cells to reorganise the structure and function of the lost tissue by encouraging the secretion of their own matrix to recreate it (Carletti et al., 2011; Lee et al., 2008).

1.1.2 2D versus 3D influence on cell function

TE approaches are often followed by several challenges that need to be tackled in order to make them available for clinical and surgical practice (Nerem and Schutte, 2014). One of the key difficulties is the need to develop methods to generate functional tissues for therapeutic application. This critical factor involves a major qualitative leap in the way cells are cultured. The conventional approach is bidimensional (2D) cell culture (Figure 1.1A), where cells are grown on surfaces such as microwell plates, tissue culture flasks and Petri dishes made of polystyrene or glass. The benefit of using monolayer culture lies in the high cell viability and ease of operation through which proliferating cells receive a homogenous amount of nutrients and growth factors from the medium during growth. Necrotic cells easily detach from the surface and are removed during growth medium change (Huang et al., 2013). However, owing to the nature of the substrate, the cells acquire a flat and spread morphology that adversely affects multiple processes, including cell proliferation, division, apoptosis, gene expression and protein expression (Tibbitt and Anseth, 2009). Although 2D cell culture systems are adequate to research and to analyse basic cell biology, it is widely accepted that they are not indicative of either the *in vivo* cell environment or the adhesive, topographical and mechanical forces encountered by cells in the physiological context (Carletti et al., 2011; Lee et al., 2008). The complexity of the *in vivo* context involves a thorough reconstruction of living tissue, comparable to a three-dimensional (3D) setting. The behaviour of tissues is characterized by the interaction between cells and the 3D extracellular matrix (ECM) which support them and enables communication through direct contact, paracrine and endocrine secretions. The composition and organisation of ECM components are constantly affected and remodelled by cellular changes. In turn, ECM remodelling exerts mechanical tension on cells and affects the presence of biochemical intermediaries at the cell membrane, triggering cell-signalling cascades that result in further changes in gene expression and cell activity. The underlying premise of dynamic reciprocity is this sustained mutual interaction, and it plays a vital role in development and adult tissue homeostasis.

Contrary to that, the flattened morphology of 2D culture can cause cells to assume abnormal phenotypes and behaviour, raising the need for alternate means to meet the *in vivo* cellular requirements due to the lack of a specific ECM environment (Lee et al., 2008). In contrast to 2D monolayer culture, to achieve an effective cell therapy strategy, cell phenotype and functionality must be aligned towards that observed *in vivo* by controlling the microenvironment, emulating the ECM, the mechanical stress under which they are subjected, and the biochemical context (Nerem and Schutte, 2014). 3D culture of cells is therefore critical to support and maintain cell function and requires the design of an *in vitro* microenvironment that can sustain cell development, organisation and differentiation (Carletti et al., 2011; Lee et al., 2008). Examples of cells grown in 3D systems as part of a cell therapy/strategy are the formation of aggregates or spheroids either on a matrix (Figure 1.1B), inside a matrix (Figure 1.1C) or in suspension medium (Figure 1.1D). In these settings, the interactions between cells and cell–ECM mimic more closely the complex environment seen *in vivo*, with mechanical, chemical and biological features that promote physiological morphology and behaviour. In addition, 3D aggregates consist of cells in multiple phases of the cell cycle, typically involving proliferating, quiescent, apoptotic, hypoxic, and necrotic cells, a variability that is somewhat close to *in vivo* tissues (Kim, 2005).

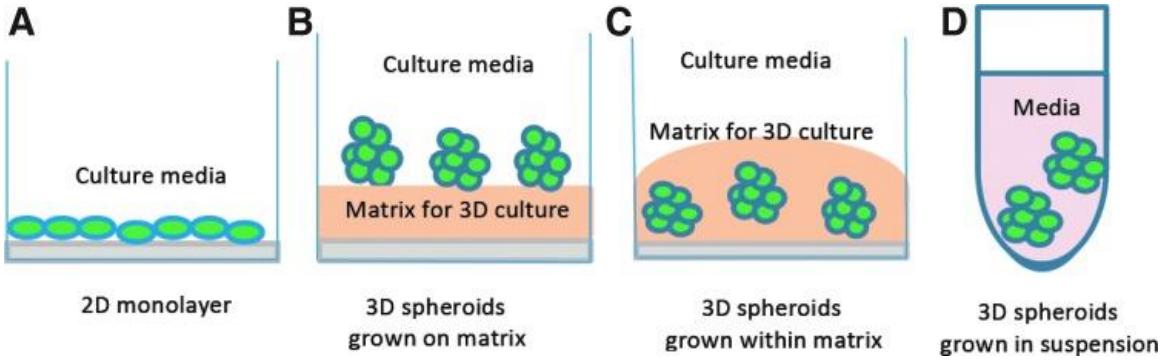


Figure 1.1 Schematic diagram of 2D monolayer cell culture (A) and the three main examples of 3D cell culture, that is cell spheroids/aggregates grown on matrix (B), cells embedded within a matrix (C), or scaffold-free cell spheroids in suspension (D). Image reproduced from Edmondson *et al.*, 2014.

1.2 How mechanobiology influences Mesenchymal Stem Cells

1.2.1 Mesenchymal Stem Cell Fundamentals for Tissue Engineering applications

The development of stem cell-based tissue engineering strategies for the treatment of disease, injury and conditions associated with ageing relies on the ability to direct stem cells safely and efficiently to specific lineages. Biological tissues include populations of differently specialised cells that are closely regulated in tissue homeostasis according to their functions and a number of progenitor cells (Nakada et al., 2011). The latter, thanks to their properties of self-renewal and multilineage differentiation, together with the collective properties in the cellular microenvironment, are referred to as the stem cell niche (Ferraro et al., 2010; Moore and Lemischka, 2006) and are crucial in maintaining tissue homeostasis by regulating cell quiescence and activation. Present knowledge is that numerous microenvironmental signals inside and between *in vivo* niches interact to regulate progenitor cell fate and function (proliferation, migration and differentiation) (Chacón-Martínez et al., 2018; Discher et al., 2009). Among these, mechanical factors have emerged as one of the main determinants together with chemical signalling. Stiffness and morphology of the substrate, cell and tissue deformation arising from mechanical packing, and shear stress associated with fluid motion are all mechanical factors that can influence cell fate (d'Angelo et al., 2019; Fioretta et al., 2012).

Multipotent mesenchymal stromal/stem cells (MSCs) are found in connective tissues and play important roles in tissue homeostasis. A feature these cells possess is the potential to differentiate into osteogenic, chondrogenic and adipogenic lineages (Nagai et al., 2007; Pittenger, 1999), and also showing in some instances the capacity to commit into myogenic, neurogenic and neuroglial lineages (George et al., 2019; Pittenger, 1999; Shih et al., 2005). Traditionally, the majority of research in this area has been linked to biochemical signalling regulating MSC functions; however, it has been shown that mechanical signals are also important regulators of MSCs behaviour. Studies in the field of mechanobiology have reported how the lineage specification of MSCs is influenced by substrate rigidity (Engler et al., 2006; Olivares-Navarrete et al., 2017), geometry (Kilian et al., 2010; McBeath et al., 2004a) and complex mechanical forces that facilitate the commitment to one

lineage at the cost of another to mirror tissue-level physiological changes (Kumar et al., 2017; Luu et al., 2009; Naqvi and McNamara, 2020; Vining and Mooney, 2017). MSCs have also been shown to be influenced by microscopic internal forces that arise as the cells pull on each other or the neighbouring extracellular matrix (Ambriz et al., 2018; Moore and Lemischka, 2006; Pongkitwitoon et al., 2016).

Current knowledge indicates that the combination of the various mechanical signals between and within *in vivo* stem cell niches is a critical determinant of MSCs fate and behaviour (Engler et al., 2006). The difficulty of investigating the latter is aggravated by the restricted accessibility to *in vivo* niches and the combination of multiple non-additive environmental effects (Atta-ur-Rahman and Anjum, 2017). These challenges have motivated the creation of experimental platforms which recapitulate the main properties of *in vivo* niches, and are used to screen multi-factor effects which control cell fate and address MSCs heterogeneity through an analysis of cell behaviour (Atta-ur-Rahman and Anjum, 2017).

1.2.2 Mechanobiology of Bone Marrow-derived Mesenchymal stem cell

Cell behaviour is the product of a complex interplay of inhibitory and stimulatory signalling pathways, and the interaction between molecules must be closely defined in order to understand their mutual effect on cell fate. MSCs feel the stiffness of their supporting substrates by applying contractile forces through adhesion complexes that bind intracellular structures to the ECM (Ambriz et al., 2018; McBeath et al., 2004a; Östlund et al., 2009). Adhesion proteins such as integrins connect the ECM to the force-generating cellular cytoskeleton, causing associated molecular transduction signalling to be triggered depending on binding affinities and stresses produced during contraction (Gauthier and Roca-Cusachs, 2018; Moore et al., 2010). Like most transmembrane molecules, integrins may move sideways through the cell membrane and also cluster into complexes named focal adhesion sites (Figure 1.2). These complexes are dynamic structures that contribute to cell adhesion by binding to the ECM and they provide physical links to the contractile architectural framework of the cytoskeleton and assemble according to substrate

rigidity and topography. As such, they act as major mechanical signalling mediators between the external environment and molecular networks of intermediate filaments, microtubules and actin-based microfilaments (Doyle and Yamada, 2016; Gauthier and Roca-Cusachs, 2018). The resulting formation of stress inside the cytoskeleton after cellular adhesion constitutes the transmission of information from the ECM to the nucleus, thereby translating a mechanical signal into a biochemical signal, a mechanism called mechanotransduction (Gauthier and Roca-Cusachs, 2018; Moore et al., 2010; Östlund et al., 2009; Shafrir and Forgacs, 2002).

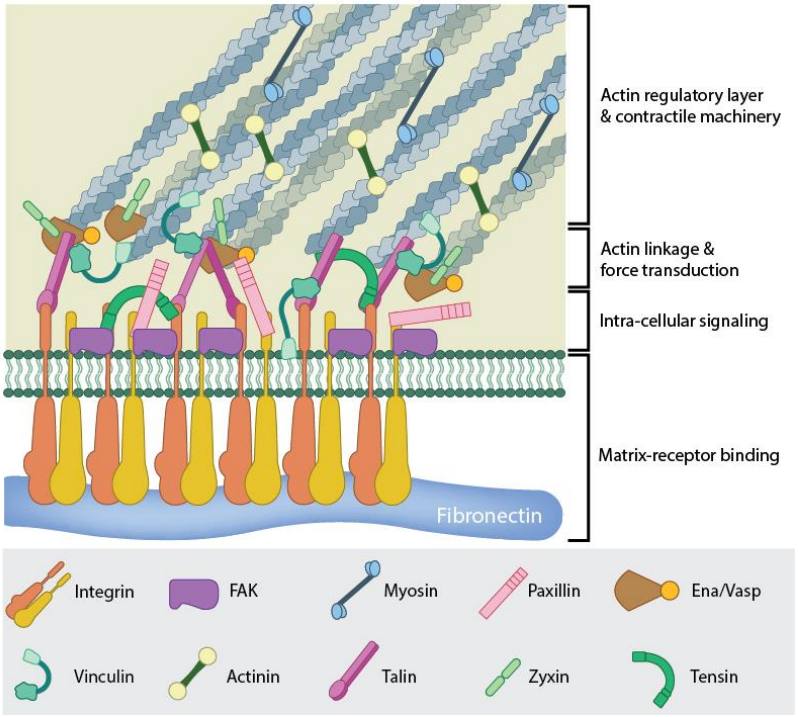


Figure 1.2 Schematic diagram of a focal adhesion. Focal adhesions comprise hundreds of proteins classified based on their contribution to four fundamental processes: receptor/matrix binding, actin cytoskeleton binding, intracellular signal transduction and actin polymerisation. By adjusting to intracellular and extracellular contractile forces, the collective action of mechanosensitive components forms the mechanoresponsive network of the cell. Image reproduced from mechanobio.info website (accessed 2021-01-03).

From the available evidence it is suggested that focal adhesions experience controlled turnover at any given time regulated by different environmental signals (Bershadsky et al., 2003; Gauthier and Roca-Cusachs, 2018; Yim et al., 2010), among which, the main determinants of integrin rigidity sensing that have been identified are (Moore et al., 2010):

1. Integrin-ECM bond strength
2. Cell protrusion/retraction ratios
3. Force produced during protrusion/retraction
4. Elasticity of the mechanosensitive proteins involved.

The elaborate composition of mechanosensitive and signalling components of cell-matrix adhesions provides greater flexibility than any other individual surface receptor. Mechanotransduction is most likely attributable to protein conformational changes in multi-domain proteins functioning as molecular switches (Gauthier and Roca-Cusachs, 2018; Moore et al., 2010; Pongkitwitoon et al., 2016; Vogel, 2006) contributing to subsequent signalling pathways via phosphorylation or to the binding of additional components due to internal/external mechanical perturbation (Dalby et al., 2014; Johnson et al., 2007). These eventually affect prominent protein-protein interactions that cause the adhesion unit to be self-assembled and/or remodelled, cascading into the activation of force-induced signal transduction pathways involving adhesion components and different targets, resulting in downstream signalling events (Dalby et al., 2014; Vogel, 2006).

After the initial integrin-ECM protein interaction, integrins undergo changes in their conformation and affinity, which in turn contributes to integrin clustering and immature focal complex formation. The binding of a variety of integrin-binding receptors, such as RhoA kinase and focal adhesion kinase (FAK), leads to the activation of a number of intracellular signalling pathways, including extracellular signal-regulated kinase/mitogen-activated protein kinase (ERK/MAPK), controlling multiple cellular processes such as proliferation and differentiation (McBeath et al., 2004a; Miyamoto et al., 1995). Subsequent recruitment of binding proteins, i.e. vinculin, talin and paxillin, triggers the formation of actin stress fibres, causing changes in cytoskeletal tension whereto the cell

responds by adjusting focal adhesion size (Atherton et al., 2016; Kawakami et al., 2001), further accentuating the influence of intracellular tension in regulating MSC processes such as differentiation and self-renewal (Dalby et al., 2014; Kilian et al., 2010; Yim et al., 2010). Research has demonstrated that direct mechanotransduction is the result of cytoskeletal changes that are transmitted through the linkers of nucleoskeleton and cytoskeleton (LINC) complexes to the intermediate filaments of the nucleoskeleton, in particular lamin (McNamara et al., 2012; Östlund et al., 2009). This causes changes to the spatial arrangement of lamin-bound chromatin, inducing chromosomal packing or chromatin rearrangement which ultimately affects gene expression (Abbasi et al., 2018; McNamara et al., 2012; Tsimbouri et al., 2013; Wang et al., 2009).

1.2.3 Mechanotransduction signalling in Bone Marrow-derived Mesenchymal stem cell inducing lineage differentiation

Time-dependent regulation of proliferation, matrix plasticity, and in certain cases (e.g. during osteogenesis) mineralisation are needed for MSC maturation across specific lineages. This is controlled by MSC-ECM interactions and the interplay of signalling molecules such as those reported in Figure 1.3A.

Initially, the study on the effects of elasticity cues was mainly focused on the motion and contractility of cells, such as cell motility, morphology or spreading area (Guvendiren and Burdick, 2012; Kuznetsova et al., 2007; Plotnikov et al., 2012) and not on the differentiation of stem cells. These experiments, however, also have shown that Young's modulus (E) for the elasticity of substrates can regulate the intracellular structure of stress fibres (F-actin), resulting in the regulation of the modality and degree of cellular traction. One remarkable example is the work of Engler et al., who found that collagen-coated polyacrylamide hydrogels with elasticity mimicking brain (E~0.1-1 kPa), muscle (E~8-17 kPa) or bone (E~40 kPa) tissue stiffnesses can selectively induce MSC differentiation in the corresponding pathways (Engler et al., 2006).

Indeed, by finding the close association between cell traction and substrate elasticity, the concept of 'mechanosensing' was introduced. Mechanosensing enables cells to detect the elasticity of the

external area by producing a contractile force of their own (Discher et al., 2005), which then propagates in the intracellular environment in a process called mechanotransduction, namely the translation of mechanical signals into cellular responses via crosstalk with intracellular signalling pathways. Among these, β-catenin signalling via Focal Adhesion Kinase (FAK), Rho-associated protein kinase (ROCK) and extracellular signal-regulated kinases (ERK) (Figure 1.3B) are among the most crucial signalling cascades in mediating complex cellular responses (Goetzke et al., 2018).

Cells probe the stiffness of the newly bound matrix by triggering myosin II motor activation and contraction (Ghassemi et al., 2012). These intrinsic forces induce conformational modifications in some adhesion components, such as talin, vinculin and FAK, resulting in the recruitment of additional proteins belonging to mechano-signalling pathways (Atherton et al., 2016). In particular, ECM resistance against cell forces modulates the stability of focal adhesions through FAK activation, which phosphorylates and activates RhoA. The RhoA signaling pathway includes the activation of ROCK, which phosphorylates myosin light chain (MLP), generating more intrinsic forces (Gattazzo et al., 2014).

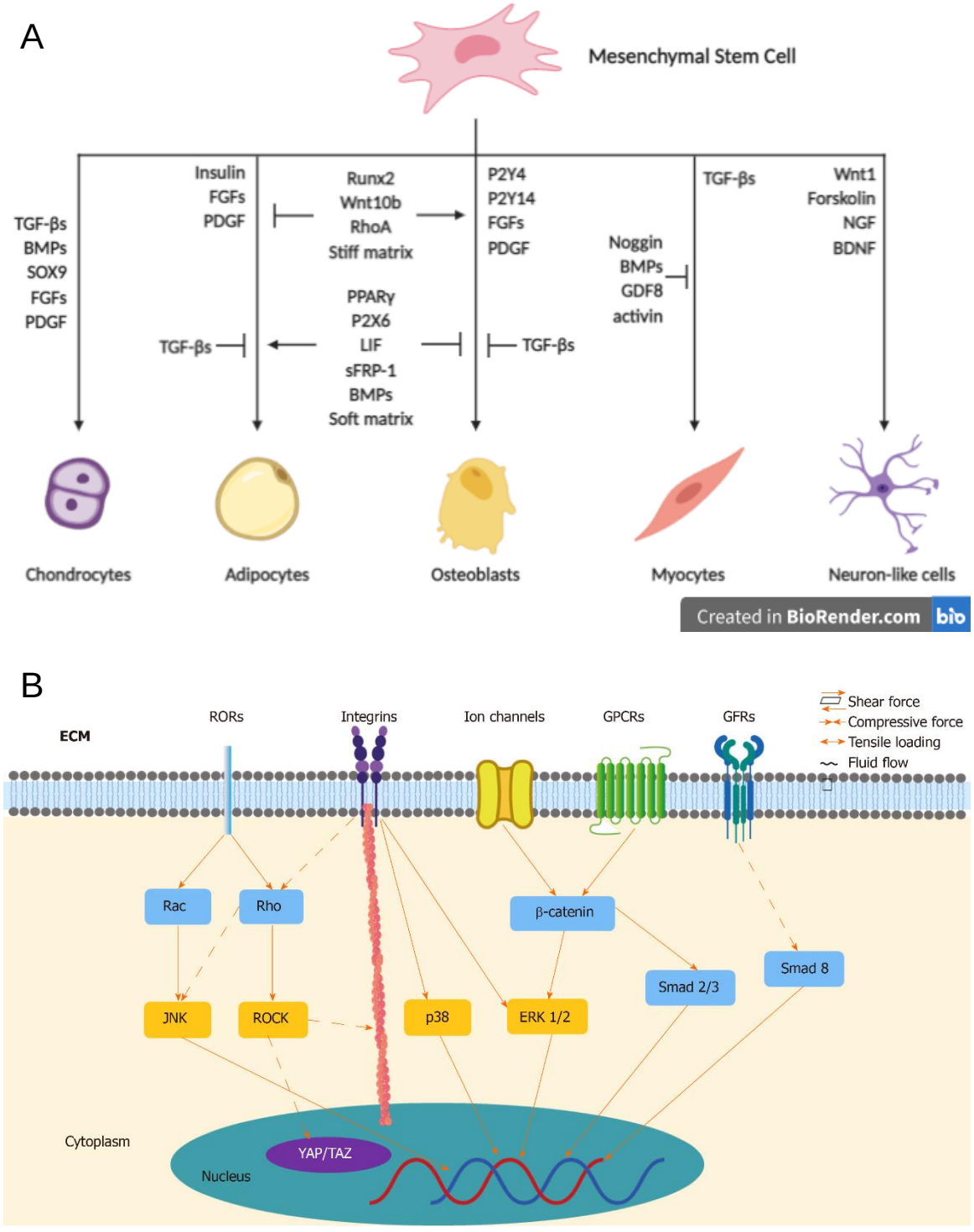


Figure 1.3 (A) Several signalling molecules help regulate the commitment and differentiation of MSCs towards diverse lineages. The molecules shown and lineages affected are adapted upon references (Almalki and Agrawal, 2016; Engler et al., 2006; Neirinckx et al., 2013). Signalling pathways are triggered by mechanical stimuli applied to a cell. The presence of external forces that increase tension on the cytoskeleton activating integrins and/or induce matrix-bound factor release which activates mechanosensory proteins such

as G-protein coupled receptors (GPCR), ion channels and growth factor receptors (GFRs), allow the cell to detect mechanical loading and activate a variety of downstream signalling pathways, promoting gene expression and/or cytoskeleton reorganisation. Image reproduced from Wang, Huang and Ni, 2020.

Focal adhesions are thus able to sense the mechanical properties of the ECM and convert the information into remodelling forces on the actin cytoskeleton that can induce several mechanosensitive transcription factors such as yes-associated protein 1 (YAP), transcriptional coactivator with PDZ binding motif (TAZ) and myocardin-related transcription factors (MRTFs) (Low et al., 2014), or transmit directly the forces from focal adhesion to the nuclear membrane, modulating nuclear activities such as transcription. This is further demonstrated by the use of specific drugs that impair cytoskeleton structures. For instance, cytochalasin D is a small molecule that inhibits the polymerisation of F-actin, blebbistatin inhibits myosin II, and Y-27632 inhibits ROCK, all of which cause reduction of contractility in the cytoskeleton. Therefore, when MSCs are cultured on polydimethylsiloxane substrates patterned with octadecanethiolate islands, the presence of these inhibitors minimise the geometry-directed MSC osteogenesis in favour of adipogenesis (Kilian et al., 2010). Moreover, inhibition of non-muscle myosin II with blebbistatin blocked substrate elasticity-directed lineage specification (Discher et al., 2005; Engler et al., 2006), indicating that the determination of MSC lineage by substrate geometry and elasticity show a dependency on the assembly of MSC focal adhesions and cytoskeleton contractility.

Similarly, when MSCs were cultured in osteogenic medium on substrates with varying stiffness, increased ROCK, FAK and ERK activity was observed on stiffer matrices (E~40 kPa, mimicking pre-calcified bone compared to E~7 kPa mimicking fat) and inhibition of FAK or ROCK decreased expression of osteogenic markers in those cells cultured on the stiffer matrices (Shih et al., 2011). In the presence of antibodies that inhibited the integrin subunit β1 (Gronthos et al., 2001), the ability of MSCs to form a mineralized matrix was also decreased, and integrin-β1 was localized to the cell surface when MSCs were cultured on rigid substrates (E~50-100 kPa) as opposed to cytoplasmic distributions observed on soft substrates (E~0.1-1 kPa) (Du et al., 2011).

As research progresses in the area of mechanosensing and mechanotransduction, other elements emerge to complicate the overall picture (Higuchi et al., 2013). Even though the influence of substrate elasticity on the initial commitment of MSCs remains essential, it is unable to alter the fate of committed MSCs. Guvendiren et al. cultured MSCs on soft methacrylated hyaluronic acid (MeHA) substrates in a 14-day combination of osteogenic and adipogenic mediums (Guvendiren and Burdick, 2012). The majority of MSCs, cultured on soft gels, differentiated into fat cells, as predicted (adipogenic pathway). However, the majority of the MSCs differentiated into bone cells (osteogenic) when the soft hydrogels were stiffened at day 1 and only a small fraction differentiated into fat cells (adipogenic). The pattern continued to rise with the stiffening of hydrogels on days 3 and 7. Such results showed that, before the substrates stiffened, MSCs interpreted the low elasticity cues and differentiated down the adipogenic pathway accordingly. However, after stiffening of the substrate, the undifferentiated MSCs no longer sensed the soft substrate but rather a high elastic one, with the outcome that the MSCs committed to osteogenesis. The fact that some adipogenic cells persisted after stiffening the gels showed that once committed (early MSCs into adipogenic cells), cells would be insensitive to elasticity changes. This appears to be confirmed by recent research wherein, as the process of cell differentiation progresses after the early commitment, much of the initial cell-hydrogel connections are presumably lost when cells, encased in covalently crosslinked hydrogels that restrict cell spreading, secrete and assemble a pericellular matrix that is necessary for the progression of tissue maturation (Cai et al., 2015; Ferreira et al., 2018). This presents a challenge for tissue engineering as any tissue-engineered scaffold, be them made from natural ECM or synthetic polymers, evolve constantly as the materials are remodelled and/or, degrade which may have a variable impact on cell phenotype. This information confirms the need for careful consideration and fine-tuning of the modulus of tissue engineering scaffolds, since they can influence the regeneration, structure, function and commitment of stem cells to differentiate into target cells (Kerscher et al., 2016), but also the need to maintain a certain degree of deformability and flexibility to accommodate the process of differentiation up to its final stages (Assis-Ribas et al., 2018; Wen et al., 2014).

1.3 Biomaterials for Tissue Engineering

1.3.1 Biomaterials to influence Mesenchymal stem cell behaviour

Biological signals, such as growth factors, hormones, small chemicals, and ECM, can determine stem cell fate. However, if at first research primally focused on discovering soluble differentiation factors to replicate the chemical microenvironment of the stem cell, many groups moved to other aspects influencing cell behaviour. Among these are physical cues on MSCs, such as cell shape, cell culture substrate stiffness, mechanical forces (shear stress, compressive forces) and external forces (electrical force, magnetic force) (Burdick and Vunjak-Novakovic, 2009; Clause et al., 2010; Engler et al., 2006; Kasten et al., 2010; Lee et al., 2011; Park et al., 2007; Yim et al., 2010). This suggests that the approach of inducing cell differentiation *in vitro* through soluble factors alone may not be sufficient. The limited accessibility of *in vivo* niches, in conjunction with the scarcity and susceptibility of MSCs to different stimulants, has encouraged the creation of experimental platforms that accurately capture key properties of *in vivo* niches, screen multi-factor effects that control cell fate, and resolve MSCs heterogeneity by evaluating adequate cell numbers on an individual basis. This has led to the development of biomaterials that can promote the production of large numbers of stem cells and/or stimulate the differentiation of cells for *in vitro* regenerative medicine and tissue engineering.

The design and optimisation of bioactive scaffolds require an understanding of the responses of cells cultured upon them. The initial site of interaction with cells is the surface of the biomaterial. Its properties include both chemical and topographical characteristics, such as hydrophilicity/hydrophobicity ratio, bulk chemistry, surface charge and charge distribution, roughness and rigidity (Boyan et al., 1996). Moreover, surface properties can be selectively modified to enhance biomaterial performance through chemical functionalisation and biomolecule immobilisation. Biomolecules include adhesive proteins like collagen, fibronectin, RGD peptides but also growth factors such as FGF and EGF. These elements can either be covalently attached, electrostatically adsorbed or self-assembled on the surface (Wilson et al., 2005).

Since any TE scaffold should facilitate cell attachment, polymers that favour the formation of large and accessible surface areas are preferable. High internal surface-area-to-volume ratios are essential in order to accommodate a great number of cells for regeneration purposes, and in this regard, porosity play an important role in providing a large surface area (O'Brien et al., 2005). Pore size determines the number of struts and the density of ligands available for cell adhesion. As pore size decreases, specific surface area increases but, at the same time, this denser network of struts limits choice in the direction of the movement of the cells and creates resistance to scaffold penetration, extracellular matrix production and neovascularisation of the inner areas of the scaffold (Harley et al., 2008). Conversely, if the pores are too large a decrease in the surface area occurs, which in turn limits cell adhesion.

Thus, changing the biomaterial surface and scaffold microarchitecture may influence cell behaviour concerning individual processes such as proliferation, differentiation and motility (chemoattraction, adhesion, migration) which in turn will affect matrix deposition (Ravindran et al., 2010). This feature is imperative to achieve biocompatibility, biodegradability and interconnectivity in the formation of new tissue (Nair and Laurencin, 2007).

The meaning of biocompatibility is to elicit a biological response without resulting in toxicity, inflammation or immunological response that may lead to rejection. Although limited local inflammation can promote healing and neovascularisation, chronic inflammation and/or an adverse immune response can compromise both the implant and the patient (Nair and Laurencin, 2007). Biocompatibility involves not only the material used but also the surrounding cells/tissue that interacts with it. Dynamic interaction between cell, substrate and cytoskeleton is required for tissue homoeostasis, which occurs employing specific ligand-integrin interactions and mechanotransduction as the cell develops tensile stress to feel its surroundings (Figure 1.4).

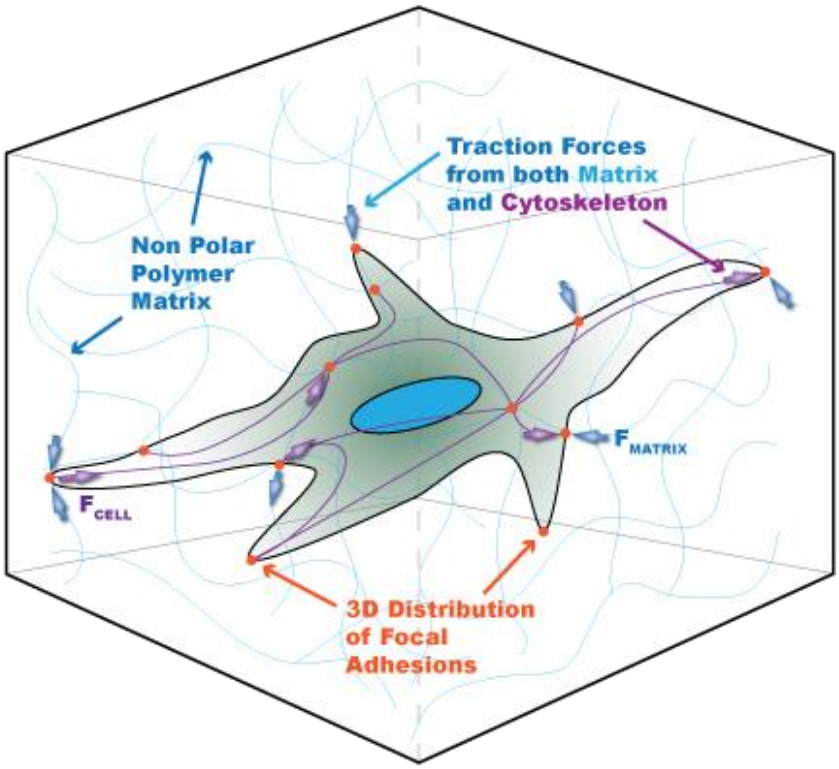


Figure 1.4 Schematic representation of a cell inside a 3D ECM. In this context, cellular traction forces are evenly distributed and propagated along ECM fibres, causing both ECM and cytoskeleton remodelling and cell reshaping. Image adapted from Breuls, Jiya and Smit, 2008.

Since the recognition of biomaterials by cells is typically mediated by adhesion proteins, adjusting their composition can lead to a difference in ligand density, availability and subsequent integrin binding, thus improving the overall cellular response (Wilson et al., 2005). Some observations also highlight that shape could drive stem cell differentiation alone, overruling the instructive messages provided by soluble differentiation factors (Rodrigues et al., 2014). Finally, mechanical properties are critical in choosing a suitable biomaterial (Polo-Corrales et al., 2014). The biostability of a polymer depends also on factors such as strength and elasticity, which are essential for the scaffold to modulate the remodelling of the cytoskeleton, cell polarisation, intracellular signalling and for the tissues to withstand continuous loads and stresses (Balani et al., 2014). One such parameter is the elasticity of the material, as represented by the elastic modulus or Young's modulus (*E*, Pa = N/m^2), which refers to the resistance to elastic deformation (Khetan et al., 2013). The elasticity of

2D substrates or 3D matrices can be calculated by atomic force microscopy (AFM) (Wen et al., 2014), compression testing (Rowlands et al., 2008), tensile testing (Zoldan et al., 2011) or by using a rheometer (Kumar et al., 2013).

1.3.2 Natural and Synthetic Polymers

While materials intended for implantation were in the past designed to be biologically inert, the scope has shifted toward the design of bioactive materials that integrate with biological molecules or cells to regenerate tissues. Biomaterials can be categorised into different types in terms of structural, chemical, and biological characteristics. Their quality is ultimately determined by the ability to influence mechanical properties, cell responses and tissue formation. Natural polymers are those materials that have natural occurring long-chain molecular structures while synthetic polymers are derived mainly from oil-based materials (hydrocarbon) with the resulting properties of high expansion coefficient, low density and low thermal conductivity (Nair and Laurencin, 2007).

Natural polymers were among the first biodegradable materials used clinically (Reddy et al., 2021). They usually have more complex structures than synthetic polymers and concerning tissue engineering, natural polymers perform a diverse set of functions due to their native settings. Natural polymers, especially the protein-based ones, have the benefit of copying the features of an ECM and thus have the potential to direct the migration, growth and formation of cells during tissue regeneration and wound healing and for stabilization of cells (Malafaya et al., 2007). Table 1.1 shows several natural polymers found in application in the field of tissue engineering.

TABLE 1.1 Examples of natural polymers **(Malafaya et al., 2007)**

Natural Polymers	Examples
Protein-origin polymers	Collagen, gelatin, silk fibroin, fibrin (fibrinogen), elastin, soybean
Polysaccharides	Chitosan, starch, alginate, hyaluronan, chondroitin sulphate, dextran, carrageenans, gellan gum and cellulose.
Polyhydroxyalkanoates	Poly(β-hydroxybutyrate) (PHB) and poly(hydroxybutyrate-co-valerate) (PHBV)

Collagen, the most abundant protein in the human body, has been used in a wide range of tissue engineering applications due to its predominance in the ECM. In the work of Sell *et al.*, 2009, collagen type I was dissolved in hexafluoro-2-propanol (HFP) ranging the concentration from 0.03 to 0.10 g of collagen/ml of HFP and electrospun it to fabricate fibres for tissue scaffold potential. The experiment resulted in scaffolds composed of 100 nm to 5 μm diameter fibres. Fibrin, a major component of blood clots, has been employed as a coating agent on metallic implants to improve cell dispersion and responsiveness, as well as to release growth factors. Preincubation of Ti surfaces with whole human blood increased the number of adherent cells, increased ALP and collagen-I protein expression, and accelerated mineralisation, according to (Kopf *et al.* (2015). Another is chitosan, a cationic polymer from chitin, which can produce a scaffold with a hydrophilic surface and cell adhesive/differentiating characteristics, while its inherent osteoconductive nature endows its potential use for bone tissue engineering (Aguilar et al., 2019; Cruz et al., 2008) as well as skin grafting (Pandey et al., 2017).

Composed of hydrophilic elements, natural polymers provide innate biological informational guidance to cells favouring cell interactions and promoting chemotactic responses. This allows them to enhance cells performance in biological systems, however, concern exists over their

immunogenicity, potential risk of disease transmission, poor handling, and inadequate mechanical properties (Prestwich and Atzet, 2013).

Synthetic polymers offer a versatile alternative (Docheva et al., 2007). They have an advantage over natural polymers in the way that they can be tailored to give a wide range of properties and which are more predictable (Liu et al., 2007). They are easily processed concerning porosity, degradation time and mechanical characteristics; moreover, the possibility to be tailored for specific applications makes them an even more attractive cellular delivery device. Synthetic polymers are often cheaper than biological scaffolds, can be produced in large quantities under controlled conditions and have a long shelf-life. Furthermore, they exhibit predictable and reproducible mechanical and physical properties such as tensile strength and elastic modulus (Gunatillake et al., 2006).

Also, many studies and investigations discussed that synthetic biodegradable polymers were already approved by the Food and Drugs Administration (FDA) (Liu et al., 2007). Table 1.2 shows different examples of synthetic polymers used for medical applications.

TABLE 1.2 Examples of synthetic polymers and their uses

Synthetic Polymers	Properties
Polyvinylchloride (PVC)	Amorphous and rigid polymer, high melt viscosity, made flexible and soft by the addition of plasticisers. Used for: blood and solution bag, surgical packaging
Polymethylmethacrylate (PMMA)	Resistant to inorganic solutions, excellent optical properties. Used for: blood pump and reservoir, implantable ocular lenses, bone cement
Polypropylene (PP)	High tensile strength, excellent stress-cracking resistant Used for: blood oxygenator membrane, artificial vascular grafts
Polystyrene (PS)	Good transparency, ease of fabrication, thermal stability, relatively high modulus Used for: tissue culture flasks, vacuum canisters, filterware

Despite their positive characteristics, success can be limited because of their recognition by the body as non-self, leading to an unwanted immune response and release of acidic degradation by-products altering the pH in the surrounding tissue (Yang et al., 2001). Furthermore, most of them lack cell recognition sites, which limits cell adhesion on 3D scaffolds (Hutmacher, 2000).

1.3.3 Hydrogels and gelatin-derived composites

Hydrogel is a characteristic biomaterial that differs significantly from other materials due to its hygroscopic nature, similar to native tissues. One of the most attractive features of hydrogels is the possibility to be delivered in a minimally invasive manner and gelled *in situ* (photo-crosslinked or ionically) to provide a 3D microenvironment with high water content (Gupta, 2019; Kim et al., 2012). Their viscoelastic material properties seem particularly suitable for cartilage regeneration, although many applications in bone have also been explored (Cushing and Anseth, 2007; Liu et al., 2017). The advantage of hydrogels is that chemical biofunctionalisation, cell encapsulation and delivery are relatively straightforward (Cushing and Anseth, 2007).

Gelatin, a derivative of collagen hydrolysis, has attracted much interest in this regard. Gelatin can form hydrogels in aqueous solutions, shows good biocompatibility and contains Arg-Gly-Asp (RGD) motifs within its structure that favour cell adhesion (Grover et al., 2012). Manufacturing gelatin is relatively simple and cheaper compared with that of collagen, however, gelatin-based hydrogels display low mechanical stability due to their high hydration and poor durability, limiting their use (Toh and Loh, 2014). To improve their stability, several approaches including crosslinking have been used, and one promising example is the semi-synthetic biomaterial gelatin methacrylate (GelMA) (Van Den Bulcke et al., 2000; Yue et al., 2015). In this instance, methacryloyl groups from methacrylic anhydride react and replace a significant number of amino groups found on the side chains of gelatin (Figure 1.5A). This GelMA is similar to gelatin in that the temperature still determines its solid-liquid transformation. However, due to the inclusion of methacryloyl groups, it is possible to cross-link (Figure 1.5B). When adding the photoinitiator, a water-soluble GelMA crosslinks immediately under UV light, giving rise to GelMA hydrogels that have excellent

thermostability. In this regard, GelMA hydrogels are engineered to imitate the normal ECM due to the tuneability of the mechanical strength towards native ECM and are capable to promote cell growth in a 3D environment, encouraging the formation of functional tissues, maintaining mechanical integrity and the survival of implanted cells (West, 2011). GelMA hydrogels have been shown to promote the formation of 3D vascular endothelial networks (Nichol et al., 2010), as well as support osteocyte, chondrocyte, myocyte and adipocyte viability and differentiation by matching the natural functions of scaffolds in mechanical and geometrical properties (Gao et al., 2015; Kim et al., 2020).

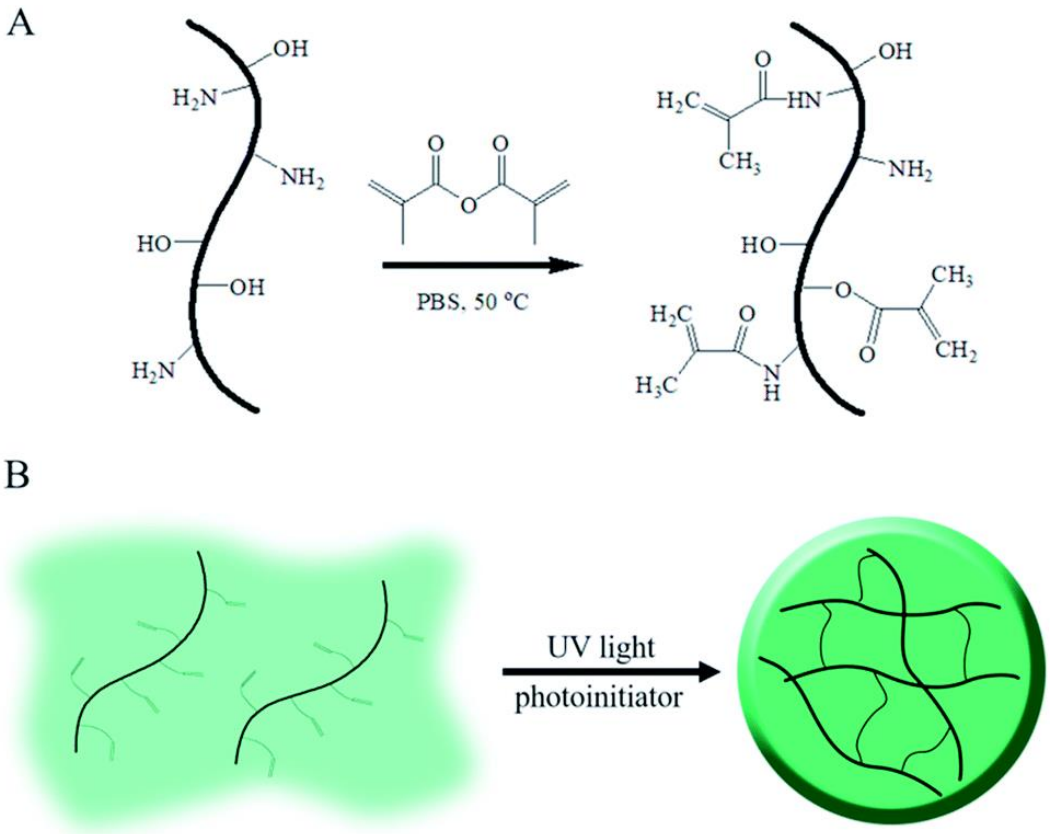


Figure 1.5 Schematic of (A) GelMA synthesis from gelatin and methacrylic anhydride and (B) formation of hydrogels via UV-catalysed crosslinking. Image reproduced from Dong *et al.*, 2019.

1.4 Polymeric microparticles for Tissue Engineering

1.4.1 The Microparticle-based approach

Microparticles have been suggested as a viable alternative to traditional bulk scaffold-based approaches. Polymeric microparticle morphology is usually spherical and ranges from 1 to 1000 μm in diameter. These systems offer several benefits including ease of fabrication, biochemical stability and chemical composition customisation (Chau et al., 2008). Modification of parameters like size, shape, porosity and elasticity allows control over morphology and physicochemical characteristics; moreover, control of molecule incorporation and tailoring their release kinetics allows for a fine-tuned system for multiple specific applications (Berkland et al., 2003). Indeed, bioactive agents and *in vitro* pre-seeded cells can both be encapsulated, attached to the microparticle surface and delivered using the microparticles as vectors and injected into the defect, obviating the need for invasive surgical procedures (Kirby et al., 2011; Oliveira and Mano, 2011; White et al., 2013).

1.4.2 Applications of polymeric microparticles in Tissue Engineering

Microparticles can be employed for diverse applications, as summarised in Figure 1.6.

Biodegradable polymeric microparticles have been extensively used as vehicles for the *in situ* delivery of bioactive molecules with short systemic circulation half-life and their controlled release over time (Coombes et al., 1997). Microparticles can encapsulate growth factors, morphogenetic proteins or drugs and release them per diffusion, polymer degradation or triggered release (Figure 1.6A,B). The modulation of release rates by exploiting degradation kinetics can be achieved by employing polymers with different chain lengths and compositions (Ravivarapu et al., 2000). One of the applications for this system is the induction of cell migration, growth and differentiation to promote tissue regeneration in specific areas (Freiberg and Zhu, 2004). This has been carried out with encapsulated transforming growth factor-β1 (TGF-β1), BMP, FGF and VEGF, both in single and dual delivery systems (Santo et al., 2013).

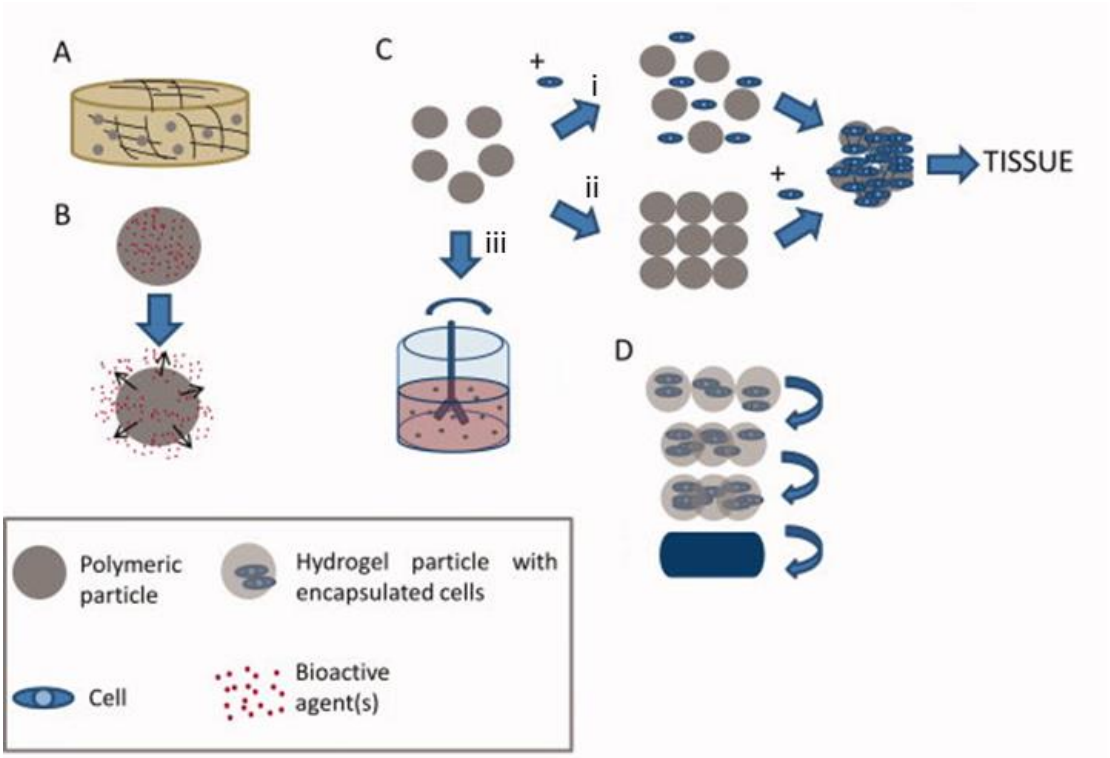


Figure 1.6 Schematic representation of the applications of polymeric microparticles in TE. Briefly, these include: (A) Incorporation in hydrogels, matrices or porous scaffolds as an added factor for modifying their porosity and viscoelastic properties, or as delivery systems for macromolecules; (B) Injectable delivery systems for controlled-release of bioactive molecules; (C) Scaffolds obtained by (i) cell agglomeration, (ii) chemical agglomeration or sintering; (iii) Microcarriers for cell expansion; (D) Hydrogel particles with encapsulated cells for organ printing and mesoscale self-assembly. Image adapted from Oliveira and Mano, 2011.

Microparticles are also known for their use as cellular microcarriers, employed *in vitro* for cell population expansion (Figure 1.6Ciii) either as a monolayer on the surface or as multilayers within a porous structure. Separate particles offer a high ratio of surface area per volume, allowing high yields of therapeutically relevant quantities of cells, up to 200 million per mL (Blüml, 2007). They can also be shaped into larger, complex structures with high interconnectivity for bottom-up construct fabrication, as it minimises the number of steps in the overall process, namely detaching cells from the microparticles before further processing (Chau et al., 2008). Cell-laden microparticles can be led to form aggregates *in vivo* or suspension cultures through cell-cell, cell-

ECM or cell-scaffold interactions (Figure 1.6Ci), which could be further enhanced via functionalisation with adhesive proteins (Custódio et al., 2014). This method was attempted with chondrocyte-laden PLGA microparticles for *in vivo* cartilage regeneration with promising results (Chun et al., 2004). Alternatively, these scaffolds can be obtained via sintering (Figure 1.6Cii). This has been applied for osteochondral TE to produce a comprehensive bone and cartilage interface, using biphasic, sintered PLGA and nanohydroxyapatite microsphere scaffolds (Shalumon et al., 2016). Finally, approaches of cell encapsulation inside hydrogel microparticles led not only to delivery systems for cell therapy, but also mesoscale fabrication methods for organ printing (Figure 1.6D).

1.4.3 Polymeric microparticle production

Most fabrication methods aim to achieve microparticles of optimal size and low polydispersity. For TE, the former should be small enough for a higher surface-area-to-volume ratio, increasing the area available for cell adhesion, preventing phagocytosis (Champion et al., 2008). As for polydispersity, narrow size distribution is desirable to maximise experimental homogeneity, reproducibility, repeatability and consistency. This feature is essential for obtaining reliable and unambiguous results due to intra-system uniformity in regards to outputs, such as drug release profile and cell response (Kawaguchi, 2000).

One of the most common methods for microparticle production is the emulsion of two or multiple immiscible solutions. As a basic rule, polymers are dissolved in an organic solvent, which is usually volatile and with low water miscibility, such as dichloromethane (DCM) or chloroform. This solution, called the disperse phase, is then emulsified via stirring or homogenisation into an aqueous solution, the continuous phase, which contains surfactants such as poly(vinyl alcohol) (PVA) to stabilise the formed microparticles. Microparticles are produced after organic solvent extraction or evaporation and are eventually dried or lyophilized. Size control is achieved by altering the viscosity of the solutions and the stirring or shear rate, though control is limited (Chau et al., 2008). The emulsion type can be varied according to the solubility of the polymer or drug to be

encapsulated. In this regard, the method is divided into two main variants, oil-in-water (O/W) and water-oil-water (W/O/W) emulsifications. Stability is crucial to impede microparticle coalescence and drug loss and can be achieved by increasing the concentration of the surfactant, which conversely reduces the average size of microparticles (Nihant et al., 1994). Another widespread method is spray drying, which is a single-step production approach based on the direct injection of a polymer-based aerosol through a heated nozzle, followed by its rapid evaporation via a hot stream of gas and deposition of dried product. Spray drying is a low-cost and easy to scale up continuous process, however, its high temperature can cause denaturation of thermally labile molecules such as proteins (Chau et al., 2008). Polymers can also be subjected to phase separation, also known as coacervation. It can be achieved by decreasing the solubility of the polymer-containing solution via the introduction of a coacervation agent, which interacts with the solvent but not with the polymer. This results in two distinct phases, one coacervated with the polymer and one supernatant phase. This process is suitable for encapsulation of both hydrophilic and hydrophobic drugs and ensures minimal loss of both polymers and drugs. The main disadvantages are the need for high concentrations of polymers and strong solvents, batch to batch variability and agglomeration of microparticles due to the absence of stabilising agents (Chau et al., 2008).

1.4.4 Microfluidic-based fabrication of microparticles

The methods until now considered, though effective, result in wide particle size distributions. Compared with emulsion-based approaches, microfluidics has emerged thanks to many of its specific advantages. such as the capability of precisely controlling the size and shape of the microparticles allowing for monodispersed populations with a wide range of shapes and compositions (Leng et al., 2010; Utada et al., 2005). Microfluidic systems are also suitable for monitoring the rate of reaction, heat and mass transfer, minimising waste. In addition, composite particles can be created with accuracy and reproducibility by mixing various streams and using double-emulsion techniques or photolithography. Particle processing can be combined also with

other parts, such as sensors, heaters, coolers, visualisation windows to further affect or monitor the output. Finally, microfluidics can be scaled up by parallelisation, enabling large-scale production.

Droplet microfluidics is the most direct way to manufacture hydrogel microparticles in microfluidic systems. A typical flow-focusing microfluidic system comprises two immiscible co-flowing streams, employing the break-up of these streams to produce homogenous, discrete droplets. Usually, a disperse phase composed of an aqueous polymer solution is directed into a faster-flowing oil continuous phase, which drags polymer droplets out from its source. The flow ratio is adjusted in a way that the inner fluid forms droplets rather than a jet of fluid, balancing between the shear force of the liquid that pulls out the nascent droplet, and surface tension. The size of the particles can be altered by modulating the flow rate ratio of the two phases, allowing easy control over particle diameter in a continuous process (Xu et al., 2009). The most popular designs are T-junction, flow-focusing and co-flow geometries to create microdroplets by hydrodynamic manipulation (Christopher and Anna, 2007). In a T-junction arrangement (Figure 1.7A), the continuous phase flowing through the main channel is intersected by the dispersed phase flowing through the secondary channel. In a flow-focusing configuration (Figure 1.7B) the flow of the dispersed phase in the main channel is squeezed by the continuous phase flow entering by two lateral channels (Samanipour et al., 2016). Finally, the co-flow configuration (Figure 1.7C), similar to the flow-focusing configuration, consists of the disperse and continuous phases flowing in the same direction in parallel microchannels (Christopher and Anna, 2007), with the disperse phase in the inner flow and the continuous phase in the outer flow. The size of the droplets produced depends on the viscosity and density of the fluids, surface tension, flow speeds, surface properties, and system geometry (Teh et al., 2008). Dimensional measurement results in a correlation between the droplets' non-dimensional size and the Capillary and Reynolds numbers of disperse and continuous phases, the viscosity ratio (λ) and the contact angle and the flow rate ratio (φ).

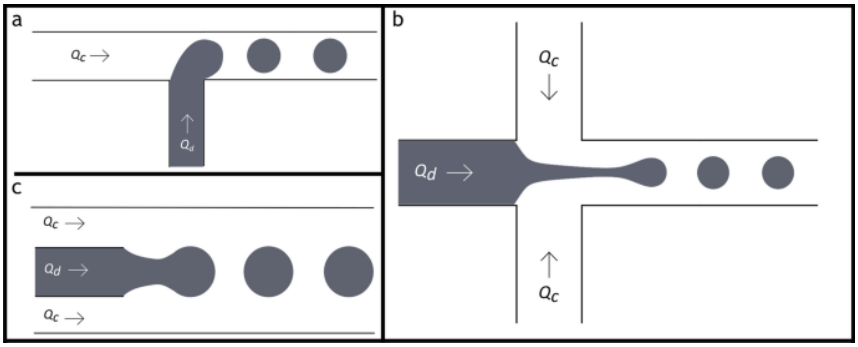


Figure 1.7 Most common designs used in droplet microfluidics: T-junction system (A); flow-focusing system (B); Co-flow system (C). Q_c: Continuous phase flow rate; Q_d: Disperse phase flow rate. Image adapted from (Moreira et al., 2021).

Typical flows are characterised by very low Reynolds numbers in microfluidic systems, wherein viscous forces are predominant with no significant changes in the flow (Teh et al., 2008). Whereas in high-speed flows, the inertial forces become important and so the Reynolds number effects should be assessed (Baroud et al., 2010).

Some instruments are needed to predict the flow regime, polydispersity and particle size to generate particles with defined characteristics. Only in the dripping and jetting regimes are microdroplets formed, as evidenced by Carneiro et al. (Carneiro et al., 2016), who characterised PDMS droplet formation in a microfluidic flow-focusing system, concluding that the dripping regime is the optimal flow condition to acquire monodispersed microdroplets. The study of particle size patterns is not a straightforward matter either, because size trends are geometry-dependent and, as the findings of many papers in the literature demonstrate, it is heavily dependent on regime changes. For example, Dang et al. (Dang et al., 2012) produced monodisperse PEG microparticles in a flow-focusing system and observed a reduction in the size of the droplets with the increase in the continuous phase flow rate, whilst high concentrations of PEG led to larger microdroplets. Indeed, concentrated PEG solutions have high viscosity and increased surface tension, with a dominant rise in viscosity. For this reason, high concentrations contribute to elevated disperse phase Capillary numbers.

In this regard, hydrogel microparticles have great potential in many biomedical applications, and the use of microfluidics enables precise control over the formation of the particles and is useful to meet most of the specific needs of these applications. Significant challenges remain when using microfluidics as the flow rate of the two phases must be kept to relatively slow speeds to reduce the size distribution, which impacts the timing when fabricating sufficient quantities not only for experimentation but possibly for large-scale production. With these considerations in place, it is of particular interest to develop a technique for the production of microparticles that allows both an increase in yield and the retention of the viscoelastic characteristics of the microparticles themselves, a crucial factor to enable the study of MSCs in influencing their behaviour and commitment, together with the capacity to obtain relevant quantities for future clinical translation.

1.5 Aims of the Thesis and Research question

Current methods on understanding the effect of matrix stiffness on MSC differentiation have been carried over in 2D format, i.e. hydrogel discs with varying matrix stiffness and coated with adhesion molecules. However, the cellular microenvironment is in 3D, and the signalling and geometric effects are much different when cultured in such a manner. The author, therefore, aims to and hypothesises that the cell culture conditions that induce differentiation in 2D can be translated into 3D using a hydrogel-based microparticle format. As mentioned before, it has been decided to use a platform material: a hydrogel in a microparticle form. Hydrogels mimick the porous nature of the ECM along with its matrix stiffness (i.e., bone marrow and neotissues), whereas the microparticle format constitutes a loose 3D space in which cells could proliferate and interact dynamically in a similar manner to their native tissues.

Thus the objective of the research was to develop a platform to translate the observations of matrix stiffness-induced differentiation of mammalian cells from a 2D phenomenon to a 3D culture system. The reason why the author pursued this rationale is that a unitary vision relating to the cellular response to mechanical stimuli in a 3D perspective is lacking since research has mainly focused on biomaterials in a 2D format and limitedly in 3D environments, wherein volume adaption

plays a crucial role in cellular dynamics (Labriola et al., 2018; Major et al., 2019; Wang et al., 2019). Secondly, the use of hydrogels stems from the fact that these biomaterials are more flexible and, when naturally sourced, contain peptide motifs for protein receptor binding, increasing the survivability of cells and influencing their behaviour (Docheva et al., 2007; Du et al., 2011; Luu et al., 2009), which also translates into the activation of pathways that can guide their differentiation without providing external growth factor signals (Olivares-Navarrete et al., 2017). Thirdly, the use of microparticles produced via microfluidics allows a more scalable, replicable and manipulable platform (Moreira et al., 2021; Xu et al., 2009), granting cells free interactions with their surroundings by interconnecting colonies on a particle to another (Neto et al., 2019).

A co-flow microfluidic system was developed, and by adjusting its operating and solution parameters, one could produce monodisperse, hydrogel-based microparticles of tuneable size and matrix stiffness. The microparticles fabricated were evaluated in their capacity to support the culture of human bone marrow-derived mesenchymal stem cells (MSC) and to support their differentiation into varying lineages through the surface modulus of the microparticle alone. It is hypothesised that matrix stiffness in a 3D environment could differentiate MSCs into the desired lineage.

The repercussions of this research expand the experimental horizon related to GelMA hydrogel microparticles thanks to multiple crucial advantages: they constitute an architecture for 3D cell culture, they represent a bottom-up element that allows desirable scaling-up from laboratory to industrial processes, and also provide means to avoid costly exogenous and xenogenic growth factors for cell differentiation.

2. METHODS

2.1 Consumables and Materials used

All general chemicals and reagents were purchased from Sigma-Aldrich (Poole, UK) except where stated otherwise. All analytical grade solvents were obtained from Fischer Scientific (Loughborough, UK).

2.2 GelMA synthesis via precipitation method

GelMA synthesis was conducted following the experimental conditions reported by Shirahama *et al.* (2016). Briefly, a 10% w/v gelatine Bloom 175 was prepared in 0.25 M carbonate-bicarbonate buffer at 60°C and with stirring at 500 g on a hot-plate stirrer (11-100-16SH Fisherbrand Isotemp, Thermo Fisher Ltd. UK). Upon complete dissolution, the pH of the solution was adjusted to 9.0 using 5.0 N NaOH. While stirring, methacrylic anhydride was added at a ratio of 0.02, 0.1 or 0.2 ml/grams gelatine (the latter 4.4x times excess towards the theoretical moles of available primary amines) at a rate of 0.5 ml/min through manual pipetting. The reaction was conducted in a light-free condition and in a minimised air uptake environment, where a narrow-necked reaction vessel was covered by aluminium foil. After 2 h of stirring, the reaction was halted by neutralising the solution (pH 7.4) by adding 5.0 N NaOH or 1 M $NaHCO_3$. The reaction liquid was precipitated readily by adding the solution dropwise in a large volume of denatured alcohol. The precipitate was removed from the solvent via filtration (Whatman® Grade 1 Qualitative Filter Paper) and was dissolved in 50 ml deionized water at 60°C and 500 g. The resulting solution was precipitated again, and this process was repeated 3 times to ensure the complete removal of unwanted by-products and unreacted components. The precipitated GelMA was manually pressed between filter papers to remove the remaining excess solvent, and then freeze-dried at -50°C for two days. The resulting product was a lump of solid material which was powdered using a coffee grinder (GT203840, Tefal, UK) and stored at -20°C until use.

2.3 Characterisation of GelMA degree of substitution via 2,4,6-trinitrobenzene sulfonic acid assay

2,4,6-trinitrobenzene sulfonic acid (TNBS) test was used to assess the degree of methacrylation of the three GelMA formulations prepared as described in section 2.2. Briefly, 15 mg of the sample was dissolved in 2 ml of 4% w/v $NaHCO_3$ containing 0.01 M TNBS and reacted at 40°C and 100 g for 3 h. Afterwards, 3 mL 6.0 N HCl was added to the solution and the temperature was raised to T=80°C and left to react for 1 h. The solution was then cooled to room temperature by immersing the reaction vial in a water bath, and the solution was further diluted by administering 5 ml of distilled water. Absorbance was then determined at 345 nm using a 96-well plate reader (Infinite Pro, Tecan) and the degree of substitution (DS) was estimated from three different, triplicate samples, using the following equation:

$$DS = 100 \times \left(1 - \frac{A_{GelMA} - A_{blank}}{A_{Gelatin} - A_{blank}}\right) \quad (3.1)$$

2.4 GelMA 2D discs generation

GelMA 2D discs were produced by mould casting, adding 250 µL of GelMA Bloom 175 precursor solution at the concentration (Degree of Substitution, DS) of 5% (30% DS), 5% (68% DS), 5% (93% DS), 8% (93% DS) or 13% (93% DS) w/v with 0.5% w/v photoinitiator 2-Hydroxy-4′-(2-hydroxyethoxy)-2-methylpropiophenone (Irgacure D-2959) in a cylindrical PTFE mould (diameter = 12mm). The DS was determined using the TNBS assay. The solution was crosslinked under a 25-W 365 nm UV Bench lamp for 10 min. Afterwards, the cylinders were washed with PBS 3 times and incubated in DMEM without phenol red (Gibco) at 37°C before use.

2.5 GelMA microparticles production using co-current flow microfluidic system

Manufacturing of GelMA microparticles was performed via a custom-made co-current flow microfluidic system. A schematic of the setup is shown in Figure S1. Briefly, two syringes (one

containing the disperse phase and the other containing the continuous phase), were loaded on two syringe pumps (WZ74905-02, Cole-Parmer, UK) respectively. The disperse phase syringe and the continuous phase syringe are connected, directly and via PTFE tubing (1.5 mm I.D.) respectively, to a coaxial needle (ramé-hart instrument co., Succasunna, NJ, USA), composed of gauges 20 and 13 as the inner and outer capillaries, respectively. A heating band (TBSO-052-060, BriskHeat, Cole-Parmer UK) is wrapped around the disperse phase syringe to maintain the temperature of the solution at 60°C to prevent gelling. A silicon tube (1.3 mm I.D.) connects the output of the coaxial needle to a UV chamber, containing a UV lamp (OmniCure® S1000, Lumen Dynamics, Mississauga, Canada) and a metal mesh sieve with a 50 μm cut-off (60.131.000050, Retsch, Haan, Germany) installed on a metal pan for microparticle retention and continuous phase recovery.

Following the microfluidic approach, the disperse phase and continuous phase flow in the same direction and meet at the point of outflow of the internal capillary into the outer one, producing an emulsion of single droplets of disperse phase dragged within the continuous phase. The parameters affecting the production are thus the flow rates of disperse and continuous phases. The advantages of this approach are the potential for large-scale production of monodisperse microparticles with precise size distribution.

For the initial screening using a Design of Experiment process (as described in section 2.6), the disperse phase consisted of GelMA Bloom 175 at 5% (93% degree of substitution as determined via TNBS) w/v in 0.5M Magnesium chloride (added as a chaotropic agent) dissolved in deionised water, whilst the continuous phase consisted of Span80 (Sorbitan monooleate) at a concentration of 10% v/v in mineral oil. The photoinitiator 2-Hydroxy-4′-(2-hydroxyethoxy)-2-methylpropiophenone (Irgacure D-2959) was added in the disperse phase at a concentration of 0.5% w/v as a crosslinking agent of the methacrylate groups of GelMA.

Similarly, for the experiments on cells viability and differentiation, another series of disperse phase formulations were used: GelMA Bloom 175 at 5% (30% DS), 5% (68% DS), 5% (93%

DS), 8% (93% DS) or 13% (93% DS) w/v in 0.5M Magnesium chloride dissolved in deionised water. The flow rates used were 3 ml/hr and 100 ml/hr for the disperse phase and continuous phase, respectively, producing microparticles of ~250μm in diameter. The aim was to produce high quantities of GelMA microparticles with a defined diameter and low polydispersity so as to maintain the morphological and elastic properties of the single microparticles as homogeneous as possible.

After collection, microparticles are washed three times with hexane, three times with IMS and three times with deionised water in order to remove the remaining mineral oil and photoinitiator. Finally, the sample suspended in water is transferred into a 7 ml Bijou sample container and stored at 4ºC until future use.

2.6 Design of Experiment

To understand mathematically and statistically the effect of operating conditions with the minimum number of trials, a Design of Experiment (DoE) was performed. Initially, pre-trial experimentations were done to evaluate the region of operability of the microparticle production. The extremity values were then used as the upper and lower limits in the DoE. The microparticle production experiment has been carried out with 17 runs whose determining factors (disperse and continuous flow rates) were set up following a response surface methodology - Central Composite Design. Central composite designs are a factorial design organised with a set of centre points, i.e. runs in which the values of each factor are medians of the values used as starting factors, and a set of axial points, i.e. runs identical to the centre points except for one factor that takes values both below and above the median of the starting factors. Duplicate runs were included in the design to estimate errors, as well as 5 central points to increase the robustness of the model. Pre-trial runs were performed to determine the range of operability of the flow rates of each phase. Responses measured were average diameter, Young's modulus, span and coefficient of variation (CV). Design expert v.11 was used in mathematically generating design points for the study (Table 2.1).

TABLE 2.1 Experimental Runs using Central Composite Design for assessment of disperse and continuous flow rates in determining size and surface modulus of GelMA microparticles.

	Factor 1	**Factor 2**
Run	Disperse phase flow rate	Continuous phase flow rate
	ml/hr	ml/hr
1	5.5	300
2	1	500
3	1	100
4	10	100
5	10	500
6	10	100
7	5.5	300
8	5.5	100
9	10	300
10	5.5	300
11	1	100
12	1	300
13	10	500
14	5.5	300
15	1	500
16	5.5	300
17	5.5	500

2.7 Co-current flow microfluidic simulation

A 2D symmetric simulation was made to evaluate temporal changes on the formation of droplets in the microfluidic system. Finite element method was used to solve computationally the co-flow system, with the laminar flow, level set interface for resolving the two-phase flow regime of the setup. An incompressible formulation of the Navier-Stokes equation was used:

$$\rho\frac{\partial \mathbf{u}}{\partial t} + \rho(\mathbf{u}\cdot\nabla)\mathbf{u} = \nabla\cdot[-p\mathbf{I} + \mu(\nabla\mathbf{u} + \nabla\mathbf{u}^T)] + \mathbf{F} \quad (4.1)$$

$$\nabla\cdot\mathbf{u} = 0 \quad (4.2)$$

Where ρ is the density of the fluid, **u** is the velocity vector, p is the pressure, t is the time, μ is the viscosity of the fluid, and **F** is the sum of the forces acting on the fluid, including the surface tension. On determining the interface between two immiscible fluids, the following equation is also added:

$$\frac{\partial \phi}{\partial t} + \mathbf{u}\cdot\nabla\phi = \gamma\nabla\cdot\left(\varepsilon\nabla\phi - \phi(1-\phi)\frac{\nabla\phi}{|\nabla\phi|}\right) \quad (4.3)$$

Where ϕ is the fluid fraction, γ is the reinitialization parameter, and ε is the interface thickness controlling parameter. Fluid parameters density and viscosity are now redefined as

$$\rho = \rho_1 + (\rho_2 - \rho_1)\phi \quad (4.4)$$

$$\mu = \mu_1 + (\mu_2 - \mu_1)\phi \quad (4.5)$$

In which the subscripts 1 and 2 denote the constant properties of fluid 1 and 2, namely the dispersed phase GelMA and the mineral oil with surfactant. The values reported in Table 2.2 are used for the simulation.

TABLE 2.2 Values of the parameters used in co-flow simulation

Parameter	Value
Inner needle diameter, D_i	0.84 mm
Outer needle diameter, D_0	1.37 mm
$Temp_{GelMA}$ for all parameters	60°C
5% w/v GelMA density, ρ_{1a}	1050 kg/m^3
13% w/v GelMA density, ρ_{1b}	1100 kg/m^3
5% w/v GelMA viscosity, μ_{1a}	5.72 x 10^{-3} Pa.s
13% w/v GelMA viscosity, μ_{1b}	39.983 x 10^{-3} Pa.s
Mineral oil density (with surfactant), ρ_2	850 kg/m^3
Mineral oil viscosity (with surfactant), μ_2	60 x 10^{-3} Pa.s
Liquid-liquid interface surface tension, σ	3 x 10^{-3} N/m
5% w/v GelMA fluid flow rate, Q_{d1}	3 mL/h
13% w/v GelMA fluid flow rate, Q_{d2}	1.5 mL/h
Mineral oil flow rate, Q_c	100 mL/h
Reinitialization parameter, γ	1
Interface thickness controlling parameter, ε	5 x 10^{-5} m

*values obtained for GelMA are similar from gelatin values (Cumper and Alexander, 1952).

Parameters of mineral oil obtained from manufacturer's specification

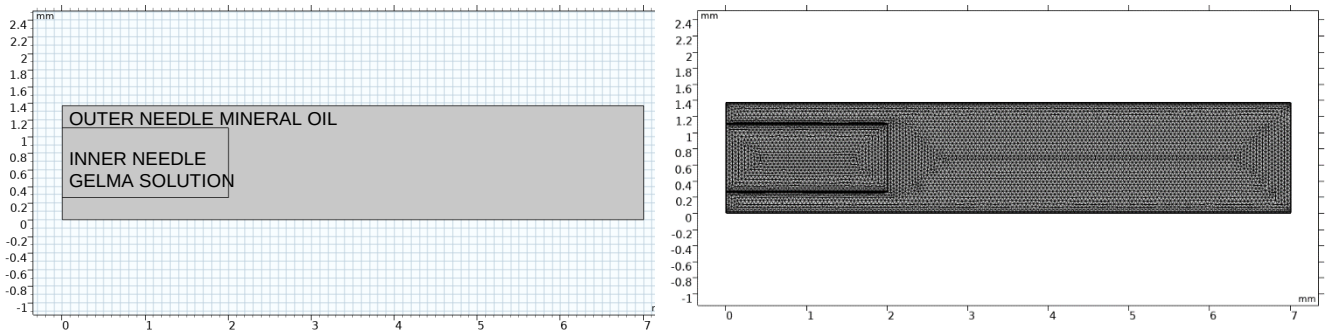


Figure 2.1 Model geometry (left) and the meshed configuration (right), where a free triangular mesh was used. Total degrees of freedom solved for was 25874 (plus 23901 internal DOFs).

On the implementation of the two-phase level set method, the quality of the mesh was increased until the mesh size is independent on the convergent value (Figure 2.1). A two-step approach was made on solving the equations, where a phase initialization step was used prior to on time-dependent simulation to ease computational time and solution stability. The time step made was 0.0001s with total time of 0.5s. The computation was carried out on a workstation with Intel Core i7-6820HQ 2.7 GHz (8 CPUs) with 32.8 GB of DDR4 RAM, using COMSOL Multiphysics as the implementing software. The maximum computational time on the simulation was 4 hours and 37 minutes.

2.8 GelMA microparticle size characterisation

GelMA microparticles were imaged with an optical light microscope (Nikon Eclipse TS 100 inverted microscope, capture unit: Nikon DS-L3) for size and morphology characterisation. For each sample of GelMA microparticles, a volume of 100 µL was inoculated in a 24-well plate in triplicate, and subsequently taking a total of 8 pictures per sample. The software ImageJ with the plugin Fiji was employed for measuring the average diameter, calculated with at least 50

microparticles per batch. To do so, a scalebar at 5X magnification was used to set in ImageJ the Global Length in pixels at 100 µm. Afterwards, lines were manually drawn along the diameter of the individual microparticles and for each the number of pixels was measured as diameter in µm.

To affirm further the size distribution measurements, a laser diffraction particle sizing instrument (Coulter LS 230 instruments, Beckman-Coulter Co., Ltd., UK) was employed. The microvolume sample cell was loaded with 18 mL of dH_2O for calibration and background normalisation, then 1 mL was removed and a suspension of microparticles to be sized was added until the optimal obscuration value (between 8 to 12%) was reached. Readings were taken three times per condition with each run over 60s. Analytical data (mean, median, mode, standard deviation, d10, d50, d90, CV, skewness, kurtosis) was generated by the inbuilt software and directly obtained from the instrument. The polydispersity index of the microparticles was measured in terms of Span factor and Coefficient of Variation, expressed as:

$$Span = \frac{(d_{90} - d_{10})}{d_{50}} \qquad (3.2)$$

$$CV\% = \frac{\sigma}{\mu} \cdot 100\% \qquad (3.3)$$

In (1), d_{90}, d_{10} and d_{50} identify the microparticle diameters at which the volume percent of the distribution fall below 90, 10 and 50, respectively; whereas in (2), σ represents the standard deviation of the sample population and µ represents the mean diameter? of the population. A low Span and CV% indicate a narrow size distribution and a low polydispersity (Dragosavac et al., 2008).

2.9 Characterisation of GelMA microparticle morphology via environmental Scanning Electron Microscope and ion residuals via energy-dispersive x-ray spectroscopy

GelMA microparticle morphology was assessed via environmental Scanning Electron Microscopy (FEI Quanta 650 ESEM, Thermo Scientific, UK). Wet samples were deposited in an

aluminium sample pin, dipped in liquid nitrogen and rapidly inserted into the ESEM chamber on a Peltier plate set at a temperature of -20°C, and sealed under low vacuum of 0.7 Torr to facilitate water sublimation on the microparticle surface. The samples were imaged at 10kV with a minimum of three different magnifications and in three different quadrants where possible.

The energy-dispersive x-ray spectroscopy (eDX) function of the eSEM (ESEM-EDX) was used to highlight the presence of residual magnesium ions from the production of microparticles. A region of interest of approximately 30 × 30 microns was selected in three different microparticle samples, and qualitative and semiquantitative element weight percentage content spectra was obtained.

2.10 Cell culture of mesenchymal stem cells

hTERT immortalised human mesenchymal stem cells (ihMSCs) were kindly provided by Dr James Dixon, generated as described in (Okamoto et al., 2002). ihMSCs were cultured in DMEM (Gibco) supplemented with 10% v/v Fetal Bovine Serum (FBS), 100 U/ml Penicillin, 0.1 mg/ml Streptomycin and 2mM L-Glutamine up to passage 20.

Human primary mesenchymal stem cells (hMSCs) were purchased from Lonza (PT-2501, Lonza, Basel, Switzerland) and cultured in Mesenchymal Stem Cell Growth Medium supplemented with Single Quots (MSCGMTM BulletKitTM, PT-3001, Lonza). The cells were cultured in an incubator at 37°C in a humidified atmosphere with 5% CO2 in air up until passage 4. Cells were obtained from three male donors aged 30 years old. Once sub-confluence was reached, media was aspirated, the cells were washed with PBS and afterwards dissociated with 0.05% v/v trypsin/0.02% w/v (0.53 mM) EDTA for 5 minutes in a humidified incubator at 37°C. A volume of 7 ml of culture media was added to neutralise trypsin, then centrifuged at 200 g for 5 minutes. The supernatant was removed and the cell pellet resuspended in warm media and transferred into new cell culture plates at a 1:6 initial dilution or plated at the density required for the experiments.

2.11 Cryopreservation and resuscitation of cells

Once cells were trypsinised and centrifuged, the supernatant was eliminated and the cells were resuspended at 90% v/v FBS containing 10% v/v DMSO at a density of 5 x 10^5 cells/ml. Aliquots of 1 ml of cell suspension were transferred into a 2 ml cryovial (Fisher Scientific) and cooled by storage in Mr. FrostyTM (Fisher Scientific) at -80°C freezer overnight. The vials were then moved to a storage tank in liquid nitrogen until required.

For cell resuscitation, the vials were withdrawn from the liquid nitrogen tank and soaked in a 37°C water bath until a minimal amount of ice was present. The thawed liquid was pipetted into 5 ml of culture media, centrifuged at 300 xg for 5 minutes, and the supernatant was collected. Cells were resuspended in 1 ml of culture media, plated in a T-175 flask and incubated for further usage.

2.12 Live&Dead assay

Live/Dead staining (Thermo Fisher Ltd. UK) was employed for the assessment of cell viability following culture on the GelMA microparticles. GelMA microparticles of small (≤300 μm), medium (>300 μm; ≤600 μm) and large (>600 μm) diameters in water were distributed in 48 well non-tissue culture treated well plates at a volume of 100 μl to cover the bottom of the wells. These were irradiated under UV light for 10 minutes, and afterwards, the water was replaced with pre-conditioning media, composed of DMEM supplemented with 200 U/ml Penicillin, 0.2 mg/ml Streptomycin and 5 ng/ml of Gibco Amphotericin B to minimise the risk of contamination, and left in the incubator at 37°C overnight. The following day, the media was removed and ihMSCs (passage 20) in fresh media were plated at a density of 2000 cells/cm^2 in wells containing the microparticles and in empty wells of tissue culture treated well plates as a control. On days 1, 4 and 7, cells were washed with PBS and incubated with 350 μl of DMEM containing 2 μM calcein-AM and 4 μM EthD-1 for 15 minutes. Afterwards, cells were imaged under a fluorescence microscope (Leica DM IRB, Leica Microsystems UK) at 5x and 10x magnification. The study was carried out for each condition in duplicate in single-batch experiments, and 3 images were taken from each technical replicate for a total of 6 images per condition. For percent

viability calculation, both live (green) and dead (red) cells in each image were counted in ImageJ, and the number of live cells was divided by the total number of cells. Mean and standard deviation were calculated on the 6 images of each condition.

2.13 Differentiation test of immortalised hMSCs grown on GelMA microparticles by visualisation of ALP and Vinculin expression

ihMSCs were grown on GelMA 13% w/v (93% DS) microparticles deposited on an 8µm mesh (Spectrum Labs™ Woven Filter Nylon, Thermo Fisher Scientific Inc. UK) held in 48-well plate crown inserts and incubated at 37°C. ihMSCs grown on TCP were used as a negative control, and ihMSCs seeded on 13% w/v (93% DS) GelMA discs were used as 2D comparison. At timepoints 7d and 14d, the cells were washed three times with PBS, fixed with 4% w/v PFA 5'-RT, washed three times with PBS for 5'-RT each and permeabilized with 0.3% v/v Triton x-100 in PBS for 10'-RT. The cells are then washed three times with PBS, incubated with blocking buffer containing 1% w/v BSA, 2% v/v Goat Serum in PBS for 1h-RT and subsequently incubated with Alkaline Phosphatase antibody (ab83259, Abcam) and Vinculin antibody (ab130007, Abcam) at 1:100 dilution in 1% w/v BSA in PBS o/n. Cells were then washed three times with PBS and incubated with anti-rabbit (AlexaFluor488 conjugated, A11008, ThermoFisher Scientific, UK) and anti-mouse (AlexaFluor555 conjugated, A21422, ThermoFisher Scientific, UK) secondary antibodies diluted 1:200 for 1h-RT. To visualise the cell nuclei, 100 ng/ml of DAPI are added to the dilution of the secondary antibody. The cells are then washed three times with PBS and imaged with a fluorescence microscope.

2.14 Screening of early lineage markers of primary hMSCs on GelMA flat discs and microparticles

hMSCs were grown on GelMA discs or microparticles at 5% (30% DS), 5% (68% DS), 5% (93% DS), 8% (93% DS) or 13% (93% DS) w/v, placed in 24-well plates and incubated at 37°C. hMSCs grown on empty wells (on TCP) and cultured with MSCGM™ (Lonza) were used as

negative controls, whilst hMSCs cultured with adipo-inductive (Adipogenic Differentiation BulletKit™ Medium, PT-3004, Lonza) or osteo-inductive (Osteogenic Differentiation BulletKit™ Medium, PT-3002, Lonza) differentiation media were used as positive controls. At timepoint 7d, the cells were washed three times with PBS, fixed with 4% w/v PFA 5'-RT, washed three times with PBS for 5'-RT each and permeabilised with 0.3% v/v Triton x-100 in PBS for 10'-RT. The cells are then washed three times with PBS, incubated with blocking buffer containing 1% w/v BSA, 2% v/v Goat Serum in PBS for 1h-RT and subsequently separated in two different subsets, henceforth called Neurogenic-Osteogenic (N-O) array and Myogenic-Adipogenic (M-A) array, that will be immunodecorated separately. N-O arrays were incubated with MAP2b antibody (MA119425, host mouse, Thermo Fisher Scientific Inc. UK) and Osterix antibody (12847664, host rabbit, Thermo Fisher Scientific Inc. UK), at 1:100 dilution in 1% w/v BSA in PBS o/n. M-A arrays were incubated with Myogenin antibody (15838668, host mouse, Thermo Fisher Scientific Inc. UK) and PPARγ antibody (ABN1445, host rabbit, Sigma-Aldrich, Poole, UK), at 1:100 dilution in 1% w/v BSA in PBS o/n. Cells were then washed three times with PBS and incubated with anti-rabbit and anti-mouse secondary antibodies diluted 1:200 for 1h-RT. 100 ng/ml of 4,6-diamidin-2-phenylindole (DAPI) are added to the dilution of the secondary antibody. The cells are then washed three times with PBS and visualised with Super resolution confocal fluorescence microscope (PS1 Super Resolution Microscope, ZEISS, Oberkochen, Gemany).

2.15 Atomic force microscopy

The MFP-3D Standalone Atomic Force Microscope (AFM) (Oxford Instruments, Asylum Research Inc., CA) was used to obtain force-displacement curves of GelMA microparticles for Young's modulus calculation.

The principle of the AFM rests on the cantilever as its key element, using a tip mounted at the outermost side to measure the force applied to the sample surface using spring loading (Vakarelski et al., 2007). A laser beam, reflected from the gold-coated back of the cantilever, is detected by a

position-sensitive photodiode, which measures the position change of the incident laser. The deflection and the movement of the piezo in the Z-direction resulting from the interaction tip-sample are corrected via the following equations for obtaining a Force-Distance (F-D) curve (Cappella and Dietler, 1999):

$$F = k_c Def \qquad (3.4)$$

$$d = Z - Def \qquad (3.5)$$

where F is the tip-sample interaction force as a function of Hooke's law, Def is the cantilever deflection, k_c is the cantilever spring constant, d is the tip-sample distance and Z the piezo displacement. The piezo height must be corrected for the cantilever deflection for proper F-D curve generation and subsequent analysis.

An AFM silicon nitride probe MLCT-C (Bruker Nano Inc., CA) with nominal tip radius of 30 nm, 2.5-8 μm tip height, 7 kHz Resonant Frequency and 0.01 N/m Spring Constant was used (Figure 2.2A). The actual tip base radius, tip height and conical half-angle were calculated via SEM imaging of the probe (Figure 2.2B and 2.2C), with values of 2.32 μm, 2.923 μm and 28.439°, respectively. The tip radius was characterised by measurement of a standard sample, with a value of 32±4 nm. The sharp, pyramidal tip of the cantilever was used to indent the top most surface of GelMA microparticles (a relatively flat surface) in order to gather the elastic recoil of the material, which is then registered by the instrument as a change of laser deflection. To increase the level of accuracy when measuring the porous hydrogel structure of GelMA samples (Galluzzi et al., 2016), which was essential to evaluate the exact range of elasticity shown by the microparticles for the cell experiments, a polystyrene microparticle of 20 μm of diameter was glued onto the tip of the cantilever (Figure 2.2D). The higher surface area of the colloidal beads would increase the contact area on the GelMA microparticle, producing a smoother and wider elastic recoil of its surface, thus providing a better understanding of its modulus.

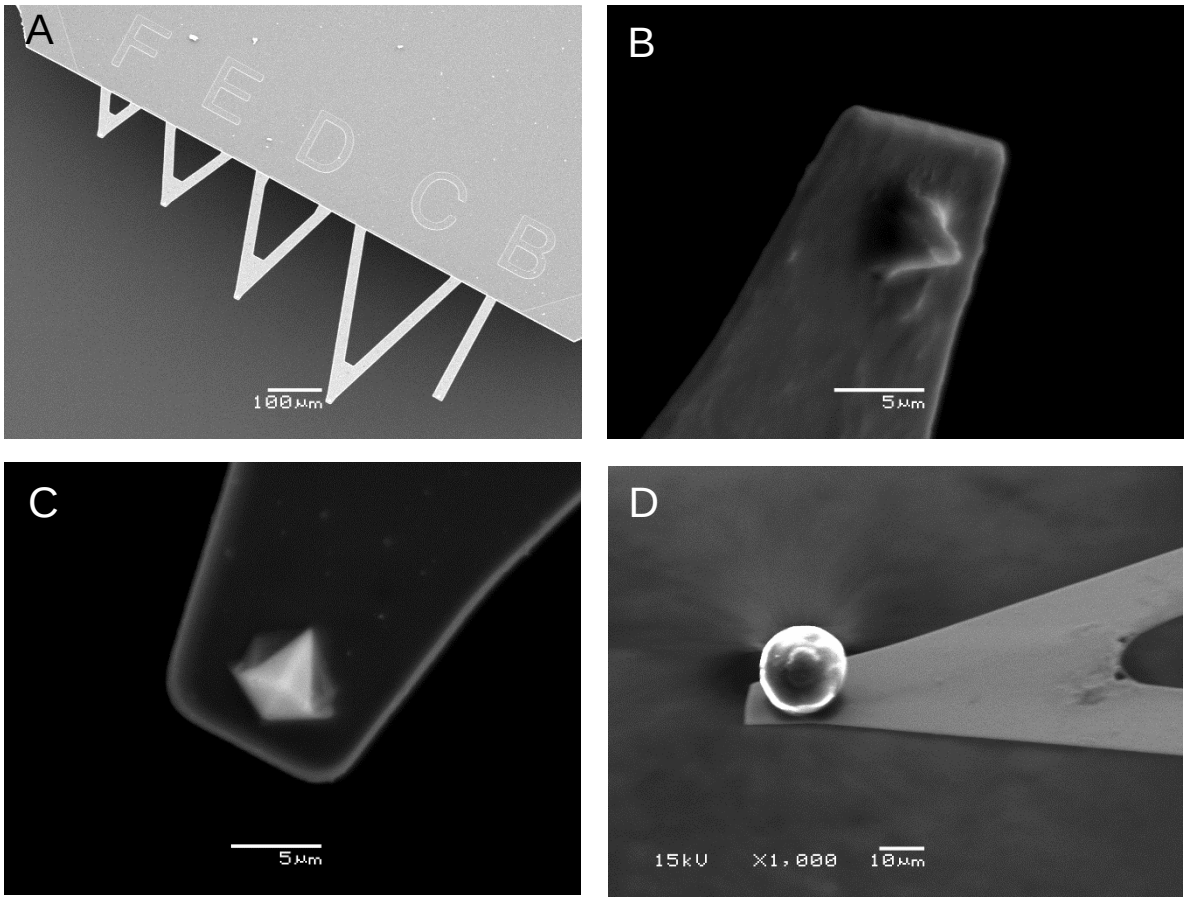


Figure 2.2 (A) Silicon nitride MLCT cantilevers, of which the cantilever C was used; (B-C) Rotated (pyramidal) tip of cantilever C. (D) 20µm diameter polystyrene microparticle attached to MLCT-C tip. Images were generated via SEM.

2.16 Atomic force microscopy: Young's modulus calculation with the Derjaguin-Muller-Toporov model

Young's modulus (E) was extracted from the uppermost part of the retracting curve using an appropriate mathematical model. The one used in this study was the Derjaguin-Muller-Toporov (DMT) spherical model (Derjaguin et al., 1975) (Figure 2.3). The advantages of this method are the inclusion in its equation of the attractive interaction forces of the sample surface towards the tip as an increase of F value, plus the area of contact defined by the tip-sample indentation.

The model predicts the shape of the retracting curve in order to fit it with the slope of the raw curve, using the ordinary least squares method. This generates a fitted F-D curve that displays the elastic behaviour of the material as the surface is displaced, i.e. deformed by the increasing force of the tip. The fitting process is done by solving the following four equations (Ha et al., 2004), correlating the contact radius (a), the adhesion force (F_{ad}), the indentation depth (δ) and the tip-sample distance (d) (3), in order to obtain E:

$$a = \sqrt[3]{\frac{R}{E}(F + 2\pi Rw)} \qquad (3.6)$$

$$\delta = \frac{a^2}{R} - \frac{2}{3}\sqrt{\frac{6\pi wa}{E}} \qquad (3.7)$$

$$F_{ad} = 2\pi Rw \qquad (3.8)$$

$$F = -\frac{2\pi Rw}{(1-\frac{d}{d_0})^2} \qquad (3.9)$$

where R is the tip spherical radius, F is the tip-sample interaction force, w is the surface energy and d_0 is the starting tip-sample distance. The equations are effectively solved by dedicated software on the basis of the raw data of Def and Z. For a more accurate analysis, the manufacturer specifications of the tip, including height, radius and front, back and side angles, are required.

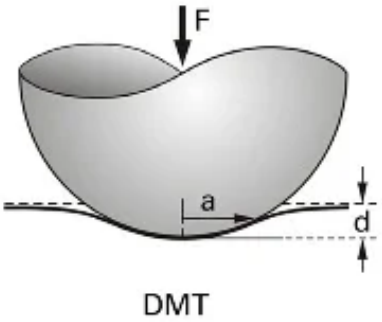


Figure 2.3 DMT model contact mechanics in AFM. The applied force (F) causes an indentation (d) that develops on the substrate in response to a non-deformable sphere with a contact area (a) closely related to the sphere radius. Figure reproduced from *azonano.com*, accessed 02/03/21.

2.17 Atomic force microscopy sample preparation and analysis

GelMA microparticle samples produced were prepared for AFM analysis. Microparticles were bonded to glass coverslips prior to AFM measurements, following a similar protocol to Nguyen *et al.*, (2015). Coverslips were incubated with 1% w/v (3-aminopropyl)-trimethoxysilane (APTMS) in absolute ethanol for 2 hours at room temperature under agitation for functionalisation with amine groups. Afterwards, they were washed with deionised water to remove excess APTMS. Microparticles were incubated with 2 mM 1-Ethyl-3-[3-dimethylaminopropyl]carbodiimide hydrochloride (EDC) and 5 mM N-hydroxylsulfosuccinimide (sNHS) in 0.1 M 2-(N-morpholino)ethanesulfonic acid (MES) activation buffer for 15 minutes, and subsequently quenched with 1.4 μL of 2-mercaptoethanol. Each MP sample was centrifuged to remove activation buffer, resuspended in PBS, incubated on a coverslip for 2 hours at room temperature and washed with PBS and placed in a plastic Petri dish in PBS before mechanical characterisation.

Samples were tested in deionised water at room temperature for force measurements. Before each series of measurements, instrument sensitivity was calibrated with the unloading curve slope of an F-Z curve of glass alone, whilst instrument thermal fluctuations were used to extract the effective spring constant of the tip, inherent to its resonant frequency. This was necessary since the difference between the nominal and effective k_c can be up to 100% (Notbohm et al., 2012). For each measurement of the sample, at least 100 F-Z curves were recorded. Acquired Deflection and Z-sensor points were converted into .txt files by the subroutine provided in the associated MPF3D-AFM software and processed in the Excel environment by the DMT model to fit the retracting curve and calculate E.

A blend of Polystyrene and Polyolefin Elastomer with nominal E of 100 MPa (PS-LDPE-12M, Veeco, CA) was used as standard for tip radius identification and accuracy assessment of the AFM. The analysis was carried out by adjusting the instrument Deflection Set-point, which defines the contact force of the tip on the sample, until the calculated E is in the order of magnitude of the nominal one. To increase the accuracy of the calculation, the nominal value of the tip radius was

manually adjusted in the software settings until the calculated E was close to the nominal value. This provided a good level of confidence concerning the characteristics of the tip and force load for the subsequent analysis.

2.18 Image analysis via Ilastik and CellProfiler

A pipeline of the image analysis process is presented in Figure 2.4. Raw images generated as discussed in section 2.14 were pre-processed in ImageJ with the plugin Fiji. Using the functions Process>Subtract Background and Image>Adjust Brightness/Contrast, the excessive background signal was removed and the fluorescent signal made sharper respectively. Afterwards, the three channels composing the images (blue channel: nuclei; green channel: AlexaFluor488; red channel: AlexaFluor555) were split to be processed separately for the subsequent image analysis.

The software Ilastik (Berg et al., 2019) was applied to facilitate the identification of signals amidst the strong autofluorescence of the GelMA hydrogels and discriminate between non-cellular features. To do so, the split channels were loaded in the software and the pixels as either belonging to the cell or background were annotated through its labelling feature. With these annotations, the program can then compute pixel features based on edge and texture filters. These filters include Gaussian Smoothing, Laplacian of Gaussian, Gaussian Gradient Magnitude, difference of Gaussian, Structure Tensor Eigenvalues, and Hessian of Gaussian Eigenvalues. (Sommer, Straehle, Kothe, & Hamprecht, 2011). Ilastik then applies a convolution process to produce probability masks, which are the result of the segmentation of positive signals to either nucleus (blue channel), fluorescent green (green channel) and fluorescent red (red channel) signals. These probability masks (which now represent a clearer localisation of the actual signals) are then processed in CellProfiler (McQuin et al., 2018) in order to identify the hMSCs nuclei (blue channel) as the primary object and localise around them the positive signal from the cytoplasmic marker of differentiation as the secondary object (green or red channels). Finally, the cells showing markers were counted and rendered as a percentage of positives against the total number of cells. A total of 120 images per marker pair (N-O & M-A, N = 3; n = 2) were analysed.

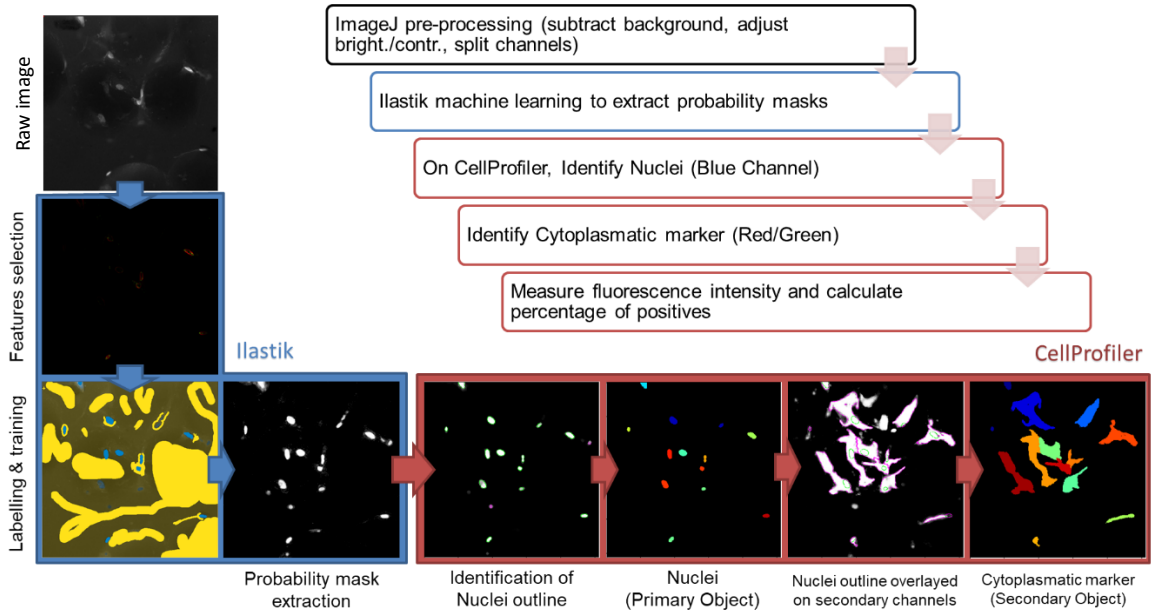


Figure 2.4 Pipeline of the image analysis of hMSCs showing positive signal to the marker screening. The raw image as taken by the microscope is first pre-processed with ImageJ for clearing up the image of background, then rendered through Ilastik machine learning training to recognise eligible pixels and batch processing to extract probability masks showing the signal of interest. The probability mask is then listed in the CellProfiler software for image segmentation and counting of positives to evaluate the percentage of marker positive cells.

2.19 Statistical Analysis

The experimental data for the different studies are expressed as the mean ± standard deviation (SD), the error bars on the figures were calculated from the standard deviation of the mean. All experiments were carried out in triplicate. The mean and SD of each experiment were calculated using statistical Microsoft Excel® 2013 and GraphPad Prism (version 9.0) software. One way ANOVA was used with Tukey's post-hoc test to assess differences in means, in which p-values less than 0.05 were considered significant.

3. PRODUCTION, MECHANICAL CHARACTERISATION AND BIOCOMPATIBILITY OF GELATIN METHACRYLATE MICROPARTICLES FABRICATED VIA A CO-CURRENT FLOW CAPILLARY SYSTEM

3.1 Introduction

The use of hydrogel-based microparticles (MPs) has been explored in multiple instances over the past two decades (Daly et al., 2020). Hydrogel MPs have a wide range of uses in biomedicine, from cell and drug transport to the creation of scaffolds for tissue healing and bioinks for 3D printing (Daly et al., 2020; Lu et al., 2015). A number of manufacturing procedures, such as batch emulsion, microfluidics, lithography, electrohydrodynamic spraying and mechanical fragmentation, can be used to encapsulate biological material (cells and drugs) into MPs of predetermined shapes and sizes (Contessi Negrini et al., 2020; Custódio et al., 2014; Daly et al., 2020). Hydrogel MPs can be made as suspensions to deliver medicines, as granular hydrogels to build microporous scaffolds that encourage cell infiltration, or embedded within a bulk hydrogel to achieve multiscale behaviour.

Gelatin MPs have been widely researched for their ability for a variety of applications, including deliver of growth factors to induce angiogenesis (Zhao et al., 2011), cartilage TE (Holland et al., 2005), stem cell differentiation within scaffolds (Ogawa et al., 2010) or within aggregates (Bratt-Leal et al., 2011; Solorio et al., 2012). Gelatin MPs are commonly made by creating a water-in-oil emulsion and then cross-linking with reagents such as glutaraldehyde (GA) (Holland et al., 2005; Patel et al., 2008), genipin (Solorio et al., 2012), or carbodiimides (Liang et al., 2004). Even though is the most common method of collagen-based materials crosslinking, the major caveats of GA use is a narrow crosslinking range that rarely comprises a 60% degree of crosslinking and below, as well as difficulty in accurately predicting crosslinking *a priori* (Bigi et al., 2001; Sung et al., 1999; Tomihata and Ikada, 1996). Additionally, GA itself is cytotoxic and can cause

calcification and inflammation *in vivo* (Bigi et al., 2001; Sung et al., 1999). Genipin has been shown to be a viable alternative to GA, as it has comparable crosslinking mechanical properties and is far less toxic (Cheng et al., 2013; Pinheiro et al., 2016), however its use can be very expensive. Moreover, genipin/protein crosslinking often leads to the formation of dark blue pigment, thus limiting its applications for biomaterial purposes (Zhao and Sun, 2017).

Conversely, gelatin methacrylation has been shown to be less cytotoxic and to allow for a wider variety of cross-linking density (Hoch et al., 2012). Glycidyl methacrylate (GyMA), methacryloyl chloride (MC), or methacrylic anhydride (MA) can be used to replace amino groups on gelatin (Hoch et al., 2012; Nichol et al., 2010). The methacrylate groups on GelMA restrict the maximum cross-linking density achievable compared to glutaraldehyde, genipin, or dehydrothermal cross-linking. In particular, MA-mediated substation affords greater control over hydrogel cross-linking density as it is independent by the presence of soluble factors or experimental conditions, such as time and temperature of crosslinking, which are difficult to control (Hoch et al., 2012; Nichol et al., 2010). The use of GelMA MPs in several applications has been explored, such as controlled release of growth factors such as recombinant human BMP-4 or FGF-2 (Nguyen et al., 2015), use of composite calcium carbonate/GelMA MPs for 3d cell culture in bone TE (Xu et al., 2020) and 3D bioprinted Chitosan/GelMA MPs as a modular bioink for enhancing 3D neurite outgrowth and elongation (Chen et al., 2020).

One of the most successful approaches for the production of GelMA MPs in a reproducible way and narrow size distribution is microfluidics (Utada et al., 2005). Different attempts have been explored for either gelatin-based MPs (Park et al., 2016) and GelMA (Suvarnapathaki et al., 2018; Zhao et al., 2021) using mainly flow focusing devices. However, from a process scalability perspective, the flow speed as achieved by traditional systems are usually low, on the scale of 30–80 µL/min (Suvarnapathaki et al., 2018). Furthermore, the gelation properties complicate the droplet formation process as the solution tends to clog the microfluidic capillaries at room temperature (Suvarnapathaki et al., 2018; Wang et al., 2017).

To overcome this problem, one possibility is to exploit a material other than glass or plastic for the microfluidic chip which can withstand pressures higher than 14 psi (Suvarnapathaki et al., 2018), such as steel capillaries, in order to sustain increased flow rates and mobilise the disperse phase quicker. Secondly, steel is a good thermal conductor which allows to use heating belts to maintain temperatures higher than the room temperature to prevent gelation of the disperse phase even at high polymer concentration (Park et al., 2016; Suvarnapathaki et al., 2018). This allows to increment remarkedly the amount of solution travelling in the capillary and as such the mass of produced MPs per hour. Also, adding a cooling step at the end of the droplet formation process (Park et al., 2016), eases their gelation, prevents their coalescence and thus makes the crosslinking process under UV light more reliable.

Based on these assumptions, this chapter of the thesis focused on the development of a custom microfluidic device that utilises co-current flow dynamics. The concept was prompted by the possibility of finely controlling the polydispersity of fabricated microparticles in terms of size, as well as increasing the overall quantity per hour as compared to traditional methods. It has been shown that by varying the flow rates of continuous and disperse phases in a microfluidic system, it is possible to modify the size of the microparticles in a precise, reproducible and monodisperse manner (Dragosavac et al., 2008; Vladisavljević et al., 2014). Moreover, a correlation between particle diameter and surface Young's Modulus has been observed (Guo et al., 2014; Hashmi and Dufresne, 2009; Promkotra and Kangsadan, 2013), although most of the studies were conducted on the nanometre scale, whilst few at the present knowledge have studied the same effects at the micrometre scale. In this regard, it is hypothesised that size affects the modulus of the microparticles, and the said properties affect immortalised human mesenchymal stem cells (ihMSCs) growth and proliferation. The confirmation of the hypothesis will signify the realisation of a reliable process for the production of monodisperse hydrogel microparticles with controllable elastic properties as a platform for future experiments designed to assess their influence, and therefore the ability to control, on hMSCs behaviour and differentiation *in vitro*.

3.2 Results

3.2.1 Simulation of co-current flow production of GelMA microparticles

Simulation of GelMA microparticle production was carried out to evaluate *in silico* the performance of the two most used oil continuous phases in droplet formation, namely corn seed oil and mineral oil. The velocity profile observed a parabolic laminar flow as expected, where initial ejections normalised into steady-state conditions after 0.0013s for 5% w/v and 0.001s for 13% w/v GelMA solution (Figure 3.1B and D). The highest ejection velocity achieved from the annulus was at about 7.5 m/s for the 5% w/v and 8 m/s for the 13% w/v GelMA (Figure 3.1A and C). For the centreline velocity, a single value of 3.1 m/s was achieved for 5% w/v and 13% w/v GelMA respectively.

As observed also experimentally, there is the intermittent formation of tailings in the co-current flow system (Figure 3.2). This two-phase flow regime is due to the Plateau-Raleigh instability of the setup, where droplet breakup is axisymmetric in certain periods that results in tailings. The unwanted crosslinked tailings were reduced in numbers due to filtration using a predefined mesh as a collector.

Given the overall performance of the mineral oil, which stabilises the droplet formation rate as the laminar flow is achieved as compared to the corn seed oil, it was chosen as the constituent of the continuous phase for the next experimental steps.

A

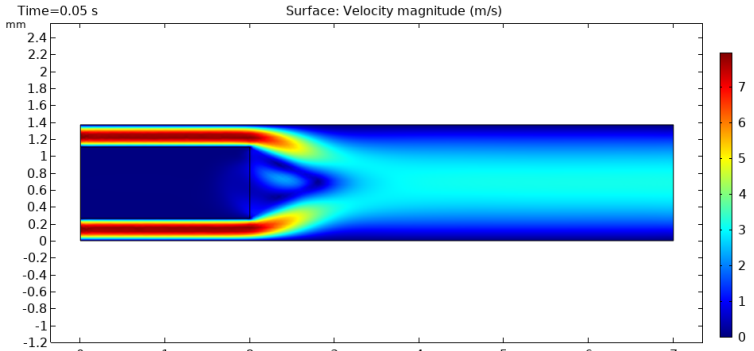


Figure 3.1 Velocity plots of the microfluidic system with 5% w/v (a) and 13% w/v (d) GelMA solutions. The 2D plots are accompanied by a 1D plot which is obtained from the solutions in a cut line at (5.5, 0) and (5.5, 1.4), where time-dependent velocity profiles are shown as a function of arc length. Q_{d1} = 1.5 mL/h, Q_{d2} = 3 mL/h, and Q_c = 100 mL/h.

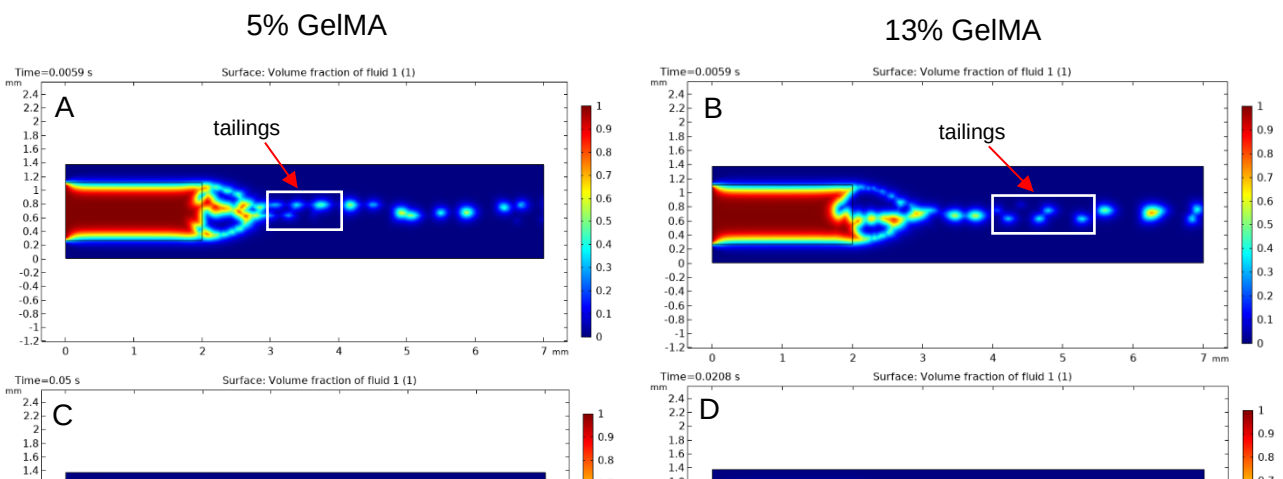


Figure 3.2 Droplet formation regime of 5% w/v and 13% w/v GelMA solutions. Plot shows tailing (A) and (B) regime and a steady, consistent droplet formation (C) and (D). 1D plot of arc length vs volume fraction (E) and (F) show inconsistent volume fractions at predefined arc length (measured at (3.5, 0.7) and (4.5, 0.7) of the 2D plot), indicative of tailing flow regime.

3.2.2 GelMA microparticle size characterisation

Following the Design of Experiment, as stated in section 2.6, GelMA microparticles were produced and characterised as listed under Table 3.1. Varying responses were obtained by simply tuning the dispersed and continuous phase, where the diameters ranged from 170-758 µm, with a coefficient of variation and span range of 7.22-19.86% and 0.14-0.40 respectively. It is noteworthy to mention that 8 out of 17 runs were in the IUPAC range of monodispersity (CV values of ~10% or lower). A wide range of surface modulus could be obtained from 26.3-130.2 kPa. The use of a heating band and the addition of magnesium chloride as a chaotropic agent (Moelbert et al., 2004) in the solution were deemed necessary to further reduce the viscosity of the GelMA solution and to avoid gelation prior to microparticle formation. Important data that can be deduced is the low Span and CV% obtained through this method, as the produced microparticles are very similar in size (Figure 3.3A). This has been confirmed by the DLS analysis, of which representative size distribution plots are reported in Figure S2.

TABLE 3.1 Data obtained from the experimental runs examining the effect of flow rates in determining the responses of diameter, surface modulus, Span and CV% of GelMA microparticles.

	Factor 1	**Factor 2**	**Response 1**	**Response 2**	**Response 3**	**Response 4**
Run	DP flow rate	CP flow rate	Diameter	Surface Young's modulus	Span $\frac{d_{90}-d_{10}}{d_{50}}$	CV $\frac{\sigma}{\bar{x}}\cdot 100$
	ml/hr	ml/hr	µm	kPa		%
1	1	100	427±30	87.7±19.9	0.171345	7.22777
2	1	100	404±45	42.9±33.2	0.16806	11.2333
3	1	300	203±30	90.3±15.7	0.341803	14.6025
4	1	500	215±16	76.3±37.6	0.182793	7.3859
5	1	500	170±15	130.2±13.1	0.213626	8.65106
6	5.5	100	755±77	26.3±9.3	0.292162	10.1755
7	5.5	300	650±33	30.7±15.2	0.146716	11.5594
8	5.5	300	559±43	82.2±9.1	0.180848	7.62989
9	5.5	300	606±56	70.6±16.4	0.202056	9.17018
10	5.5	300	532±102	59.3±18.8	0.248219	19.2659
11	5.5	300	492±59	69.9±16.3	0.284859	12.0794
12	5.5	500	441±74	87.4±10.9	0.40079	16.7253
13	10	100	703±91	43.1±20.7	0.341493	19.8582
14	10	100	752±86	45.9±8	0.313683	11.4329
15	10	300	758±67	50.3±31.6	0.213679	8.81336
16	10	500	546±52	60.7±18.3	0.237789	9.55687
17	10	500	462±83	59.3±19.7	0.272053	17.9909

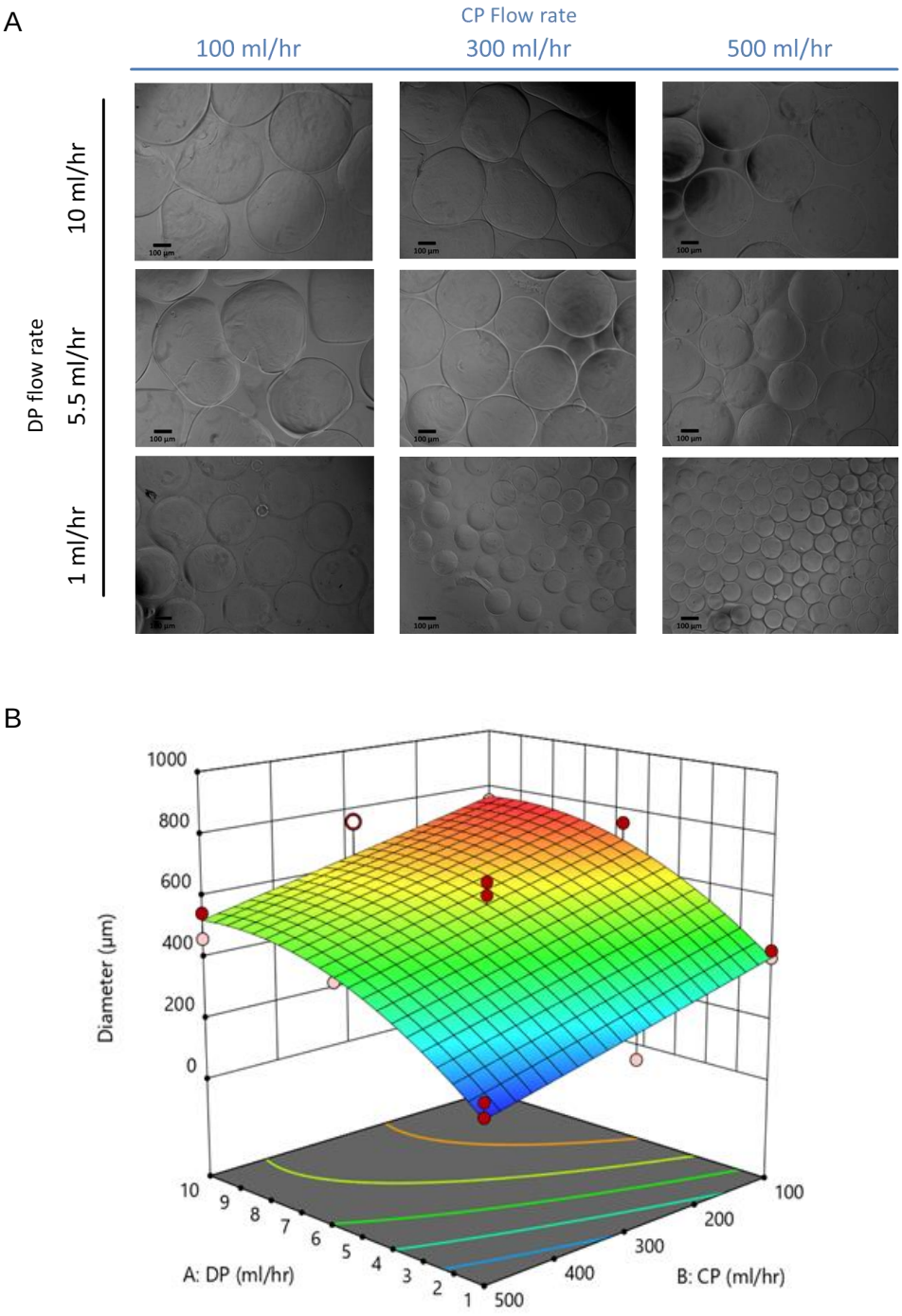


Figure 3.3 (A) Microparticles imaged under optical microscope; (B) Surface plot of the diameter response with respect to the disperse phase (DP) and continuous phase (CP) flow rates. The graph shows the direct proportionality between DP flow rate and diameter and the inverse proportionality between CP flow rate and diameter. Red dots are the experimental values, in which a surface function is fitted.

Microparticles were categorised in terms of size in small (≤300 μm), medium (>300 μm; ≤600 μm) and large (>600 μm) for subsequent experiments. Furthermore, it was revealed that when the ratio of continuous to disperse phase flow rates increases, the diameter of the microparticles tends to decrease (Figure 3.3B). This is related to the fact that decreasing the disperse phase flow rate will reduce the amount of polymer released as a droplet in a given time, whilst increasing the continuous phase flow rate will augment the shear dragging force necessary to break up the disperse phase into droplets, following Rayleigh instability (Mansard et al., 2016; Vladisavljević et al., 2014). The interaction of the two variables was further studied in a mathematical fitting with a quadratic function to evaluate how predictive this method is in producing microparticles of a pre-determined size. The model fitting in terms of the response "diameter" is shown in Table S1, where in particular the model F-value and p-value show statistical significance in the response prediction. As shown also in Table S2, the model fitting reaches a predicted R^2 of 0.8382, which is in reasonable agreement with the Adjusted R^2 of 0.8831. Figure S3A shows the correlation between Predicted and Actual values, which is confirmed also by the first-order interaction plot in Figure S3B. Through modelling, the interaction between factors generated an empirical equation to predict the size by calculating the required flow rates:

$$d = 369.336 + 101.09 \cdot Q_{DP} - 0.602 \cdot Q_{CP} - 5.547 \cdot {Q^2}_{DP} \qquad (4.8)$$

Where d is the microparticle diameter, Q_{DP} the disperse phase flow rate and Q_{CP} the continuous phase flow rate.

3.2.3 GelMA microparticle structure characterisation

GelMA microparticles were imaged using eSEM to reveal their surface structure. Initial tests with conventional SEM led to microparticle flattening, probably caused by the sudden escape of water under vacuum conditions. This same phenomenon happened in the eSEM chamber even with humidity at 80%, therefore a protocol involving snap freezing in liquid nitrogen was adopted to preserve the microparticle structure even after water sublimation in low vacuum conditions. The results are shown in Figure 3.4A.

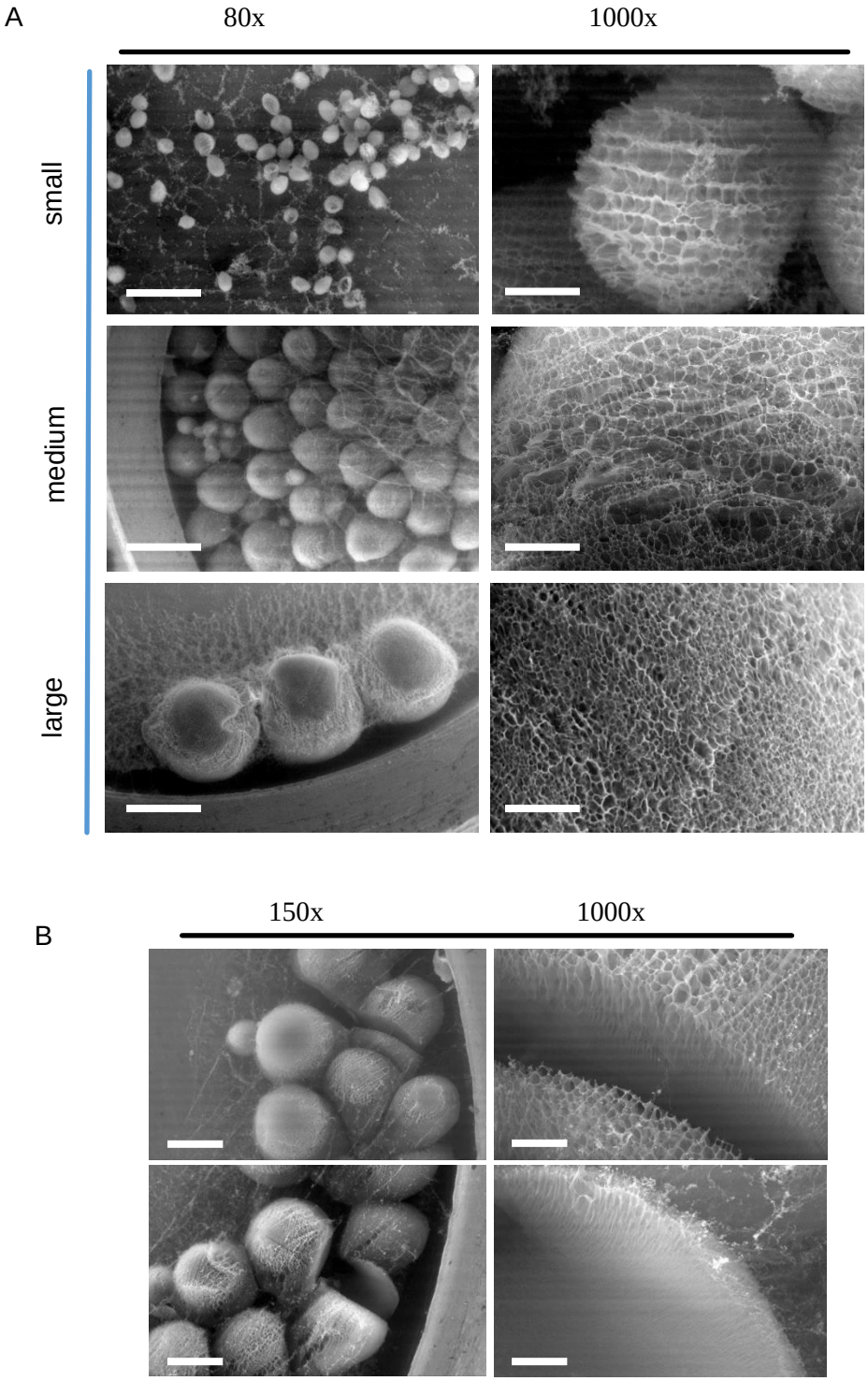


Figure 3.4 (A) Representative eSEM images of GelMA microparticles at small, medium and large diameter ranges. The porous surface structure is revealed after water sublimation at low pressure. Scale bar, left column = 500 μm; right column = 40 μm. (B) Representative eSEM images of GelMA microparticles of medium diameter range, showing an internally porous structure. Alignment is seen on the wall pores tangent to the surface, indicating a vertical alignment from the core to the surface. Scale bar, left column = 200 μm; right column = 40 μm.

After the snap freezing, the microparticles assumed a tear-shaped structure. This is likely due to the quick sublimation of ice under vacuum in eSEM. Interestingly, the surface of the microparticles displayed a larger and more ordered pore structure as the microparticle size decreases. This might be reflected by the way the polymer chains of GelMA stack together, as in small diameter microparticles they require less time to align in ordered layers before being fixed in position by the crosslinking reaction. The core structure was also revealed, showing how these porous structures were organized after crosslinking (Figure 3.4B). To confirm if any impurities are present in the final product that might affect cell culture, as is the case for magnesium cations which exhibits osteo-inducing effects on MSCs differentiation (Qi et al., 2021), edX analysis was carried out during eSEM imaging (Figure 3.5). The spectra of the total atomic content in terms of weight percentage displayed an average of 0.6% content of magnesium.

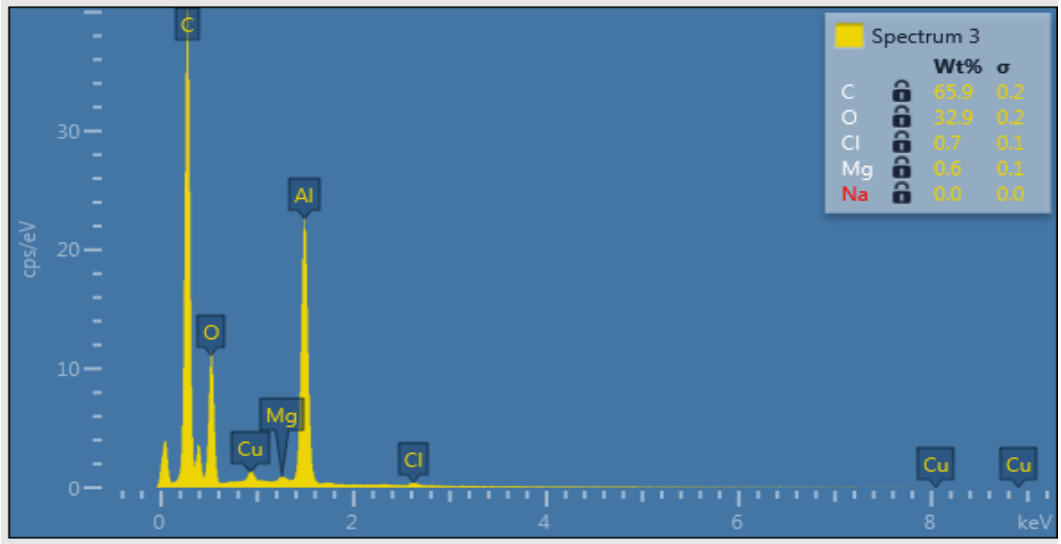


Figure 3.5 eDX spectra of GelMA microparticle spectra (image is a representative of three samples taken).

Assuming a total volume of $V = \frac{4}{3}\pi\left({}^{\sim 250}/_{2}\right)^{3} = 8.18 \cdot 10^{-6} cm^{3}$ per microparticle, multiplied by the density of GelMA (1.6 g/cm^3), one microparticle overall weight is $1.31 \cdot 10^{-5}\ g$. Considering thus magnesium content to be 0.6%, Mg weight in a microparticle is $7.85 \cdot 10^{-8}\ g$, or: $mol = \frac{7.85 \cdot 10^{-8}\ g}{24.305\ {}^{g}/_{mol}} = 3.23 \cdot 10^{-9} mol$. Assuming a total of 1 ml of occupied space, the concentration of magnesium in a microparticle sample would be ${}^{3.23 \cdot 10^{-9} mol}/_{0.001\ l} = 3.23 \cdot 10^{-3} mM$, which is lower than the concentration of magnesium (in the form of magnesium sulphate $MgSO_4$) in DMEM medium (0.81 mM) and negligible when compared to the minimum required to exert induction of osteogenesis (5mM) (Yoshizawa et al., 2014).

3.2.4 GelMA microparticle surface modulus characterisation

GelMA microparticles were lastly characterised via AFM to assess how the surface modulus of the microparticle varies in response to a change in the microparticle diameter. Values for each experimental run are reported in Table 2.1. The analysis of the Force-Displacement curves, when grouping the runs in terms of microparticle sizes (Figure 3.6A) suggests that the size of the microparticles and the degree of deformation follow an inverse proportionality to the modulus towards the diameter (Figure 3.6B). Clustering the microparticle sizes in terms of small (≤300 μm), medium (>300 μm; ≤600 μm) and large (>600 μm) diameters show a significant intra-batch difference between the samples (Figure 3.6C). These results might be explained by the porous structure the GelMA microparticles assume, which becomes more ordered as the microparticle diameter decreases. It could be that the more compacted, homogenously distributed array of pores better transmit the indenting force on the structure, resulting in a higher surface stiffness.

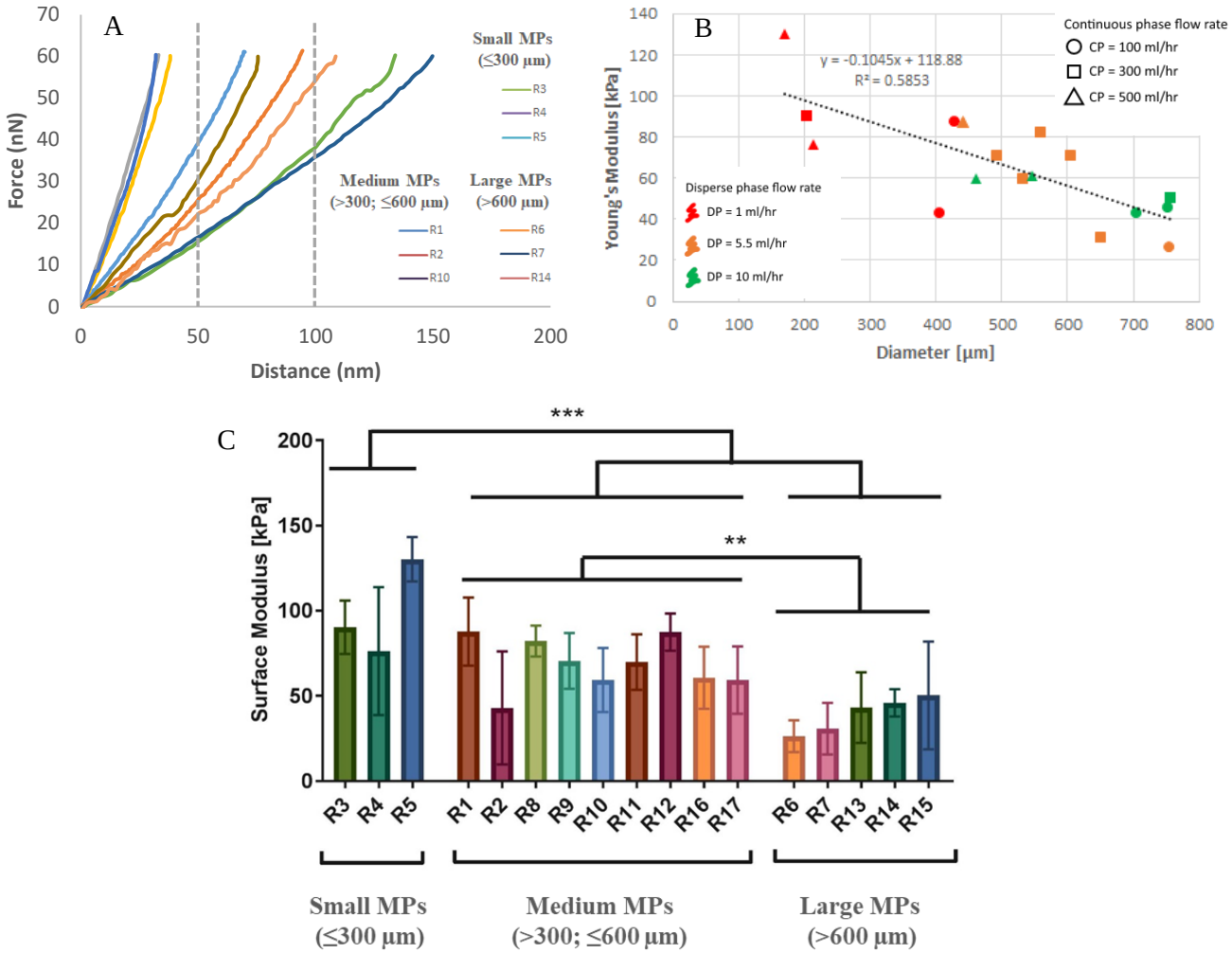


Figure 3.6 (A) F-D curves of representative experimental runs (R), showing the different degree of deformation for small, medium and large microparticle diameters; (B) Scatter plot of microparticle diameter versus Young's modulus. The graph shows the inverse correlation equation between the two responses. (C) Histogram plot of Young's modulus values for each experimental run in water. Error bars indicate the standard deviation of the mean, calculated on 100 points per each sample (n=5). Statistical significance calculated via two-way ANOVA at 5% significance level (**: $p<0.01$, ***: $p<0.001$).

A further point of interest was linking the flow rates of the two phases with surface Young's modulus, as an indirect cause of the effect of microparticle size. The aim was to outline a model that could predict the elastic modulus from the manufacturing process settings. The data were well fit using a linear function, which F-value and p-value are significant as shown in Table S3, whilst the R^2 values in Table S4 suggest that the values predicted by the model are in reasonable agreement with the experimental values, as displayed also in the correlation and factors interaction scatter plots, defining an inverse proportionality between the two factors (Figure S5).

The microparticles' Young's modulus has been plotted against CP and DP in (Figure 3.7), which shows that Young's modulus can be controlled using the relative flow rates using Equation 4.9.

$$E = 60.91 - 3.737 \cdot Q_{DP} + 0.084 \cdot Q_{CP} \qquad (4.9)$$

Where E is the microparticle Young's modulus, Q_{DP} the disperse phase flow rate and Q_{CP} the continuous phase flow rate.

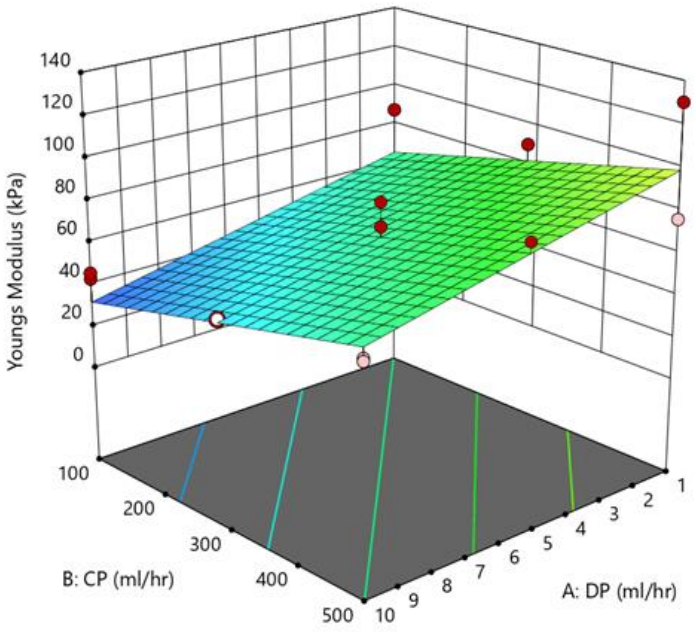


Figure 3.7 Surface plots of surface Young's modulus response with respect to the disperse phase (DP) and continuous phase (CP) flow rates. Considering the inverse proportionality between surface Young's modulus and the microparticle size, the effect of the DP flow rate is inversely proportional and the effect of CP flow rate is directly proportional.

3.2.5 Cell viability

The assessment of ihMSCs viability on GelMA microparticles was performed to evaluate the biocompatibility of the material. After 7 days, the viability of the cells was maintained at approximately 80% except for those adhering to the large microparticles which by day 7 reached 73% viability (Figure 3.8).

Tethering density of the ligands can affect the rate of proliferation of a cell (Cavalcanti-Adam et al., 2007; Engler et al., 2006; Fischer et al., 2007), therefore it is plausible that large

microparticles, displaying a high number of large pores, could also show the increased distance between the RGD domains and thus reduced instances of cell attachment and survival (Figure 3.9). Additionally, the stiffness of the material can also influence the viability, as previously reported by Tse and Engler (2011), where they showed that MSCs grown on hydrogels having physiological stiffness gradients tend to accumulate onto stiffer hydrogel regions assuming a spindle-like morphology and increased contractility, denoting a myogenic commitment, whilst on low stiffness areas they are less proliferative and express the neural marker β3 tubulin. In conclusion, the coupling effects of ligand density and substrate stiffness could have a compounding effect with regards to the overall viability of the ihMSCs.

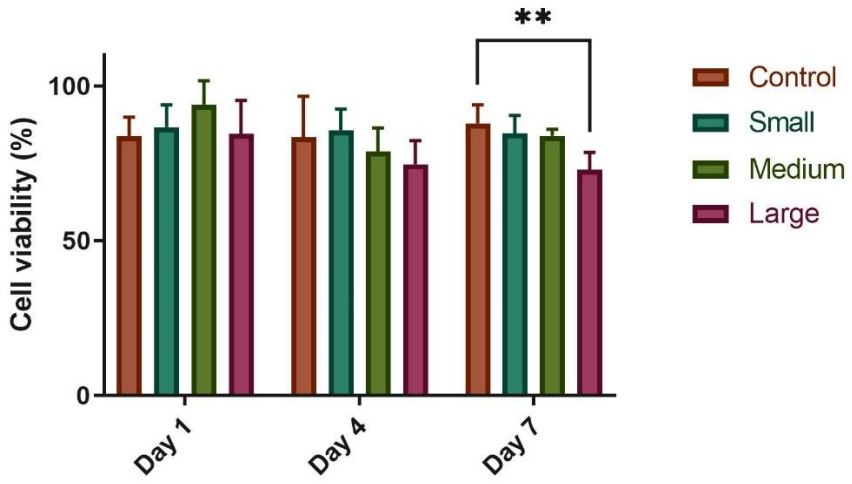


Figure 3.8 Histogram plot of percent cell viability obtained as ratio of live cells per total cell number for small (≤300 μm, teal), medium (>300 μm; ≤600 μm, green) and large (>600 μm, purple) microparticles on days 1, 4 and 7. The number. Error bars indicate the standard deviation of the mean, calculated from 6 images per each condition, evaluating the number of live cells divided by the total number of cells. Statistical significance calculated via two-way ANOVA at 5% significance level (**: $p<0.01$)

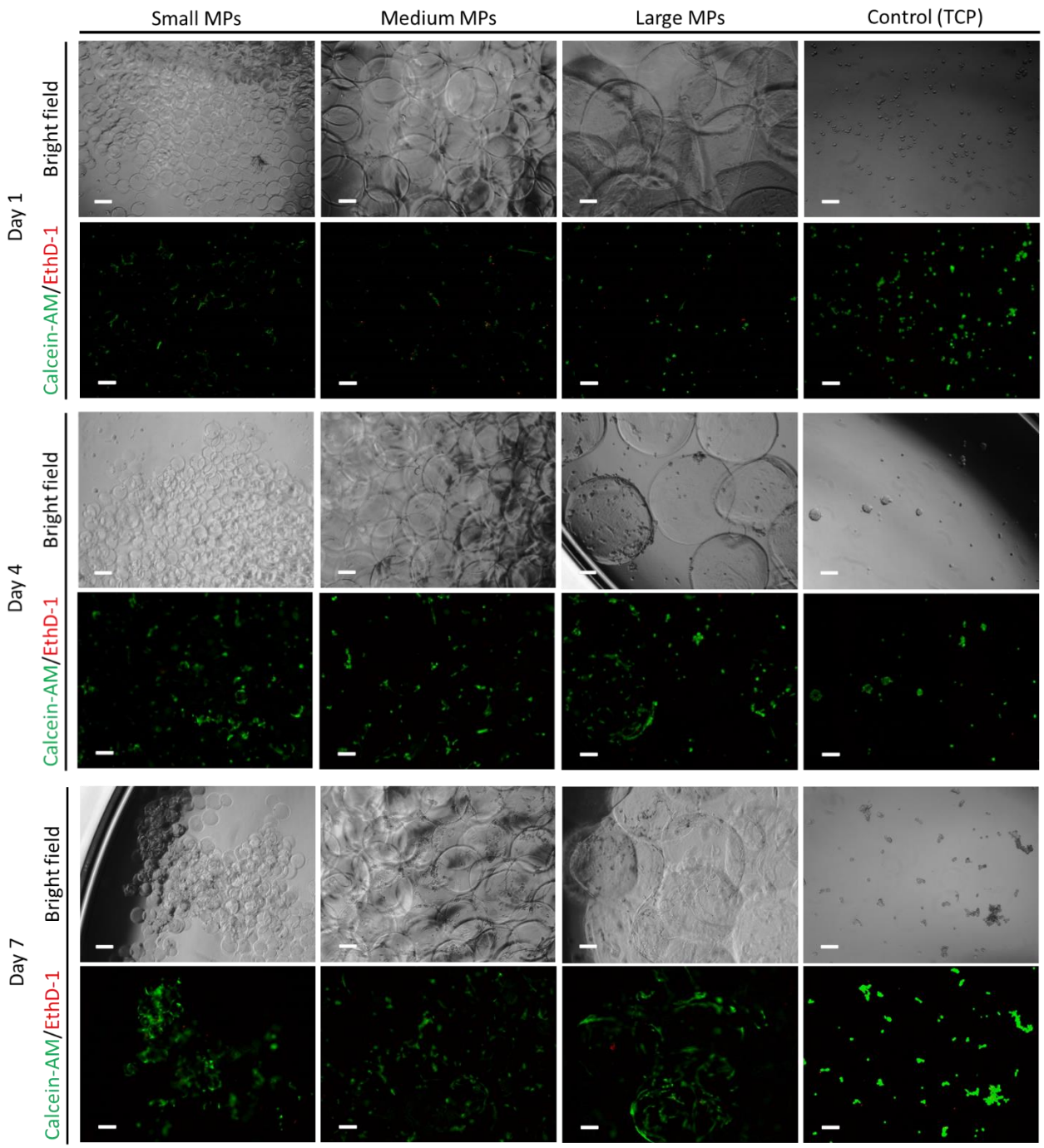


Figure 3.9 Representative bright field (top) and fluorescence (bottom) images of the experimental conditions, as displayed. Live cells were stained with Calcein-AM (green), whilst dead cells were stained with Ethidium homodimer (red). Scale bar =100 μm.

3.3 Summary and Discussion

Current methods of producing GelMA microparticles are either using homogenisation or microfluidic approaches. The former method is high-throughput but there is a large heterogeneity of both mechanical strength and particle diameter, and controlling cannot be fine-tuned (Nguyen et al., 2015). The microfluidic approach offers high tuneability, but the rate of production is low (Jung and Oh, 2014). With the work presented, we have shown that a co-current microfluidic platform could be used to produce GelMA microparticles with monodisperse characteristics of size and surface Young's modulus. The production of microparticles are also increased, with a throughput rate comparable to the homogenisation method (1-10 mL/h). This process could be easily scaled up by using parallel scale-up approaches, which has been done previously for other polymers of interest (Mulligan and Rothstein, 2012) . In addition, the tuneability of Young's modulus with similar diameters or varying diameters with similar Young's modulus is one of the significant features of this production route. Decoupling the size and modulus is important to remove any confounding variables (i.e. the interaction of surface area and modulus) to the overall conclusion of the study. This decoupling is only feasible using DoE, since through mathematical and statistical optimisation, one can obtain a desired modulus and diameter based on experimental needs. The researcher believes, in the best of his knowledge, that this is the first study to obtain decoupled matrix stiffness and diameter, since several studies (summarised in this review Daly *et al.*, 2020) have controlled either the size or diameter, but not both parameters. The DoE also eases the production method wherein the desired material property is predetermined by obtaining the process conditions through the model.

In this work, microparticle diameter was assessed with phase-contrast microscopy and DLS, showing a microparticle diameter ranging from 170-760 µm, which increased with the increase of disperse phase flow rate and the decrease of continuous phase flow rate. The microparticles produced possessed a narrow size distribution, as evidenced by the Span index and CV% not higher than 0.35 and 20%, respectively. The elastic properties of the microparticles were assessed

via AFM, displaying surface Young's modulus values ranging from 26-130 kPa. The values obtained followed an inversely proportional trend in regards to the microparticle size, showing a significant change in small (≤300 μm), medium (>300 μm; ≤600 μm) and large (>600 μm) classes of microparticles. The structural properties of the microparticles, which are seemingly dependant on the size, were further characterised by environmental Scanning Electron Microscopy, showing that as the diameter decreased, the porous structure appeared increasingly ordered and the pore size appeared to be larger. The polymer chains of GelMA could favourably stack in smaller sized microparticles, creating stronger crosslinked networks that translate to a stiffer material. The mathematical modelling of the method allowed the formulation of two separate equations for diameter and surface Young's modulus prediction from the two phases flow rates, which consolidate the relationship between the flow rates in determining the properties of GelMA microparticles. Moreover, the size and the stiffness might also affect cell proliferation, as revealed by the Live&Dead assay which confirmed approximately 80% ihMSCs viability after one week across different microparticle sizes. Albeit maintaining acceptable levels of cell viability, the larger microparticles exhibited a lesser percentage of live cells, which may be related to the lesser density of the RGD domains, affecting cell attachment and survival.

These findings enable the fabrication of a 3D platform for cell culture, with tuneable elasticity and particle size (curvature). This platform will translate most 2D effect of differentiation into a 3D order, where the applications are likely for high-througput production of differentiated cells without using exogenous factors. With the use of DoE, this also allows scaling of the production, because other confounding and noise factors are included in the model for robustness. Such technology for producing highly tuneable particles allows not just investigation in *in vitro* models, but also could be applied in a commercial scale for potential clinical and GMP-manufacturing usage of materials. As a final remark, the co-current flow methodology allows the production of monodisperse GelMA microparticles that follow a size-stiffness correlation. This method will be employed to explore the applicability of microparticles with tuneable elasticity to

influence MSCs behaviour. The next chapter will focus on the production of microparticles with similar sizes but different elasticities by controlling initial GelMA concentration and degree of methacrylation. The ultimate aim is to produce a library of hydrogel microparticles with defined elastic surface moduli to be used in a medium to high-throughput perspective for 3D culturing of hMSCs, to induce specific lineage commitment in serum-free conditions.

4. GELATIN METHACRYLATE MICROPARTICLES INFLUENCE ON MESENCHYMAL STEM CELLS MULTI-LINEAGE DIFFERENTIATION

4.1 Introduction

Adult stem cells, as part of natural regenerative processes, are assumed to recede and migrate away from their niche (Katayama et al., 2006) and eventually re-implant and differentiate across a variety of microenvironmental tissues. This one aspect derives from the capacity of cells to obtain and incorporate input from their microenvironment to regulate their activities at local and systemic levels, which is critical as it directs cell fate during growth, homeostasis and regeneration after injury. Mesenchymal stem cells (MSCs) in particular can alter the direction of differentiation in response to biochemical factors (ion levels, gases, nutrients and macromolecules) and protein (ECM components, growth factors and signalling molecules) composition of the microenvironment, however in the last decade evidence has been reported to illustrate that the mechanical forces acting on cells are equally essential in driving differentiation (Discher et al., 2017; Humphrey et al., 2014; Iskratsch et al., 2014).

When it comes to MSCs, several studies have demonstrated that these cells are sensitive to substrate properties, such as surface texture, elasticity and chemistry, and can differentiate into various anchorage-dependent cell types including neurons (Deng et al., 2006; Scuteri et al., 2011), adipocytes (Hu et al., 2018; Li et al., 2018; Sekiya et al., 2004), myoblasts (Dezawa et al., 2005; Hodgson et al., 2018), and osteoblasts (Hu et al., 2018; Li et al., 2018; McBeath et al., 2004b). The forerunner of this understanding on mechanobiology in regards to the response of MSCs to the elasticity of the substrate was a report from Engler et al. (Engler et al., 2006). MSCs were cultivated on collagen I-coated polyacrylamide gels, with matrix elasticity determined by the degree to which the gels were cross-linked. Cells on gels exhibiting the softest Young's modulus (E ~ 0.1–1 kPa) similar to the elasticity of brain tissue, and displayed the highest expression of neuron-specific

markers. Likewise, MSCs on medium stiffness close to muscle tissue (E ~ 8–17 kPa) expressed six times higher levels of myogenic markers, whilst when grown on the stiffest substrate (E ~ 25–40 kPa) the cells expressed four times higher osteogenic markers. Given the capacity of ECM stiffness to modulate stem cell adhesion, differentiation and signalling, and to activate mechanotransduction pathways in the latter, it should be noted that most studies focusing on this aspect have been performed predominantly in 2D experiments, which do not completely recapitulate the physiological scenario of a 3D microenvironment (Burdick and Vunjak-Novakovic, 2009; Scadden, 2006; Underhill and Bhatia, 2007). Moreover, although approaches have been attempted to modify the elasticity of microparticles for tissue engineering applications, they exhibit narrow ranges of stiffness, and in particular hydrogel ones display low elasticity (up to 1 kPa), not covering the large differences in elasticity and not specifically targeting the mechanical properties alone of the material in microparticle-format (Chan et al., 2014; Gomez-Florit et al., 2020; Lee and Kim, 2018; Oliveira and Mano, 2011). At the author's best knowledge, there is no evidence in literature of the use of hydrogel MPs exhibiting an ample range of stiffness that could potentially cover the phyiosological elasticity of the body tissues, brain to bone.

Thus, the focus of this chapter was to explore the elastic properties of one such hydrogel material, Gelatin Methacrylate (GelMA), in inducing changes in bone marrow-derived hMSC behaviour towards specific lineages and providing an appropriate 3D environment (the microparticle) suitable for translational purposes. Atomic force microscopy was employed to characterise flat discs and microparticles generated by increasing GelMA degree of substitution and concentrations to evaluate their surface elasticity, and thus tailoring the selection for specific stiffness to induce primary human bone marrow-derived mesenchymal stem cell (hMSCs) differentiation. An initial translational strategy with immortalised human mesenchymal stem cells (ihMSCs) seeded onto GelMA microparticles produced via the co-flow microfluidic system as reported in the previous chapter (Chapter 3), and in this chapter, we have produced microparticles that vary in modulus with similar diameters. The hypothesis was to verify surface modulus in 3D

can influence the differentiation state of hMSC via GelMA microparticles. The analysis explored providing evidence of lineage commitment through the screening of early lineage markers of neurogenesis (MAP2b), adipogenesis (PPARγ), myogenesis (Myogenin) and osteogenesis (Osterix) via immunocytochemistry. Afterwards, a machine learning procedure and high-throughput image analysis were carried out through the integration of the software Ilastik to CellProfiler, to highlight the yes-no response rate to the marker concerned.

4.2 Results

4.2.1 GelMA flat discs and microparticles elasticity characterisation

GelMA flat discs and microparticles were characterised via AFM to assess the change of stiffness in response to a change of concentration and degree of methacrylation. Values for each sample are reported in Table 4.1 As shown on the histograms in Figure 4.1A and 4.2B, reporting the Young's moduli of GelMA flat discs and microparticles respectively, the stiffness of GelMA is directly proportional to the concentration of the polymer and to the degree of methacrylation of the same.

TABLE 4.1 Young's modulus of GelMA discs as obtained by AFM measurements.

Format	**Concentration [% w/v]**	**Degree of substitution [%]**	**AFM E [kPa] (N = 3)**
Flat discs	5%	30%	0.2±0.1
	5%	68%	1.6±0.4
	5%	93%	5.9±0.3
	8%	93%	14.6±1.5
	13%	93%	43.1±3.1
Microparticles	5%	30%	0.23±0.03
	5%	68%	1.5±0.2
	5%	93%	5.9±0.9
	8%	93%	15.6±4.8
	13%	93%	44.5±6.9

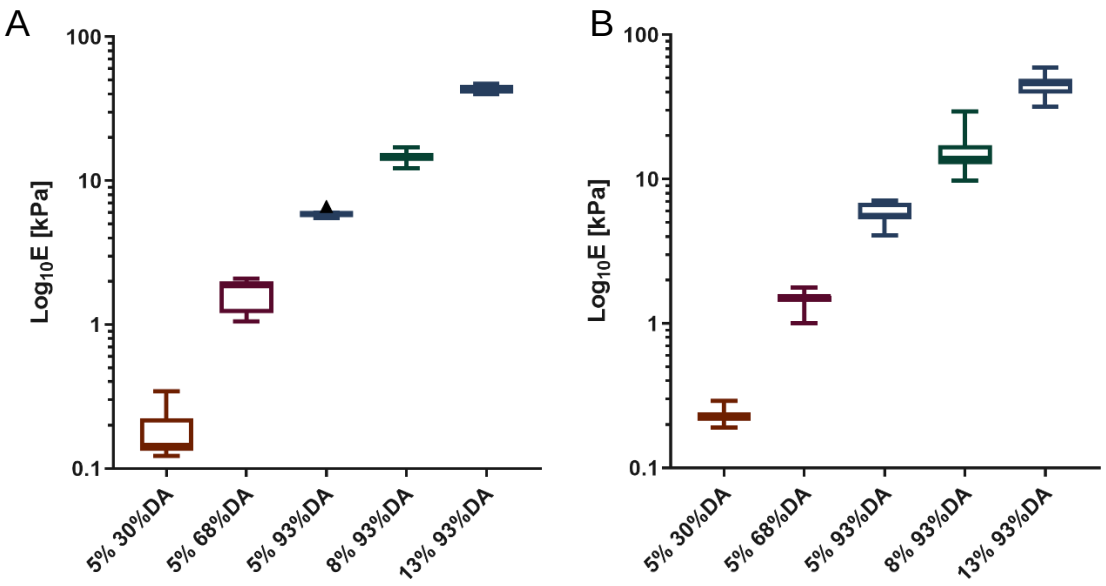


Figure 4.1 Box plot graphs of Young's modulus of GelMA flat discs (A) and microparticles (B) stiffness change concerning different degrees of methacrylation and concentration. Values have been calculated on 3 different samples, measuring 3 force maps of 100 spots per condition.

On this basis, the parameters for desirable GelMA elastic properties are tailored for the culture of primary hMSCs, to assess GelMA capacity to induce cell differentiation through stiffness alone, as shown by the previous work of Engler et al. (Engler et al., 2006). The formulation of GelMA presented above, exhibiting altogether a broad spectrum of stiffness, were used for the 2D and 3D cell studies as discussed in the following sections.

4.2.2 Alkaline Phosphatase and Vinculin expression of ihMSCs cultured on GelMA discs and microparticles

In order to translate the 2D perspective of the GelMA discs to a 3D environment, a pre-trial study to evaluate if ihMSCs can attach, grow and differentiate on GelMA microparticles was carried out. GelMA microparticles (13% w/v, 93% DS) were produced according to section 2.5, displaying a diameter of 251±35 μm with a low polydispersity (Figure 4.2A) and had an overall spherical shape (Figure 4.2B). These were used to test whether they can be viable as microcarriers for cell proliferation towards clinically relevant quantities and cell delivery strategies, altogether inducing the elasticity-driven differentiation of primary hMSCs.

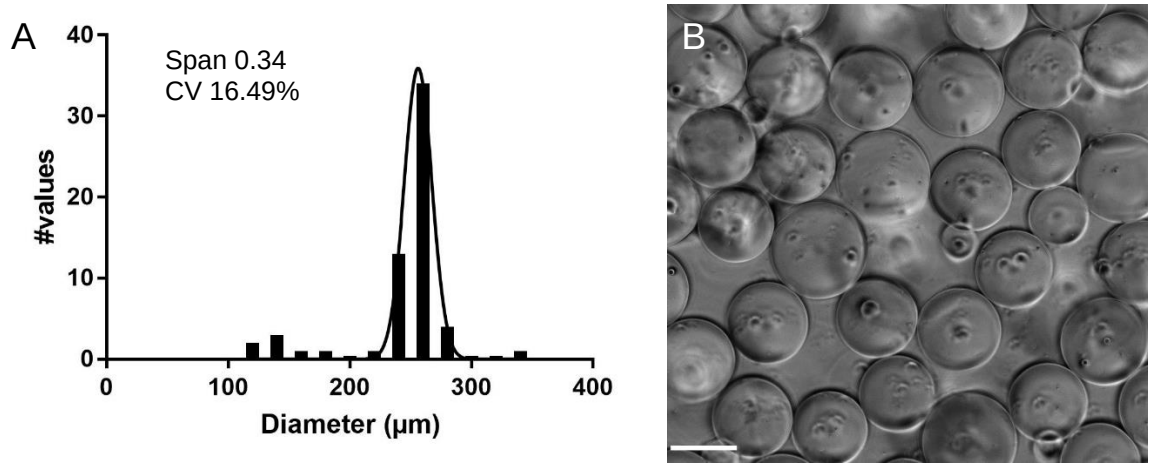


Figure 4.2 (A) Frequency distribution of GelMA microparticles diameters, calculated on a total of 100 microparticles; (B) Microparticles imaged under an optical microscope. Scale bar = 200 µm

Subsequently, ihMSCs were seeded and assessed at 7 and14 days to evaluate their attachment and survivability. It has been shown that immortalised lines of MSCs are able to maintain their receptivity to substrates as observed in primary cells, thus rendering them useful as a stiffness reporter (Torre et al., 2018), and capable to partially recapitulate the differentiation capacity of primary MSCs (Nagai et al., 2007). In this regard, Alkaline Phosphatase (ALP) and Vinculin expression were visualised by immunostaining, as the former is a known marker for MSCs commitment to the osteogenic lineage (Kuroda et al., 2017; Štefková et al., 2015), whilst the latter gives insights on the morphology and cell behaviour when under mechanical tension (Chang et al., 2019). In particular, ALP activity in MPs shows an expression peak around day 7 which subsides at later timepoints, whilst higher expression of vinculin is related to focal adhesion formation and mechanosensing (Chang et al., 2019).

As shown in Figure 4.3, ihMSCs grown on GelMA both in a flat disc and microparticle format, respond to the substrate similarly, showing stronger ALP staining at 7d and quasi-absence at 14d. In parallel, the morphology of the ihMSCs changes as evidenced by the expression of vinculin which shows how the cells assumed a globular appearance at 14d. The results of this preliminary study show that the microparticle format is able to induce phenotypic changes in ihMSCs, thus opening the way to further studies towards a 3D culture of primary hMSCs.

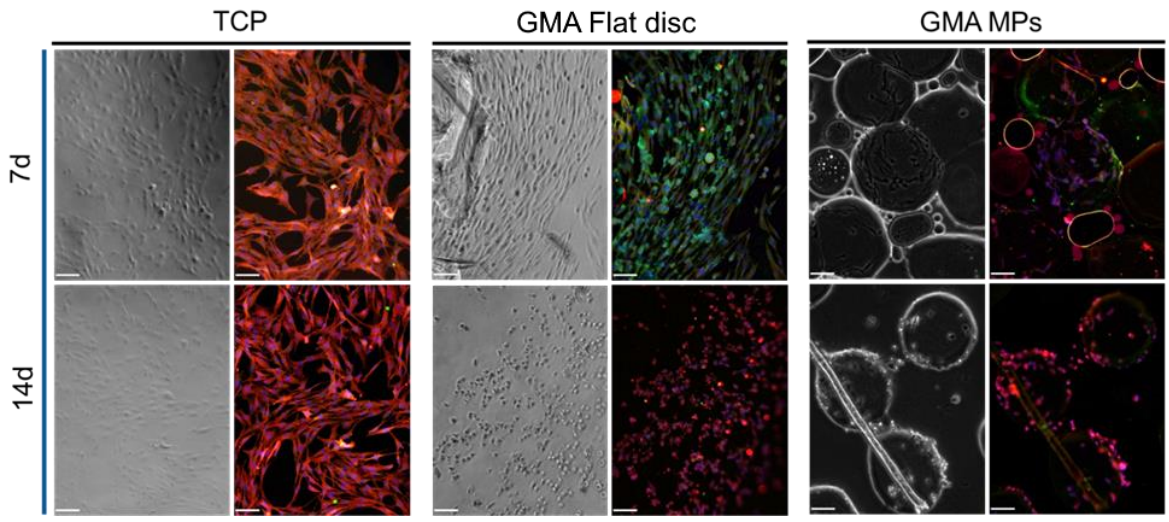


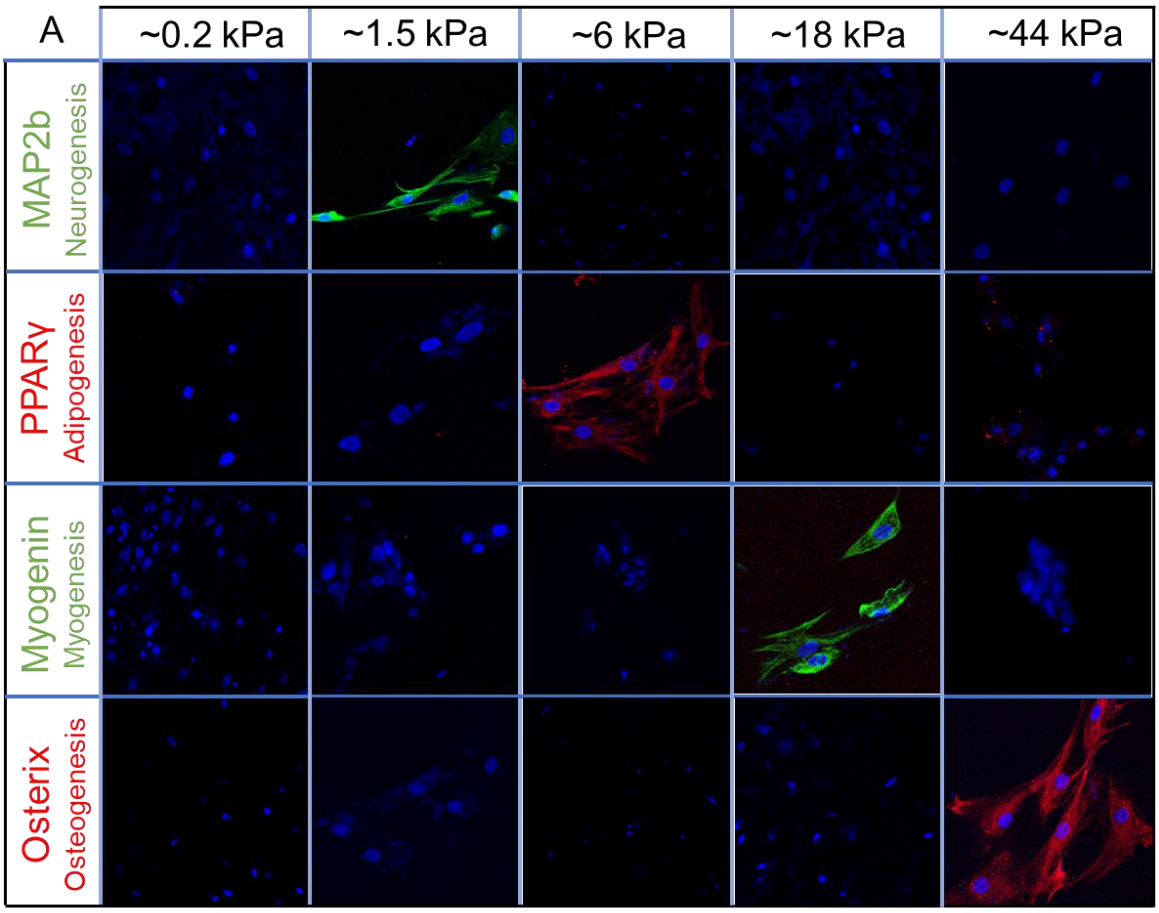
Figure 4.3 Bright field (left) and Fluorescence (right) images of the experimental conditions, as displayed. Cells were stained for Alkaline Phosphatase (green), Vinculin (red) and DAPI (blue). The peak of expression of ALP at 7d and its decrease at 14d, correlated with a stronger signal of vinculin at the 14d rather than at 7d, suggesting that both the GelMA disc and GelMA MPs can induce the variation of marker expression in ihMSCs. Scale bar = 100 μm.

4.2.3 Primary hMSCs lineage marker screening

Differentiation capacity of primary hMSCs on GelMA flat discs and microparticles with increasing stiffness was tested using five formulations of GelMA as discussed in section 4.2.1. The choice of these particular elasticities was reinforced by previous studies about the optimal values that can induce a behavioural change in hMSCs into a commitment towards defined lineages (Engler et al., 2006; Sekiya et al., 2004; Wen et al., 2014). In particular, the elasticities of produced discs and microparticles are within the range of physiological values that have been shown to promote differentiation towards the neurogenic (E_{GelMA}~0.2-1.5 kPa, E_{brain}~0.1-1 kPa), adipogenic (E_{GelMA}~6 kPa, E_{fat}~3-7 kPa), myogenic (E_{GelMA}~18 kPa, E_{muscle}~8-17 kPa) and osteogenic (E_{GelMA}~44 kPa, E_{bone}~40 kPa) lineages (Engler et al., 2006; Shih et al., 2005, 2011). The 7th-day timepoint was chosen as this is when most of the early markers for commitment are deemed to be expressed, and among these immunohistological staining of MAP2b (Fazeli et al., 2015), PPARγ (Li et al., 2018), Myogenin (Gunetti et al., 2012) and Osterix/Sp7 (Kaback et al., 2008) were employed for their respective lineages.

As Figures 4.4 and 4.5 show, the screening revealed that hMSCs grown on GelMA discs and on microparticles with relevant stiffness were able to express early markers exclusively in the elasticity specified by their lineage, as compared to the controls (Fig. 4.6). The expression of these markers was indeed present on the respective stiffnesses and was specific for those lineages as the staining of the same markers on separate lineages did not occur. Several markers were present in other matrix stiffnesses for both flat discs and MPs, albeit in low count. PPARγ expression, for example, was identified in cells cultured on MPs with surface moduli ~1.5 kPa and ~44 kPa at 1% and 4% positive samples respectively. Similarly, Osterix is seen in ~18 kPa with 5.3% positive cells. This could be an indication that the production process of microparticles generates a non-fully homogeneous population in terms of elasticity, and that therefore needs further optimisation. However, although there seems to be an overlap of lineage commitment in adjacent ranges of stiffnesses, this is at minimum a 17-fold difference in positive cells' expression of early markers on these adjacent stiffnesses as compared with the elasticity where one would expect a certain lineage commitment.

These results overall denote that primary hMSCs could have undergone commitment to the neurogenic, adipogenic, myogenic and osteogenic lineages following culture on both 2D and 3D GelMA substrates of various stiffness as also demonstrated in previous studies (Engler et al., 2006). This confirms that the differentiation potential of hMSCs can be driven by the stiffness of the substrate alone. Coupled with the ease of fabrication of GelMA in a microparticle format, this will constitute a potential platform for cell differentiation in a 3D environment.



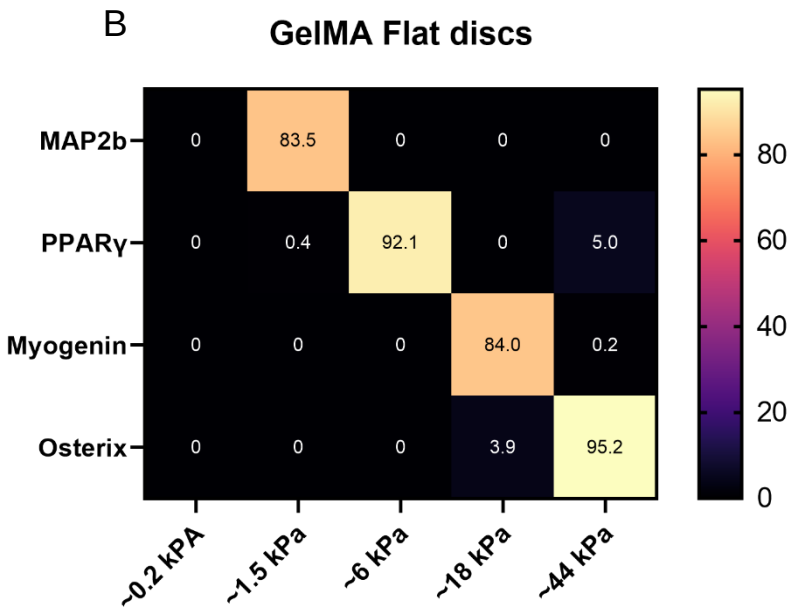


Figure 4.4 (A) Fluorescence images of MSCs cultured in GelMA Flat Discs and (B) Quantification of % positive samples based on total cell count. Standard deviations for % calculated values are as follows: MAP2b (1.5 kPa) = 7.1; PPARγ (1.5 kPa) = 0.2, (6 kPa) = 7.6, (44 kPa) = 2.7; Myogenin (18 kPa) = 6.3, (44 kPa) = 0.1; Osterix (18 kPa) = 1.9, (44 kPa) = 5.8; all at n=2 technical replicates and N=3 donors.

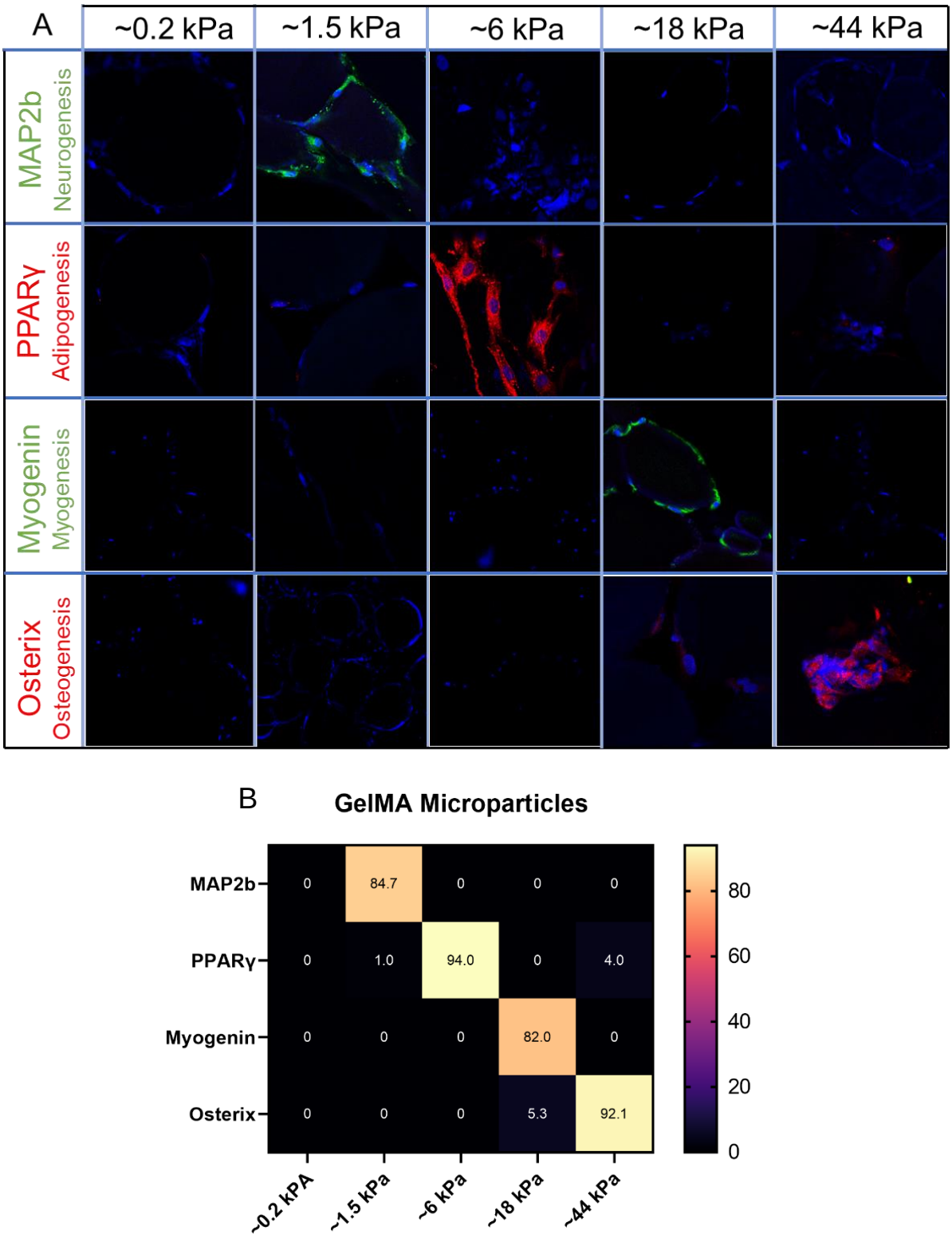


Figure 4.5 (A) Fluorescence images of MSCs cultured in GelMA MPs and (B) Quantification of % positive samples based on total cell count. Standard deviations for % calculated values are as follows: MAP2b (1.5 kPa) = 8.9; PPARγ (6 kPa) = 8.6, (44 kPa) = 1.4; Myogenin (18 kPa) = 6.8; Osterix (18 kPa) = 2.9, (44 kPa) = 4.8; all at n=2 technical replicates and N=3 donors.

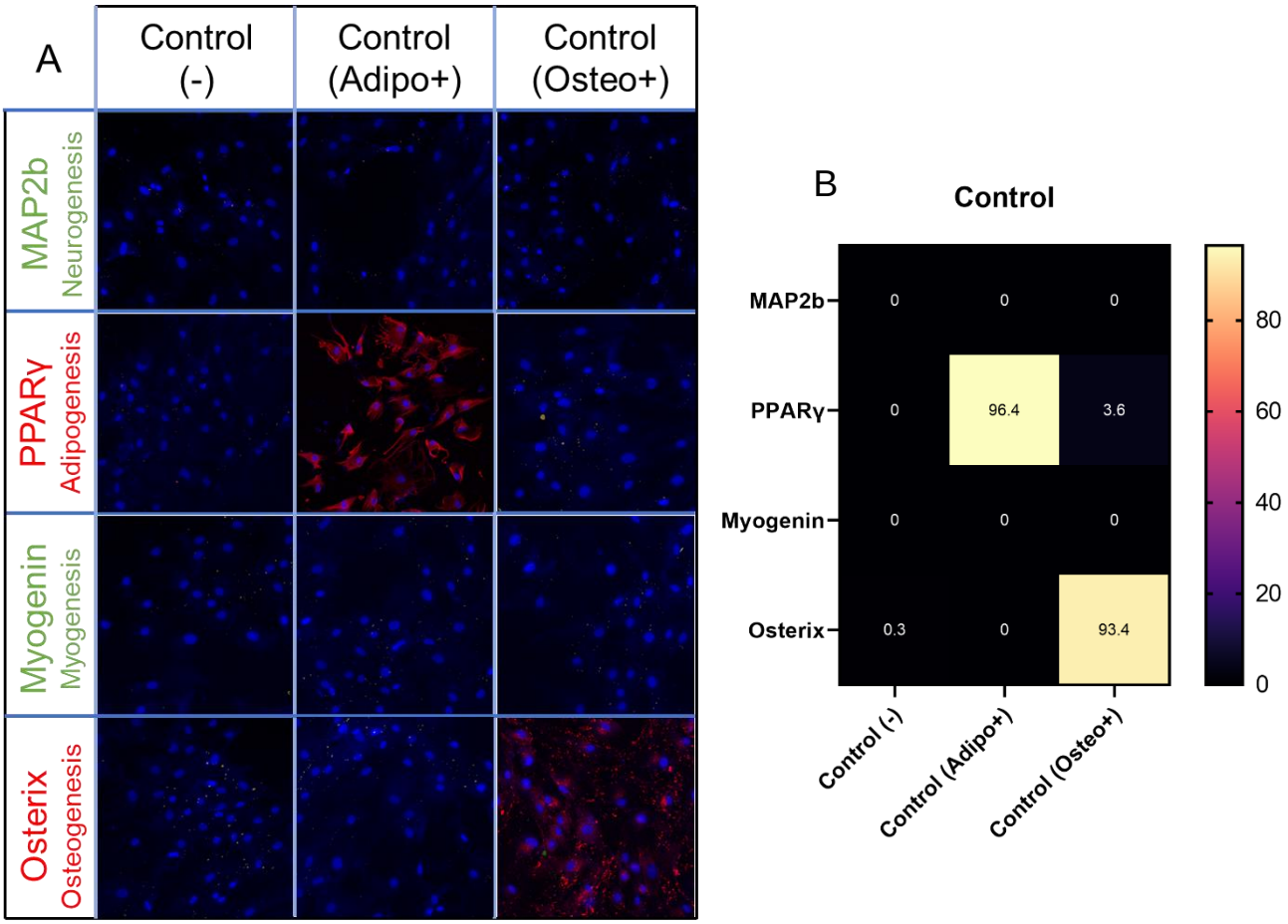


Figure 4.6 (A) Fluorescence images of MSCs cultured in Tissue Culture Plates (Controls) (B) Quantification of % positive samples based on total cell count. Standard deviations for % calculated values are as follows: PPARγ (+Adipo) = 1.8, (+Osteo) = 1.5; Osterix (-Control) = 0.3, (+Osteo) = 4.1; all at n=2 technical replicates and N=3 donors.

4.3 Summary and Discussion

The work in this chapter focused on the generation of microparticles presenting a well-defined range of stiffness in order to induce differentiation in primary hMSCs. Increasing the degree of methacrylation and concentration enables control of the matrix stiffness for both microparticles and discs of GelMA, allowing for a finely-tuned range of elasticity that is suitable for MSCs differentiation. As previous literature suggested, the elasticity attained could achieve neurogenesis (E_{GelMA}~0.2-1.5 kPa, E_{brain}~0.1-1 kPa), adipogenesis (E_{GelMA}~6 kPa, E_{fat}~3-7 kPa), myogenesis (E_{GelMA}~18 kPa, E_{muscle}~8-17 kPa) and osteogenesis (E_{GelMA}~44 kPa, E_{bone}~40 kPa)

(Engler et al., 2006). The effects of substrate stiffness for cell differentiation have been demonstrated multiple times, however, the research was focused either on already committed progenitor cells, like myofibroblasts (Huang et al., 2012) and bronchial fibroblasts aided by TGF-β1 release (Shi et al., 2013), or by using elasticity tuned polymer films coated with bioactive elements such as collagen or fibronectin (Engler et al., 2006; Evans et al., 2009; Olivares-Navarrete et al., 2017; Sun et al., 2018).

In this regard, the work here presented wanted to focus on the gap that exists between the 2D and the 3D world, by employing GelMA hydrogel capabilities to provide mechanical inputs, allow the access of intrinsic bioactive elements for cell adhesion and therefore stimulate the differentiation of MSCs without exogenous inducing factors. Several studies have performed on 2D substrates (Engler et al., 2006; Sun et al., 2018; Tse and Engler, 2011) that does not recapitulate actual cell-cell interaction with autocrine, paracrine and 3D spatiotemporal effects of matrix stiffness and overall cell curvature. There are significant differences between 2D and 3D culture, because in 2D cultures, cell-to-cell contact is only happening within their cellular boundaries. Cell signalling for 2D are the cells on its vicinity, while on 3D, autocrine and paracrine signalling is expounded (Hoarau-Véchot et al., 2018; Kapałczyńska et al., 2018). In addition to cell signalling, the curvature effect on the cellular organisation is also expounded on 3D, as cells will have more surface area exposed in contrast with 2D (Baptista et al., 2019; Chen et al., 2017). This study emphasized the effect of both matrix stiffness and 3D organisation of cells that can capture the actual dynamics in cell signalling pathways.

A prior trial-and-error study was carried out to evaluate if GelMA microparticles could be apt as microcarriers able to influence immortalised MSCs behaviour and morphology, by enabling the expression of Alkaline Phosphatase and Vinculin as compared to MSCs grown on tissue culture plastic. The study highlighted the presence of ALP expression at 7d and its absence at 14d, whilst also assuming a globular appearance has shown by the vinculin arrangement, whose presence relates to the linkage of integrin adhesion molecules to the actin cytoskeleton and focal adhesion

formation, an essential element in mechanotransduction (Ezzell et al., 1997). Finally, by growing primary hMSCs on GelMA microparticles of varying stiffnesses, it was possible to induce the expression of early lineage markers, namely MAP2b for neurogenesis, PPARγ for Adipogenesis, Myogenin for myogenesis and Osterix for osteogenesis, according to the specific matrix stiffness increase where the cells were grown upon. This was also shown by quantification of the percentage of positive cells to the marker expression which is comparable to those achieved by the adipoinductive and osteoinductive positive controls. Further validation via reproducibility studies is underway to robustly prove the stiffness induced differentiation.

The work presented here suggests that moving the cell response from a 2D matrix-induced differentiation onto a 3D surface is possible using microparticles. The significance of this work is on the usage of 3D format for scalable cultures, where a larger surface area is utilised for high-density cultures in a bioreactor and/or could be used for cell delivery to localise cells within the injection site. Emphasizing its possible role on clinical use, current cellular therapies are limited in cell numbers due to constraints in the expansion process. However, enabling the platform in a 3D format allows a multitude of increase in cell expansion throughput that are relevant in clinical applications. In addition, reduction or elimination of the use of exogenous factors used in differentiation (i.e. growth factors) could be advantageous, removing several issues such as costs, the use of xenogenic sources and the risks associated with off-target effects. Such microparticle-based culture may be beneficial for clinical use, as low cell numbers and the need for non-xenogenic differentiation induction have, to date, been the bottleneck of stem cell therapy.

5. Overall Discussion

5.1 Key Findings

In this thesis, it has been hypothesized that stiffness-induced differentiation in 2D could be translated in a 3D format using varying stiffnesses of hydrogel microparticles. A custom microfluidic co-flow setup was made to produce monodispersed GelMA hydrogel microparticles with a span index of 0.35 and a coefficient of variation of up to 20%. These microparticles were produced with diameters within the range of 170-760 µm as determined using DLS. Such particles were found out to be affected by the ratio of continuous (Mineral Oil + Span 80) and disperse phase (GelMA solution), where an increased ratio tended to reduce the size of the resulting microparticle diameter. It is thought that this is because the higher the continuous phase is, the larger the shear force is being transmitted to the dispersed phase, increasing jet breakup due to Rayleigh instability. A highly porous material was observed in eSEM, and it has been seen that the smaller the particle size, the more ordered its porous walls were. In terms of surface modulus, the range of microparticle stiffnesses measured using AFM was from 0.23-130 kPa. It was evident that matrix stiffness was inversely proportional to the particle size, i.e., the smaller the particle, the stiffer the surface properties. This relationship could be a result of the more ordered structure of the walls seen in smaller particles, in which a higher degree of crosslinking could be contributing to these structural changes in the particle microstructure.

The produced microparticles with varying stiffnesses were assessed concerning cell adherence and viability. Immortalised human MSCs were cultured for a week on these particles, and a live-dead assay was performed to quantify the overall viability of cells during static culture. On all microparticles, cell viability was recorded as >80%, but one noticeable trend was that the larger microparticles (the lower stiffness range) exhibited a lower percentage of live cells in comparison with the cells cultured on smaller, stiffer microparticles. Two reasons for this observation might be either the increased RGD peptide density on the smaller particles or the elevated stiffness caused

increased cell proliferation as has been previously described in the literature (Schrader et al., 2011; Trensz et al., 2015; Wang et al., 2012).

To compare the effects of hMSC differentiation in 2D and 3D, GelMA hydrogel discs as the 2D control and microparticles as the 3D model were used. Through the generation of microparticles with a well-defined spectrum of stiffness via increasing levels of methacrylation and concentration whilst keeping the microparticle diameter the same, it was possible to control the matrix stiffness in a range that had been previously reported to support hMSCs differentiation. The Young's modulus of the 2D and 3D formats was tailored according to previous literature values which had supported neurogenesis (E_{GelMA}~0.2-1.5 kPa, E_{brain}~0.1-1 kPa), adipogenesis (E_{GelMA}~6 kPa, E_{fat}~3-7 kPa), myogenesis (E_{GelMA}~18 kPa, E_{muscle}~8-17 kPa) and osteogenesis (E_{GelMA}~44 kPa, E_{bone}~40 kPa) (Engler et al., 2006; Sekiya et al., 2004; Wen et al., 2014). The ability for cells to attach onto GelMA microparticles was evaluated via immunocytochemistry for ALP and Vinculin expression, giving insights on both the mechanosensing ability of ihMSCs and the change of morphology as compared to the tissue culture plastic control. The cells exhibited a peak of ALP expression at day 7, whilst a phenotypical change occurred at day 14 where cells assumed a globular shape, contrary to the TCP control where cells still maintained a spread conformation. This could be an indication of integrin activation and focal adhesion formation thanks to the RGD peptides present on the GelMA surface, as they allow ihMSCs to sense further mechanical information of their surroundings (Atherton et al., 2016; Kuroda et al., 2017). The same protocol for cell culture on GelMA hydrogel microparticles were then optimised for early marker screening of MAP2b for neurogenesis, PPARγ for Adipogenesis, Myogenin for myogenesis and Osterix for osteogenesis. As the surface modules of the GelMA microparticles increased, primary hMSCs showed evidence of lineage commitment in an elasticity-specific fashion, between 82% and 94% expressing the above early markers of differentiation.

5.2 Discussion in Context of the Wider Literature

Mesenchymal stem cells have been the subject of investigation because of their potential for regenerative medicine. Factors affecting their self-renewal and differentiation have been thoroughly explored, albeit the incomplete understanding of other exogenous factors makes the direction of their differentiation not well understood. Among a plethora of factors, it has been established that mechanical effects do have a significant effect on its differentiation capacity (Wang, Tytell and Ingber, 2009; Vining and Mooney, 2017; Chang *et al.*, 2019). However, to the best of the author's knowledge, all studies performed were in 2D format, not recapitulating the microenvironment that cells grow and communicate. Translating the current knowledge into 3D can bring a close to the question about the applicability of the previous hypotheses on mechanically induced differentiation (Engler et al., 2006). We have developed a microparticle-based platform to experimentally confirm that the differentiation based on mechanical strength alone in a 3D space could induce specific lineage pathways.

Microparticles have been used as a microcarrier to expand culture conditions from 2D to 3D (Neto et al., 2019). Traditionally, materials used for microcarriers are biologically inert (i.e. glass or polystyrene), allowing only adhesion of cells without any biological feedback (Choi et al., 2018; Piskin et al., 1994; Silich et al., 1992). This passive role was replaced with more relevant materials: properties that can induce specific effects on cells being cultured. It is possible therefore nowadays to modify the inherent property of the microparticles such as chemistry, topography, and matrix stiffness, to better understand its effects on the cells (Lu et al., 2015; Mata et al., 2011; Smith et al., 2019).

On the 2D culture methods used to examine the effects of the material modulus towards MSCs differentiation, often the researchers used soft materials (e.g. polyacrylamide) coated with collagen or with any integrin-binding sites (Engler et al., 2006; Park et al., 2011; Tse and Engler, 2011). To transform works into a 3D space, we have used GelMA due to its mechanical tuneability and the availability of RGD peptide sequences for cell binding. To the author's knowledge, this is the first

work ever performed where MSCs are cultured in 3D with varying mechanical properties. Observations have shown that by mimicking Young's modulus of native tissues, MSCs express markers relevant to the stiffness in which they are cultured – results confirm that MSCs differentiate based on the mechanical strength of the material in 2D and 3D. Soft materials enabled the expression of neuronal markers, while the stiffest microparticles produced cells that has elevated osteocyte markers. Other works were performed on culturing MSCs on microparticles, and it is observed that a significant number of publications had resulted in MSCs differentiating into osteoblasts (Amer et al., 2021; Müller et al., 2017; Sezer et al., 2014). The majority of the materials used in these studies are very stiff (hundreds of MPa), and applying the findings learned in this thesis, it could be that the stiffness alone affected the MSCs differentiation into osteoblasts.

A significant effect that this work could bring is the stiffness-induced differentiation culture into 3D, where a larger number of cells could be induced without requiring exogenous factors. This may translate into higher cell densities that are relevant towards clinical use, as well as reducing the costs related to using growth factors for differentiation. The avenue in which the work has been done needs further research to realise its commercial use, but as a proof-of-concept is likely enough to warrant investigations for scale-up and (pre)clinical trials.

The particle format allows an important vertical development of 3D cell culture in various applications such as research, being an easily manipulable platform for the study of mechanotransduction and related pathways, which has remained mostly confined to the 2D perspective, failing to faithfully recapitulate the conditions to which the cell is physiologically exposed (Labriola et al., 2018; Wang et al., 2019); clinically, for the production in a bioreactor of large batches of terminally differentiated cells for transplants, tissue reconstruction and cancer modelling (Daly et al., 2020; Gong et al., 2015); industrially, for both biomedical products (Daly et al., 2020) and cellular agriculture, of which synthetic meat is one of the most relevant emerging fields (Bodiou et al., 2020).

5.3 Current limitations

Several limitations became evident during this research project. First of all, the production method requires further optimisation and suitable instrumentation for use, since the process gives rise to the formation of tailing patterns during the co-current flow dynamic, producing smaller droplets that, although eliminated after filtration, still contaminate the monodispersity of the sample. Also, the current process cannot at present control the RGD peptide density presented at the microparticle surface, which can change due to the degree of methacrylation (as it substitutes the amine portion of lysin and occasionally arginine) and concentration of the polymer.

Additionally, it was not yet possible to achieve a fully dynamic seeding protocol, wherein cells were left to sediment on the microparticles, needing to stir them occasionally to improve the homogeneous distribution on microparticles surface.

Further limitations are the lack of neuroinductive and myoinductive positive controls in the lineage marker screening, as the current restrictions due to the COVID-19 pandemic resulted in reduced laboratory time.

5.4 Conclusion

In this research work, we have successfully developed a 3D platform for cell culture with varying stiffnesses via the generation of GelMA hydrogel microparticles. Through co-flow microfluidics, this work managed to produce controllable diameters (170-760 µm) with low polydispersity by adjusting the continuous and dispersed phase of the system. The stiffnesses of such microparticles were adjusted by modifying both the polymer concentration as well as the degree of methacrylation, in which the stiffnesses obtained ranged from 0.2-44 kPa; values were obtained in both 2D discs and 3D microparticle format. A biocompatibility study was performed on the synthesised microparticles, and ihMSCs showed viabilities greater than 80%.

To evaluate the hypothesis that matrix stiffness induces differentiation in 3D, we produced 2D discs and 3D microparticles with similar stiffness. It was shown that both in 2D and 3D, primary hMSCs

show early markers of neurogenic, adipogenic, myogenic, and osteogenic lineages depending on the matrix stiffness the cells were cultured upon. This work shows that matrix stiffness in a 3D format can induce expression of specific genes for hMSCs differentiation, translating previous works of 2D mechano-induced differentiation into a 3D space. These results implicate the transitioning of the mechanical induced differentiation into a more relevant 3D culture method that may break the current limitations of cellular density and xenogenic use of growth factors in clinical applications.

5.5 Future work

The results shown in this thesis demonstrate that by using hydrogel microparticles, a translation from a 2D matrix-induced differentiation onto a 3D surface is feasible and represents the novelty of this work. Future work could include the culture of cells on these microparticles in a bioreactor for scalable high-density cultures, thanks to the increased surface area of microparticles (Figure 5.1). Also, by exploiting the mechanosensing abilities of hMSCs and the versatility of GelMA both in terms of RGD presentation to integrins and matrix stiffness control, a reduction in the use of exogenous factors involved in differentiation is plausible. This would mitigate the current limitations of using these factors such as costs, off-target effects and the utilisation of xenogenic sources.

Indeed, the production process could benefit by modifying the fluidic prototype with the necessary technical changes, such as:

1) Recirculation pump for reintroducing the continuous phase to the flow;
2) Fine control over the temperature of the disperse phase, allowing reduced viscosity but also the possibility of including cells for possible encapsulation;
3) Addition of vibrational elements to create the breaking of the jet regime to obviate the use of the oily phase;

Further investigations are needed to evaluate the extent of hMSCs differentiation, to confirm their lineage commitment to maturation as terminally differentiated cells.

Finally, interest will focus on the culture of the microparticles in bioreactors for growth and differentiation in a critical mass useful for clinical applications.

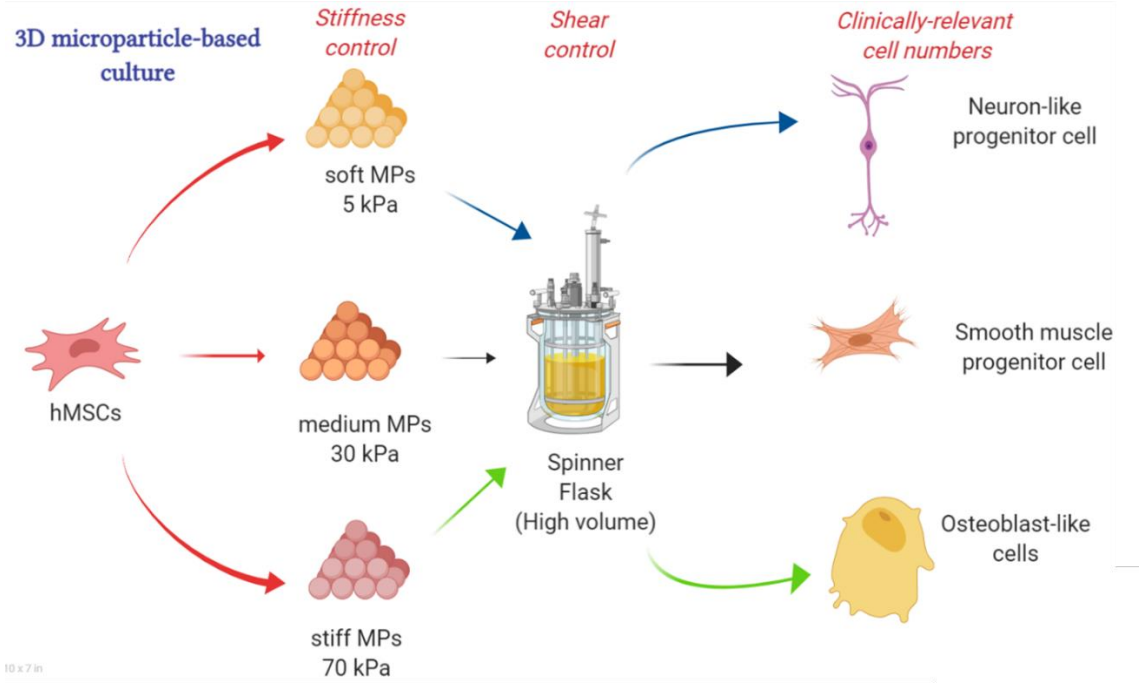


Figure 5.1 Schematic of the project workflow towards scalable production of differentiated MSCs

LIST OF REFERENCES

Abbasi, F., Ghanian, M.H., Baharvand, H., Vahidi, B., Eslaminejad, M.B., 2018. Engineering mesenchymal stem cell spheroids by incorporation of mechanoregulator microparticles. J. Mech. Behav. Biomed. Mater. 84, 74–87. https://doi.org/10.1016/j.jmbbm.2018.04.026

Aguilar, A., Zein, N., Harmouch, E., Hafdi, B., Bornert, F., Offner, D., Clauss, F., Fioretti, F., Huck, O., Benkirane-Jessel, N., Hua, G., 2019. Application of Chitosan in Bone and Dental Engineering. Molecules 24, 3009. https://doi.org/10.3390/molecules24163009

Almalki, S.G., Agrawal, D.K., 2016. Key Transcription Factors in the Differentiation of Mesenchymal Stem Cells. Differ. Res. Biol. Divers. 92, 41–51. https://doi.org/10.1016/j.diff.2016.02.005

Ambriz, X., de Lanerolle, P., Ambrosio, J.R., 2018. The Mechanobiology of the Actin Cytoskeleton in Stem Cells during Differentiation and Interaction with Biomaterials. Stem Cells Int. 2018, e2891957. https://doi.org/10.1155/2018/2891957

Amer, M.H., Alvarez-Paino, M., McLaren, J., Pappalardo, F., Trujillo, S., Wong, J.Q., Shrestha, S., Abdelrazig, S., Stevens, L.A., Lee, J.B., Kim, D.-H., González-García, C., Needham, D., Salmerón-Sánchez, M., Shakesheff, K.M., Alexander, M.R., Alexander, C., Rose, F.R., 2021. Designing topographically textured microparticles for induction and modulation of osteogenesis in mesenchymal stem cell engineering. Biomaterials 266, 120450. https://doi.org/10.1016/j.biomaterials.2020.120450

Assis-Ribas, T., Forni, M.F., Winnischofer, S.M.B., Sogayar, M.C., Trombetta-Lima, M., 2018. Extracellular matrix dynamics during mesenchymal stem cells differentiation. Dev. Biol. 437, 63–74. https://doi.org/10.1016/j.ydbio.2018.03.002

Atherton, P., Stutchbury, B., Jethwa, D., Ballestrem, C., 2016. Mechanosensitive components of integrin adhesions: Role of vinculin. Exp. Cell Res. 343, 21–27. https://doi.org/10.1016/j.yexcr.2015.11.017

Atta-ur-Rahman, Anjum, S., 2017. Frontiers in Stem Cell and Regenerative Medicine Research. Bentham Science Publishers.

Balani, K., Verma, V., Agarwal, A., Narayan, R., 2014. Physical, Thermal, and Mechanical Properties of Polymers, in: Biosurfaces. John Wiley & Sons, Inc, pp. 329–344. https://doi.org/10.1002/9781118950623.app1

Baptista, D., Teixeira, L., van Blitterswijk, C., Giselbrecht, S., Truckenmüller, R., 2019. Overlooked? Underestimated? Effects of Substrate Curvature on Cell Behavior. Trends Biotechnol. 37, 838–854. https://doi.org/10.1016/j.tibtech.2019.01.006

Baroud, C.N., Gallaire, F., Dangla, R., 2010. Dynamics of microfluidic droplets. Lab. Chip 10, 2032–2045. https://doi.org/10.1039/C001191F

Berg, S., Kutra, D., Kroeger, T., Straehle, C.N., Kausler, B.X., Haubold, C., Schiegg, M., Ales, J., Beier, T., Rudy, M., Eren, K., Cervantes, J.I., Xu, B., Beuttenmueller, F., Wolny, A., Zhang, C., Koethe, U., Hamprecht, F.A., Kreshuk, A., 2019. ilastik: interactive machine learning for (bio)image analysis. Nat. Methods 16, 1226–1232. https://doi.org/10.1038/s41592-019-0582-9

Berkland, C., Kim, K., Pack, D.W., 2003. PLG microsphere size controls drug release rate through several competing factors. Pharm. Res. 20, 1055–1062.

Bershadsky, A.D., Balaban, N.Q., Geiger, B., 2003. Adhesion-dependent cell mechanosensitivity. Annu. Rev. Cell Dev. Biol. 19, 677–695. https://doi.org/10.1146/annurev.cellbio.19.111301.153011

Bigi, A., Cojazzi, G., Panzavolta, S., Rubini, K., Roveri, N., 2001. Mechanical and thermal properties of gelatin films at different degrees of glutaraldehyde crosslinking. Biomaterials 22, 763–768. https://doi.org/10.1016/s0142-9612(00)00236-2

Blüml, G., 2007. Microcarrier Cell Culture Technology, in: Pörtner, R. (Ed.), Animal Cell Biotechnology, Methods in Biotechnology. Humana Press, pp. 149–178. https://doi.org/10.1007/978-1-59745-399-8_5

Bodiou, V., Moutsatsou, P., Post, M.J., 2020. Microcarriers for Upscaling Cultured Meat Production. Front. Nutr. 7, 10. https://doi.org/10.3389/fnut.2020.00010
Boyan, B.D., Hummert, T.W., Dean, D.D., Schwartz, Z., 1996. Role of material surfaces in regulating bone and cartilage cell response. Biomaterials, Polymer Scaffolding and Hard Tissue Engineering 17, 137–146. https://doi.org/10.1016/0142-9612(96)85758-9
Bratt-Leal, A.M., Carpenedo, R.L., Ungrin, M.D., Zandstra, P.W., McDevitt, T.C., 2011. Incorporation of biomaterials in multicellular aggregates modulates pluripotent stem cell differentiation. Biomaterials 32, 48–56. https://doi.org/10.1016/j.biomaterials.2010.08.113
Breuls, R.G.M., Jiya, T.U., Smit, T.H., 2008. Scaffold Stiffness Influences Cell Behavior: Opportunities for Skeletal Tissue Engineering. Open Orthop. J. 2, 103–109. https://doi.org/10.2174/1874325000802010103
Burdick, J.A., Vunjak-Novakovic, G., 2009. Engineered microenvironments for controlled stem cell differentiation. Tissue Eng. Part A 15, 205–219. https://doi.org/10.1089/ten.tea.2008.0131
Cai, R., Nakamoto, T., Kawazoe, N., Chen, G., 2015. Influence of stepwise chondrogenesis-mimicking 3D extracellular matrix on chondrogenic differentiation of mesenchymal stem cells. Biomaterials 52, 199–207. https://doi.org/10.1016/j.biomaterials.2015.02.033
Cappella, B., Dietler, G., 1999. Force-distance curves by atomic force microscopy. Surf. Sci. Rep. 34, 1–104. https://doi.org/10.1016/S0167-5729(99)00003-5
Carletti, E., Motta, A., Migliaresi, C., 2011. Scaffolds for tissue engineering and 3D cell culture. Methods Mol. Biol. Clifton NJ 695, 17–39. https://doi.org/10.1007/978-1-60761-984-0_2
Carneiro, J., Doutel, E., Campos, J.B.L.M., Miranda, J.M., 2016. PDMS droplet formation and characterization by hydrodynamic flow focusing technique in a PDMS square microchannel. J. Micromechanics Microengineering 26, 105013. https://doi.org/10.1088/0960-1317/26/10/105013
Cavalcanti-Adam, E.A., Volberg, T., Micoulet, A., Kessler, H., Geiger, B., Spatz, J.P., 2007. Cell spreading and focal adhesion dynamics are regulated by spacing of integrin ligands. Biophys. J. 92, 2964–2974. https://doi.org/10.1529/biophysj.106.089730
Chacón-Martínez, C.A., Koester, J., Wickström, S.A., 2018. Signaling in the stem cell niche: regulating cell fate, function and plasticity. Dev. Camb. Engl. 145, dev165399. https://doi.org/10.1242/dev.165399
Champion, J.A., Walker, A., Mitragotri, S., 2008. Role of particle size in phagocytosis of polymeric microspheres. Pharm. Res. 25, 1815–1821. https://doi.org/10.1007/s11095-008-9562-y
Chan, K.M.C., Li, R.H., Chapman, J.W., Trac, E.M., Kobler, J.B., Zeitels, S.M., Langer, R., Karajanagi, S.S., 2014. Functionalizable hydrogel microparticles of tunable size and stiffness for soft-tissue filler applications. Acta Biomater. 10, 2563–2573. https://doi.org/10.1016/j.actbio.2014.02.021
Chang, Y., Shao, Y., Liu, Y., Xia, R., Tong, Z., Zhang, J., Zhai, Z., Cheng, W., Li, H., 2019. Mechanical strain promotes osteogenic differentiation of mesenchymal stem cells on TiO2 nanotubes substrate. Biochem. Biophys. Res. Commun. 511, 840–846. https://doi.org/10.1016/j.bbrc.2019.02.145
Chau, D.Y.S., Agashi, K., Shakesheff, K.M., 2008. Microparticles as tissue engineering scaffolds : manufacture, modification and manipulation. http://dx.doi.org/10.1179/174328408X341726
Chen, J., Huang, D., Wang, L., Hou, J., Zhang, H., Li, Y., Zhong, S., Wang, Y., Wu, Y., Huang, W., 2020. 3D bioprinted multiscale composite scaffolds based on gelatin methacryloyl (GelMA)/chitosan microspheres as a modular bioink for enhancing 3D neurite outgrowth and elongation. J. Colloid Interface Sci. 574, 162–173. https://doi.org/10.1016/j.jcis.2020.04.040
Chen, S.-S., Lu, X.-M., Lu, Q.-H., 2017. Effects of concave and convex substrate curvature on cell mechanics and the cytoskeleton. Chin. Chem. Lett. 28, 818–826. https://doi.org/10.1016/j.cclet.2016.10.039

Cheng, N.-C., Estes, B.T., Young, T.-H., Guilak, F., 2013. Genipin-Crosslinked Cartilage-Derived Matrix as a Scaffold for Human Adipose-Derived Stem Cell Chondrogenesis. Tissue Eng. Part A 19, 484–496. https://doi.org/10.1089/ten.tea.2012.0384

Choi, Y.H., Chung, K.H., Hong, H.B., Lee, W.S., 2018. Production of PDMS microparticles by emulsification of two phases and their potential biological application. Int. J. Polym. Mater. Polym. Biomater. 67, 686–692. https://doi.org/10.1080/00914037.2017.1375494

Christopher, G.F., Anna, S.L., 2007. Microfluidic methods for generating continuous droplet streams. J. Phys. Appl. Phys. 40, R319–R336. https://doi.org/10.1088/0022-3727/40/19/R01

Chun, K.W., Yoo, H.S., Yoon, J.J., Park, T.G., 2004. Biodegradable PLGA microcarriers for injectable delivery of chondrocytes: effect of surface modification on cell attachment and function. Biotechnol. Prog. 20, 1797–1801. https://doi.org/10.1021/bp0496981

Clause, K.C., Liu, L.J., Tobita, K., 2010. Directed stem cell differentiation: the role of physical forces. Cell Commun. Adhes. 17, 48–54. https://doi.org/10.3109/15419061.2010.492535

Contessi Negrini, N., Lipreri, M.V., Tanzi, M.C., Farè, S., 2020. In vitro cell delivery by gelatin microspheres prepared in water-in-oil emulsion. J. Mater. Sci. Mater. Med. 31, 26. https://doi.org/10.1007/s10856-020-6363-2

Coombes, A.G.A., Tasker, S., Lindblad, M., Holmgren, J., Hoste, K., Toncheva, V., Schacht, E., Davies, M.C., Illum, L., Davis, S.S., 1997. Biodegradable polymeric microparticles for drug delivery and vaccine formulation: the surface attachment of hydrophilic species using the concept of poly(ethylene glycol) anchoring segments. Biomaterials 18, 1153–1161. https://doi.org/10.1016/S0142-9612(97)00051-3

Cruz, D.M.G., Ivirico, J.L.E., Gomes, M.M., Ribelles, J.L.G., Sánchez, M.S., Reis, R.L., Mano, J.F., 2008. Chitosan microparticles as injectable scaffolds for tissue engineering. J. Tissue Eng. Regen. Med. 2, 378–380. https://doi.org/10.1002/term.106

Cumper, C.W.N., Alexander, A.E., 1952. The Viscosity and Rigidity of Gelatin in Concentrated Aqueous Systems. I. Viscosity. Aust. J. Chem. 5, 146–152. https://doi.org/10.1071/ch9520146

Cushing, M.C., Anseth, K.S., 2007. Hydrogel Cell Cultures. Science 316, 1133–1134. https://doi.org/10.1126/science.1140171

Custódio, C.A., Santo, V.E., Oliveira, M.B., Gomes, M.E., Reis, R.L., Mano, J.F., 2014. Functionalized Microparticles Producing Scaffolds in Combination with Cells. Adv. Funct. Mater. 24, 1391–1400. https://doi.org/10.1002/adfm.201301516

d'Angelo, M., Benedetti, E., Tupone, M.G., Catanesi, M., Castelli, V., Antonosante, A., Cimini, A., 2019. The Role of Stiffness in Cell Reprogramming: A Potential Role for Biomaterials in Inducing Tissue Regeneration. Cells 8, 1036. https://doi.org/10.3390/cells8091036

Dalby, M.J., Gadegaard, N., Oreffo, R.O.C., 2014. Harnessing nanotopography and integrin-matrix interactions to influence stem cell fate. Nat. Mater. 13, 558–569. https://doi.org/10.1038/nmat3980

Daly, A.C., Riley, L., Segura, T., Burdick, J.A., 2020. Hydrogel microparticles for biomedical applications. Nat. Rev. Mater. 5, 20–43. https://doi.org/10.1038/s41578-019-0148-6

Dang, T.-D., Kim, Y.H., Kim, H.G., Kim, G.M., 2012. Preparation of monodisperse PEG hydrogel microparticles using a microfluidic flow-focusing device. J. Ind. Eng. Chem. 18, 1308–1313. https://doi.org/10.1016/j.jiec.2012.01.028

Deng, J., Petersen, B.E., Steindler, D.A., Jorgensen, M.L., Laywell, E.D., 2006. Mesenchymal stem cells spontaneously express neural proteins in culture and are neurogenic after transplantation. Stem Cells Dayt. Ohio 24, 1054–1064. https://doi.org/10.1634/stemcells.2005-0370

Derjaguin, B.V., Muller, V.M., Toporov, and Y.P., 1975. Effect of contact deformations on the adhesion of particles. J Colloid Interface Sci 53, 314–326.

Dezawa, M., Ishikawa, H., Itokazu, Y., Yoshihara, T., Hoshino, M., Takeda, S., Ide, C., Nabeshima, Y., 2005. Bone Marrow Stromal Cells Generate Muscle Cells and Repair Muscle Degeneration. Science 309, 314–317. https://doi.org/10.1126/science.1110364

Discher, D.E., Janmey, P., Wang, Y.-L., 2005. Tissue cells feel and respond to the stiffness of their substrate. Science 310, 1139–1143. https://doi.org/10.1126/science.1116995
Discher, D.E., Mooney, D.J., Zandstra, P.W., 2009. Growth Factors, Matrices, and Forces Combine and Control Stem Cells. Science 324, 1673–1677. https://doi.org/10.1126/science.1171643
Discher, D.E., Smith, L., Cho, S., Colasurdo, M., García, A.J., Safran, S., 2017. Matrix Mechanosensing: From Scaling Concepts in 'Omics Data to Mechanisms in the Nucleus, Regeneration, and Cancer. Annu. Rev. Biophys. 46, 295–315. https://doi.org/10.1146/annurev-biophys-062215-011206
Docheva, D., Popov, C., Mutschler, W., Schieker, M., 2007. Human mesenchymal stem cells in contact with their environment: surface characteristics and the integrin system. J. Cell. Mol. Med. 11, 21–38. https://doi.org/10.1111/j.1582-4934.2007.00001.x
Dong, Z., Yuan, Q., Huang, K., Xu, W., Liu, G., Gu, Z., 2019. Gelatin methacryloyl (GelMA)-based biomaterials for bone regeneration. RSC Adv. 9, 17737–17744. https://doi.org/10.1039/C9RA02695A
Doyle, A.D., Yamada, K.M., 2016. Mechanosensing via cell-matrix adhesions in 3D microenvironments. Exp. Cell Res. 343, 60–66. https://doi.org/10.1016/j.yexcr.2015.10.033
Dragosavac, M.M., Sovilj, M.N., Kosvintsev, S.R., Holdich, R.G., Vladisavljević, G.T., 2008. Controlled production of oil-in-water emulsions containing unrefined pumpkin seed oil using stirred cell membrane emulsification. J. Membr. Sci. 322, 178–188. https://doi.org/10.1016/j.memsci.2008.05.026
Du, J., Chen, X., Liang, X., Zhang, G., Xu, J., He, L., Zhan, Q., Feng, X.-Q., Chien, S., Yang, C., 2011. Integrin activation and internalization on soft ECM as a mechanism of induction of stem cell differentiation by ECM elasticity. Proc. Natl. Acad. Sci. U. S. A. 108, 9466–9471. https://doi.org/10.1073/pnas.1106467108
Edmondson, R., Broglie, J.J., Adcock, A.F., Yang, L., 2014. Three-Dimensional Cell Culture Systems and Their Applications in Drug Discovery and Cell-Based Biosensors. Assay Drug Dev. Technol. 12, 207–218. https://doi.org/10.1089/adt.2014.573
Engler, A.J., Sen, S., Sweeney, H.L., Discher, D.E., 2006. Matrix elasticity directs stem cell lineage specification. Cell 126, 677–689. https://doi.org/10.1016/j.cell.2006.06.044
Evans, N., Minelli, C., Gentleman, E., LaPointe, V., Patankar, S., Kallivretaki, M., Chen, X., Roberts, C., Stevens, M., 2009. Substrate stiffness affects early differentiation events in embryonic stem cells. Eur. Cell. Mater. 18, 1–14. https://doi.org/10.22203/eCM.v018a01
Ezzell, R.M., Goldmann, W.H., Wang, N., Parasharama, N., Ingber, D.E., 1997. Vinculin Promotes Cell Spreading by Mechanically Coupling Integrins to the Cytoskeleton. Exp. Cell Res. 231, 14–26. https://doi.org/10.1006/excr.1996.3451
Fazeli, Z., Ghaderian, S.M.H., Rajabibazl, M., Salami, S., Vazifeh Shiran, N., Omrani, M.D., 2015. Expression Pattern of Neuronal Markers in PB-MSCs Treated by Growth Factors Noggin, bFGF and EGF. Int. J. Mol. Cell. Med. 4, 209–217.
Ferraro, F., Celso, C.L., Scadden, D., 2010. ADULT STEM CELLS AND THEIR NICHES. Adv. Exp. Med. Biol. 695, 155–168. https://doi.org/10.1007/978-1-4419-7037-4_11
Ferreira, S.A., Motwani, M.S., Faull, P.A., Seymour, A.J., Yu, T.T.L., Enayati, M., Taheem, D.K., Salzlechner, C., Haghighi, T., Kania, E.M., Oommen, O.P., Ahmed, T., Loaiza, S., Parzych, K., Dazzi, F., Varghese, O.P., Festy, F., Grigoriadis, A.E., Auner, H.W., Snijders, A.P., Bozec, L., Gentleman, E., 2018. Bi-directional cell-pericellular matrix interactions direct stem cell fate. Nat. Commun. 9, 4049. https://doi.org/10.1038/s41467-018-06183-4
Fioretta, E.S., Fledderus, J.O., Baaijens, F.P.T., Bouten, C.V.C., 2012. Influence of substrate stiffness on circulating progenitor cell fate. J. Biomech. 45, 736–744. https://doi.org/10.1016/j.jbiomech.2011.11.013
Fischer, S.E., Liu, X., Mao, H.-Q., Harden, J.L., 2007. Controlling cell adhesion to surfaces via associating bioactive triblock proteins. Biomaterials 28, 3325–3337. https://doi.org/10.1016/j.biomaterials.2007.03.026

Freiberg, S., Zhu, X.X., 2004. Polymer microspheres for controlled drug release. Int. J. Pharm. 282, 1–18. https://doi.org/10.1016/j.ijpharm.2004.04.013
Galluzzi, M., Biswas, C.S., Wu, Y., Wang, Q., Du, B., Stadler, F.J., 2016. Space-resolved quantitative mechanical measurements of soft and supersoft materials by atomic force microscopy. NPG Asia Mater. 8, e327. https://doi.org/10.1038/am.2016.170
Gao, G., Schilling, A.F., Hubbell, K., Yonezawa, T., Truong, D., Hong, Y., Dai, G., Cui, X., 2015. Improved properties of bone and cartilage tissue from 3D inkjet-bioprinted human mesenchymal stem cells by simultaneous deposition and photocrosslinking in PEG-GelMA. Biotechnol. Lett. 37, 2349–2355. https://doi.org/10.1007/s10529-015-1921-2
Gattazzo, F., Urciuolo, A., Bonaldo, P., 2014. Extracellular matrix: A dynamic microenvironment for stem cell niche. Biochim. Biophys. Acta BBA - Gen. Subj., Matrix-mediated cell behaviour and properties 1840, 2506–2519. https://doi.org/10.1016/j.bbagen.2014.01.010
Gauthier, N.C., Roca-Cusachs, P., 2018. Mechanosensing at integrin-mediated cell–matrix adhesions: from molecular to integrated mechanisms. Curr. Opin. Cell Biol., Cell Architecture 50, 20–26. https://doi.org/10.1016/j.ceb.2017.12.014
George, S., Hamblin, M.R., Abrahamse, H., 2019. Differentiation of Mesenchymal Stem Cells to Neuroglia: in the Context of Cell Signalling. Stem Cell Rev. Rep. 15, 814–826. https://doi.org/10.1007/s12015-019-09917-z
Ghassemi, S., Meacci, G., Liu, S., Gondarenko, A.A., Mathur, A., Roca-Cusachs, P., Sheetz, M.P., Hone, J., 2012. Cells test substrate rigidity by local contractions on submicrometer pillars. Proc. Natl. Acad. Sci. 109, 5328–5333. https://doi.org/10.1073/pnas.1119886109
Goetzke, R., Sechi, A., De Laporte, L., Neuss, S., Wagner, W., 2018. Why the impact of mechanical stimuli on stem cells remains a challenge. Cell. Mol. Life Sci. CMLS 75, 3297–3312. https://doi.org/10.1007/s00018-018-2830-z
Gomez-Florit, M., Pardo, A., Domingues, R.M.A., Graça, A.L., Babo, P.S., Reis, R.L., Gomes, M.E., 2020. Natural-Based Hydrogels for Tissue Engineering Applications. Molecules 25, 5858. https://doi.org/10.3390/molecules25245858
Gong, J., Jaiswal, R., Dalla, P., Luk, F., Bebawy, M., 2015. Microparticles in cancer: A review of recent developments and the potential for clinical application. Semin. Cell Dev. Biol. 40, 35–40. https://doi.org/10.1016/j.semcdb.2015.03.009
Gronthos, S., Simmons, P.J., Graves, S.E., Robey, P.G., 2001. Integrin-mediated interactions between human bone marrow stromal precursor cells and the extracellular matrix. Bone 28, 174–181. https://doi.org/10.1016/s8756-3282(00)00424-5
Grover, C.N., Gwynne, J.H., Pugh, N., Hamaia, S., Farndale, R.W., Best, S.M., Cameron, R.E., 2012. Crosslinking and composition influence the surface properties, mechanical stiffness and cell reactivity of collagen-based films. Acta Biomater. 8, 3080–3090. https://doi.org/10.1016/j.actbio.2012.05.006
Gunatillake, P., Mayadunne, R., Adhikari, R., 2006. Recent developments in biodegradable synthetic polymers. Biotechnol. Annu. Rev. 12, 301–347. https://doi.org/10.1016/S1387-2656(06)12009-8
Gunetti, M., Tomasi, S., Giammò, A., Boido, M., Rustichelli, D., Mareschi, K., Errichiello, E., Parola, M., Ferrero, I., Fagioli, F., Vercelli, A., Carone, R., 2012. Myogenic Potential of Whole Bone Marrow Mesenchymal Stem Cells In Vitro and In Vivo for Usage in Urinary Incontinence. PLoS ONE 7. https://doi.org/10.1371/journal.pone.0045538
Guo, D., Xie, G., Luo, J., 2014. Mechanical properties of nanoparticles: basics and applications. J. Phys. Appl. Phys. 47, 013001. https://doi.org/10.1088/0022-3727/47/1/013001
Gupta, A., 2019. An Overview of In Situ Gel Forming Implants: Current Approach Towards Alternative Drug Delivery System 5, 14–21.
Guvendiren, M., Burdick, J.A., 2012. Stiffening hydrogels to probe short- and long-term cellular responses to dynamic mechanics. Nat. Commun. 3, 792. https://doi.org/10.1038/ncomms1792

Ha, J.-L., Fung, R.-F., Chen, Y.-C., 2004. Dynamic Responses of an Atomic Force Microscope Interacting with Samples. J. Dyn. Syst. Meas. Control 127, 705–709. https://doi.org/10.1115/1.2101851

Harley, B.A.C., Kim, H.-D., Zaman, M.H., Yannas, I.V., Lauffenburger, D.A., Gibson, L.J., 2008. Microarchitecture of three-dimensional scaffolds influences cell migration behavior via junction interactions. Biophys. J. 95, 4013–4024. https://doi.org/10.1529/biophysj.107.122598

Hashmi, S.M., Dufresne, E.R., 2009. Mechanical properties of individual microgel particles through the deswelling transition. Soft Matter 5, 3682–3688. https://doi.org/10.1039/B906051K

Higuchi, A., Ling, Q.-D., Chang, Y., Hsu, S.-T., Umezawa, A., 2013. Physical cues of biomaterials guide stem cell differentiation fate. Chem. Rev. 113, 3297–3328. https://doi.org/10.1021/cr300426x

Hoarau-Véchot, J., Rafii, A., Touboul, C., Pasquier, J., 2018. Halfway between 2D and Animal Models: Are 3D Cultures the Ideal Tool to Study Cancer-Microenvironment Interactions? Int. J. Mol. Sci. 19, E181. https://doi.org/10.3390/ijms19010181

Hoch, E., Schuh, C., Hirth, T., Tovar, G.E.M., Borchers, K., 2012. Stiff gelatin hydrogels can be photo-chemically synthesized from low viscous gelatin solutions using molecularly functionalized gelatin with a high degree of methacrylation. J. Mater. Sci. Mater. Med. 23, 2607–2617. https://doi.org/10.1007/s10856-012-4731-2

Hodgson, B., Mafi, R., Mafi, P., Khan, W., 2018. The Regulation of Differentiation of Mesenchymal Stem-cells into Skeletal Muscle: A Look at Signalling Molecules Involved in Myogenesis. https://doi.org/10.17863/CAM.33246

Holland, T.A., Tabata, Y., Mikos, A.G., 2005. Dual growth factor delivery from degradable oligo(poly(ethylene glycol) fumarate) hydrogel scaffolds for cartilage tissue engineering. J. Control. Release Off. J. Control. Release Soc. 101, 111–125. https://doi.org/10.1016/j.jconrel.2004.07.004

Hu, L., Yin, C., Zhao, F., Ali, A., Ma, J., Qian, A., 2018. Mesenchymal Stem Cells: Cell Fate Decision to Osteoblast or Adipocyte and Application in Osteoporosis Treatment. Int. J. Mol. Sci. 19. https://doi.org/10.3390/ijms19020360

Huang, H., Ding, Y., Sun, X.S., Nguyen, T.A., 2013. Peptide Hydrogelation and Cell Encapsulation for 3D Culture of MCF-7 Breast Cancer Cells. PLoS ONE 8. https://doi.org/10.1371/journal.pone.0059482

Huang, X., Yang, N., Fiore, V.F., Barker, T.H., Sun, Y., Morris, S.W., Ding, Q., Thannickal, V.J., Zhou, Y., 2012. Matrix stiffness-induced myofibroblast differentiation is mediated by intrinsic mechanotransduction. Am. J. Respir. Cell Mol. Biol. 47, 340–348. https://doi.org/10.1165/rcmb.2012-0050OC

Humphrey, J.D., Dufresne, E.R., Schwartz, M.A., 2014. Mechanotransduction and extracellular matrix homeostasis. Nat. Rev. Mol. Cell Biol. 15, 802–812. https://doi.org/10.1038/nrm3896

Hutmacher, D.W., 2000. Scaffolds in tissue engineering bone and cartilage. Biomaterials 21, 2529–2543.

Iskratsch, T., Wolfenson, H., Sheetz, M.P., 2014. Appreciating force and shape—the rise of mechanotransduction in cell biology. Nat. Rev. Mol. Cell Biol. 15, 825–833. https://doi.org/10.1038/nrm3903

Johnson, C.P., Tang, H.-Y., Carag, C., Speicher, D.W., Discher, D.E., 2007. Forced Unfolding of Proteins Within Cells. Science 317, 663–666. https://doi.org/10.1126/science.1139857

Jung, J., Oh, J., 2014. Cell-induced flow-focusing instability in gelatin methacrylate microdroplet generation. Biomicrofluidics 8, 036503. https://doi.org/10.1063/1.4880375

Kaback, L.A., Soung, D.Y., Naik, A., Smith, N., Schwarz, E.M., O'Keefe, R.J., Drissi, H., 2008. Osterix/Sp7 regulates mesenchymal stem cell mediated endochondral ossification. J. Cell. Physiol. 214, 173–182. https://doi.org/10.1002/jcp.21176

Kapałczyńska, M., Kolenda, T., Przybyła, W., Zajączkowska, M., Teresiak, A., Filas, V., Ibbs, M., Bliźniak, R., Łuczewski, Ł., Lamperska, K., 2018. 2D and 3D cell cultures – a comparison of different types of cancer cell cultures. Arch. Med. Sci. AMS 14, 910–919. https://doi.org/10.5114/aoms.2016.63743

Kasten, A., Müller, P., Bulnheim, U., Groll, J., Bruellhoff, K., Beck, U., Steinhoff, G., Möller, M., Rychly, J., 2010. Mechanical integrin stress and magnetic forces induce biological responses in mesenchymal stem cells which depend on environmental factors. J. Cell. Biochem. 111, 1586–1597. https://doi.org/10.1002/jcb.22890

Katayama, Y., Battista, M., Kao, W.-M., Hidalgo, A., Peired, A.J., Thomas, S.A., Frenette, P.S., 2006. Signals from the Sympathetic Nervous System Regulate Hematopoietic Stem Cell Egress from Bone Marrow. Cell 124, 407–421. https://doi.org/10.1016/j.cell.2005.10.041

Kawaguchi, H., 2000. Functional polymer microspheres. Prog. Polym. Sci. 25, 1171–1210. https://doi.org/10.1016/S0079-6700(00)00024-1

Kawakami, K., Tatsumi, H., Sokabe, M., 2001. Dynamics of integrin clustering at focal contacts of endothelial cells studied by multimode imaging microscopy. J. Cell Sci. 114, 3125–3135.

Kerscher, P., Turnbull, I.C., Hodge, A.J., Kim, J., Seliktar, D., Easley, C.J., Costa, K.D., Lipke, E.A., 2016. Direct hydrogel encapsulation of pluripotent stem cells enables ontomimetic differentiation and growth of engineered human heart tissues. Biomaterials 83, 383–395. https://doi.org/10.1016/j.biomaterials.2015.12.011

Khetan, S., Guvendiren, M., Legant, W.R., Cohen, D.M., Chen, C.S., Burdick, J.A., 2013. Degradation-mediated cellular traction directs stem cell fate in covalently crosslinked three-dimensional hydrogels. Nat. Mater. 12, 458–465. https://doi.org/10.1038/nmat3586

Kilian, K.A., Bugarija, B., Lahn, B.T., Mrksich, M., 2010. Geometric cues for directing the differentiation of mesenchymal stem cells. Proc. Natl. Acad. Sci. U. S. A. 107, 4872–4877. https://doi.org/10.1073/pnas.0903269107

Kim, C., Young, J.L., Holle, A.W., Jeong, K., Major, L.G., Jeong, J.H., Aman, Z.M., Han, D.-W., Hwang, Y., Spatz, J.P., Choi, Y.S., 2020. Stem Cell Mechanosensation on Gelatin Methacryloyl (GelMA) Stiffness Gradient Hydrogels. Ann. Biomed. Eng. 48, 893–902. https://doi.org/10.1007/s10439-019-02428-5

Kim, J.B., 2005. Three-dimensional tissue culture models in cancer biology. Semin. Cancer Biol. 15, 365–377. https://doi.org/10.1016/j.semcancer.2005.05.002

Kim, J.-S., Lim, J.-H., Nam, H.-Y., Lim, H.-J., Shin, J.-S., Shin, J.-Y., Ryu, J.-H., Kim, K., Kwon, I.-C., Jin, S.-M., Kim, H.-R., Kim, S.-J., Park, C.-G., 2012. In situ application of hydrogel-type fibrin-islet composite optimized for rapid glycemic control by subcutaneous xenogeneic porcine islet transplantation. J. Control. Release Off. J. Control. Release Soc. 162, 382–390. https://doi.org/10.1016/j.jconrel.2012.07.018

Kirby, G.T.S., White, L.J., Rahman, C.V., Cox, H.C., Qutachi, O., Rose, F.R.A.J., Hutmacher, D.W., Shakesheff, K.M., Woodruff, M.A., 2011. PLGA-Based Microparticles for the Sustained Release of BMP-2. Polymers 3, 571–586. https://doi.org/10.3390/polym3010571

Kopf, B.S., Schipanski, A., Rottmar, M., Berner, S., Maniura-Weber, K., 2015. Enhanced differentiation of human osteoblasts on Ti surfaces pre-treated with human whole blood. Acta Biomater. 19, 180–190. https://doi.org/10.1016/j.actbio.2015.03.022

Kumar, A., Placone, J.K., Engler, A.J., 2017. Understanding the extracellular forces that determine cell fate and maintenance. Dev. Camb. Engl. 144, 4261–4270. https://doi.org/10.1242/dev.158469

Kumar, S.S., Hsiao, J.-H., Ling, Q.-D., Dulinska-Molak, I., Chen, G., Chang, Yung, Chang, Yu, Chen, Y.H., Chen, D.-C., Hsu, S.-T., Higuchi, A., 2013. The combined influence of substrate elasticity and surface-grafted molecules on the ex vivo expansion of hematopoietic stem and progenitor cells. Biomaterials 34, 7632–7644. https://doi.org/10.1016/j.biomaterials.2013.07.002

Kuroda, M., Wada, H., Kimura, Y., Ueda, K., Kioka, N., 2017. Vinculin promotes nuclear localization of TAZ to inhibit ECM stiffness-dependent differentiation into adipocytes. J. Cell Sci. 130, 989–1002. https://doi.org/10.1242/jcs.194779

Kuznetsova, T.G., Starodubtseva, M.N., Yegorenkov, N.I., Chizhik, S.A., Zhdanov, R.I., 2007. Atomic force microscopy probing of cell elasticity. Micron, Microscopy in Nanobiotechnology 38, 824–833. https://doi.org/10.1016/j.micron.2007.06.011

Labriola, N.R., Sadick, J.S., Morgan, J.R., Mathiowitz, E., Darling, E.M., 2018. Cell Mimicking Microparticles Influence the Organization, Growth, and Mechanophenotype of Stem Cell Spheroids. Ann. Biomed. Eng. 46, 1146–1159. https://doi.org/10.1007/s10439-018-2028-4

Langer, R., Vacanti, J.P., 1993. Tissue engineering. Science 260, 920–926.

Laurencin, C.T., Nair, L.S., 2014. Nanotechnology and Regenerative Engineering: The Scaffold, Second Edition. CRC Press.

Lee, D.A., Knight, M.M., Campbell, J.J., Bader, D.L., 2011. Stem cell mechanobiology. J. Cell. Biochem. 112, 1–9. https://doi.org/10.1002/jcb.22758

Lee, J., Cuddihy, M.J., Kotov, N.A., 2008. Three-dimensional cell culture matrices: state of the art. Tissue Eng. Part B Rev. 14, 61–86. https://doi.org/10.1089/teb.2007.0150

Lee, J.-H., Kim, H.-W., 2018. Emerging properties of hydrogels in tissue engineering. J. Tissue Eng. 9, 2041731418768285. https://doi.org/10.1177/2041731418768285

Leng, X., Zhang, W., Wang, C., Cui, L., Yang, C.J., 2010. Agarose droplet microfluidics for highly parallel and efficient single molecule emulsion PCR. Lab. Chip 10, 2841–2843. https://doi.org/10.1039/C0LC00145G

Li, Y., Jin, D., Xie, W., Wen, L., Chen, W., Xu, J., Ding, J., Ren, D., 2018. PPAR-γ and Wnt Regulate the Differentiation of MSCs into Adipocytes and Osteoblasts Respectively. Curr. Stem Cell Res. Ther. 13, 185–192. https://doi.org/10.2174/1574888X12666171012141908

Liang, H.-C., Chang, W.-H., Liang, H.-F., Lee, M.-H., Sung, H.-W., 2004. Crosslinking structures of gelatin hydrogels crosslinked with genipin or a water-soluble carbodiimide. J. Appl. Polym. Sci. 91, 4017–4026. https://doi.org/10.1002/app.13563

Liu, C., Xia, Z., Czernuszka, J.T., 2007. Design and Development of Three-Dimensional Scaffolds for Tissue Engineering. Chem. Eng. Res. Des. 85, 1051–1064. https://doi.org/10.1205/cherd06196

Liu, M., Zeng, X., Ma, C., Yi, H., Ali, Z., Mou, X., Li, S., Deng, Y., He, N., 2017. Injectable hydrogels for cartilage and bone tissue engineering. Bone Res. 5, 1–20. https://doi.org/10.1038/boneres.2017.14

Low, B.C., Pan, C.Q., Shivashankar, G.V., Bershadsky, A., Sudol, M., Sheetz, M., 2014. YAP/TAZ as mechanosensors and mechanotransducers in regulating organ size and tumor growth. FEBS Lett. 588, 2663–2670. https://doi.org/10.1016/j.febslet.2014.04.012

Lu, Y.-C., Song, W., An, D., Jun Kim, B., Schwartz, R., Wu, M., Ma, M., 2015. Designing compartmentalized hydrogel microparticles for cell encapsulation and scalable 3D cell culture. J. Mater. Chem. B 3, 353–360. https://doi.org/10.1039/C4TB01735H

Luu, Y.K., Pessin, J.E., Judex, S., Rubin, J., Rubin, C.T., 2009. Mechanical Signals As a Non-Invasive Means to Influence Mesenchymal Stem Cell Fate, Promoting Bone and Suppressing the Fat Phenotype. BoneKEy Osteovision 6, 132–149. https://doi.org/10.1138/20090371

Major, L.G., Holle, A.W., Young, J.L., Hepburn, M.S., Jeong, K., Chin, I.L., Sanderson, R.W., Jeong, J.H., Aman, Z.M., Kennedy, B.F., Hwang, Y., Han, D.-W., Park, H.W., Guan, K.-L., Spatz, J.P., Choi, Y.S., 2019. Volume Adaptation Controls Stem Cell Mechanotransduction. ACS Appl. Mater. Interfaces 11, 45520–45530. https://doi.org/10.1021/acsami.9b19770

Malafaya, P.B., Silva, G.A., Reis, R.L., 2007. Natural-origin polymers as carriers and scaffolds for biomolecules and cell delivery in tissue engineering applications. Adv. Drug Deliv. Rev. 59, 207–233. https://doi.org/10.1016/j.addr.2007.03.012

Mansard, V., Mecca, J.M., Dermody, D.L., Malotky, D., Tucker, C.J., Squires, T.M., 2016. Collective Rayleigh-Plateau Instability: A Mimic of Droplet Breakup in High Internal Phase Emulsion. Langmuir 32, 2549–2555. https://doi.org/10.1021/acs.langmuir.5b04727

Mason, C., Dunnill, P., 2007. A brief definition of regenerative medicine. Regen. Med. 3, 1–5. https://doi.org/10.2217/17460751.3.1.1

Mata, E., Igartua, M., Patarroyo, M.E., Pedraz, J.L., Hernández, R.M., 2011. Enhancing immunogenicity to PLGA microparticulate systems by incorporation of alginate and RGD-modified alginate. Eur. J. Pharm. Sci. 44, 32–40. https://doi.org/10.1016/j.ejps.2011.05.015

MBINFO Defining Mechanobiology, n.d. How do Focal Adhesions Facilitate Mechanosensing? [WWW Document]. MBInfo. URL https://www.mechanobio.info/what-is-mechanobiology/how-do-focal-adhesions-facilitate-mechanosensing/ (accessed 1.3.21).

McBeath, R., Pirone, D.M., Nelson, C.M., Bhadriraju, K., Chen, C.S., 2004a. Cell shape, cytoskeletal tension, and RhoA regulate stem cell lineage commitment. Dev. Cell 6, 483–495. https://doi.org/10.1016/s1534-5807(04)00075-9

McBeath, R., Pirone, D.M., Nelson, C.M., Bhadriraju, K., Chen, C.S., 2004b. Cell Shape, Cytoskeletal Tension, and RhoA Regulate Stem Cell Lineage Commitment. Dev. Cell 6, 483–495. https://doi.org/10.1016/S1534-5807(04)00075-9

McNamara, L.E., Burchmore, R., Riehle, M.O., Herzyk, P., Biggs, M.J.P., Wilkinson, C.D.W., Curtis, A.S.G., Dalby, M.J., 2012. The role of microtopography in cellular mechanotransduction. Biomaterials 33, 2835–2847. https://doi.org/10.1016/j.biomaterials.2011.11.047

McQuin, C., Goodman, A., Chernyshev, V., Kamentsky, L., Cimini, B.A., Karhohs, K.W., Doan, M., Ding, L., Rafelski, S.M., Thirstrup, D., Wiegraebe, W., Singh, S., Becker, T., Caicedo, J.C., Carpenter, A.E., 2018. CellProfiler 3.0: Next-generation image processing for biology. PLoS Biol. 16, e2005970. https://doi.org/10.1371/journal.pbio.2005970

Miyamoto, S., Teramoto, H., Coso, O.A., Gutkind, J.S., Burbelo, P.D., Akiyama, S.K., Yamada, K.M., 1995. Integrin function: molecular hierarchies of cytoskeletal and signaling molecules. J. Cell Biol. 131, 791–805. https://doi.org/10.1083/jcb.131.3.791

Moelbert, S., Normand, B., De Los Rios, P., 2004. Kosmotropes and chaotropes: modelling preferential exclusion, binding and aggregate stability. Biophys. Chem. 112, 45–57. https://doi.org/10.1016/j.bpc.2004.06.012

Moore, K.A., Lemischka, I.R., 2006. Stem cells and their niches. Science 311, 1880–1885. https://doi.org/10.1126/science.1110542

Moore, S.W., Roca-Cusachs, P., Sheetz, M.P., 2010. Stretchy Proteins on Stretchy Substrates: The Important Elements of Integrin-Mediated Rigidity Sensing. Dev. Cell 19, 194–206. https://doi.org/10.1016/j.devcel.2010.07.018

Moreira, A., Carneiro, J., Campos, J.B.L.M., Miranda, J.M., 2021. Production of hydrogel microparticles in microfluidic devices: a review. Microfluid. Nanofluidics 25, 10. https://doi.org/10.1007/s10404-020-02413-8

Müller, W.E.G., Tolba, E., Ackermann, M., Neufurth, M., Wang, S., Feng, Q., Schröder, H.C., Wang, X., 2017. Fabrication of amorphous strontium polyphosphate microparticles that induce mineralization of bone cells in vitro and in vivo. Acta Biomater. 50, 89–101. https://doi.org/10.1016/j.actbio.2016.12.045

Mulligan, M.K., Rothstein, J.P., 2012. Scale-up and control of droplet production in coupled microfluidic flow-focusing geometries. Microfluid. Nanofluidics 13, 65–73. https://doi.org/10.1007/s10404-012-0941-7

Nagai, A., Kim, W.K., Lee, H.J., Jeong, H.S., Kim, K.S., Hong, S.H., Park, I.H., Kim, S.U., 2007. Multilineage Potential of Stable Human Mesenchymal Stem Cell Line Derived from Fetal Marrow. PLOS ONE 2, e1272. https://doi.org/10.1371/journal.pone.0001272

Nair, L.S., Laurencin, C.T., 2007. Biodegradable polymers as biomaterials. Prog. Polym. Sci., Polymers in Biomedical Applications 32, 762–798. https://doi.org/10.1016/j.progpolymsci.2007.05.017

Nakada, D., Levi, B.P., Morrison, S.J., 2011. Integrating physiological regulation with stem cell and tissue homeostasis. Neuron 70, 703–718. https://doi.org/10.1016/j.neuron.2011.05.011
Naqvi, S.M., McNamara, L.M., 2020. Stem Cell Mechanobiology and the Role of Biomaterials in Governing Mechanotransduction and Matrix Production for Tissue Regeneration. Front. Bioeng. Biotechnol. 8, 1375. https://doi.org/10.3389/fbioe.2020.597661
Neirinckx, V., Coste, C., Rogister, B., Gendebien, S.W.-, 2013. Neural Fate of Mesenchymal Stem Cells and Neural Crest Stem Cells: Which Ways to Get Neurons for Cell Therapy Purpose? Trends Cell Signal. Pathw. Neuronal Fate Decis. https://doi.org/10.5772/53260
Nerem, R.M., Schutte, S.C., 2014. Chapter 2 - The Challenge of Imitating Nature, in: Principles of Tissue Engineering (Fourth Edition). Academic Press, Boston, pp. 9–24. https://doi.org/10.1016/B978-0-12-398358-9.00002-1
Neto, M.D., Oliveira, M.B., Mano, J.F., 2019. Microparticles in Contact with Cells: From Carriers to Multifunctional Tissue Modulators. Trends Biotechnol. 37, 1011–1028. https://doi.org/10.1016/j.tibtech.2019.02.008
Nguyen, A.H., McKinney, J., Miller, T., Bongiorno, T., McDevitt, T.C., 2015. Gelatin methacrylate microspheres for controlled growth factor release. Acta Biomater. 13, 101–110. https://doi.org/10.1016/j.actbio.2014.11.028
Nichol, J.W., Koshy, S.T., Bae, H., Hwang, C.M., Yamanlar, S., Khademhosseini, A., 2010. Cell-laden microengineered gelatin methacrylate hydrogels. Biomaterials 31, 5536–5544. https://doi.org/10.1016/j.biomaterials.2010.03.064
Nihant, N., Schugens, C., Grandfils, C., Jérôme, R., Teyssié, P., 1994. Polylactide microparticles prepared by double emulsion/evaporation technique. I. Effect of primary emulsion stability. Pharm. Res. 11, 1479–1484.
Notbohm, J., Poon, B., Ravichandran, G., 2012. Analysis of nanoindentation of soft materials with an atomic force microscope. J. Mater. Res. 27, 229–237. https://doi.org/10.1557/jmr.2011.252
O'Brien, F.J., Harley, B.A., Yannas, I.V., Gibson, L.J., 2005. The effect of pore size on cell adhesion in collagen-GAG scaffolds. Biomaterials 26, 433–441. https://doi.org/10.1016/j.biomaterials.2004.02.052
Ogawa, T., Akazawa, T., Tabata, Y., 2010. In vitro proliferation and chondrogenic differentiation of rat bone marrow stem cells cultured with gelatin hydrogel microspheres for TGF-beta1 release. J. Biomater. Sci. Polym. Ed. 21, 609–621. https://doi.org/10.1163/156856209X434638
Okamoto, T., Aoyama, T., Nakayama, T., Nakamata, T., Hosaka, T., Nishijo, K., Nakamura, T., Kiyono, T., Toguchida, J., 2002. Clonal heterogeneity in differentiation potential of immortalized human mesenchymal stem cells. Biochem. Biophys. Res. Commun. 295, 354–361.
Olivares-Navarrete, R., Lee, E.M., Smith, K., Hyzy, S.L., Doroudi, M., Williams, J.K., Gall, K., Boyan, B.D., Schwartz, Z., 2017. Substrate Stiffness Controls Osteoblastic and Chondrocytic Differentiation of Mesenchymal Stem Cells without Exogenous Stimuli. PLOS ONE 12, e0170312. https://doi.org/10.1371/journal.pone.0170312
Oliveira, M.B., Mano, J.F., 2011. Polymer-based microparticles in tissue engineering and regenerative medicine. Biotechnol. Prog. 27, 897–912. https://doi.org/10.1002/btpr.618
Östlund, C., Folker, E.S., Choi, J.C., Gomes, E.R., Gundersen, G.G., Worman, H.J., 2009. Dynamics and molecular interactions of linker of nucleoskeleton and cytoskeleton (LINC) complex proteins. J. Cell Sci. 122, 4099–4108. https://doi.org/10.1242/jcs.057075
Pandey, A., Singh, U., Momin, M., Bhavsar, C., 2017. Chitosan: Application in tissue engineering and skin grafting. J. Polym. Res. 24. https://doi.org/10.1007/s10965-017-1286-4
Park, J.S., Chu, J.S., Tsou, A.D., Diop, R., Tang, Z., Wang, A., Li, S., 2011. The effect of matrix stiffness on the differentiation of mesenchymal stem cells in response to TGF-β. Biomaterials 32, 3921–3930. https://doi.org/10.1016/j.biomaterials.2011.02.019

Park, J.S., Huang, N.F., Kurpinski, K.T., Patel, S., Hsu, S., Li, S., 2007. Mechanobiology of mesenchymal stem cells and their use in cardiovascular repair. Front. Biosci. J. Virtual Libr. 12, 5098–5116. https://doi.org/10.2741/2551

Park, K.-S., Kim, C., Nam, J.-O., Kang, S.-M., Lee, C.-S., 2016. Synthesis and characterization of thermosensitive gelatin hydrogel microspheres in a microfluidic system. Macromol. Res. 24, 529–536. https://doi.org/10.1007/s13233-016-4069-6

Patel, Z.S., Yamamoto, M., Ueda, H., Tabata, Y., Mikos, A.G., 2008. Biodegradable gelatin microparticles as delivery systems for the controlled release of bone morphogenetic protein-2. Acta Biomater. 4, 1126–1138. https://doi.org/10.1016/j.actbio.2008.04.002

Pinheiro, A., Cooley, A., Liao, J., Prabhu, R., Elder, S., 2016. Comparison of natural crosslinking agents for the stabilization of xenogenic articular cartilage. J. Orthop. Res. Off. Publ. Orthop. Res. Soc. 34, 1037–1046. https://doi.org/10.1002/jor.23121

Piskin, E., Tuncel, A., Denizli, A., Ayhan, H., 1994. Monosize microbeads based on polystyrene and their modified forms for some selected medical and biological applications. J. Biomater. Sci. Polym. Ed. 5, 451–471. https://doi.org/10.1163/156856294X00149

Pittenger, M.F., 1999. Multilineage Potential of Adult Human Mesenchymal Stem Cells. Science 284, 143–147. https://doi.org/10.1126/science.284.5411.143

Plotnikov, S.V., Pasapera, A.M., Sabass, B., Waterman, C.M., 2012. Force fluctuations within focal adhesions mediate ECM-rigidity sensing to guide directed cell migration. Cell 151, 1513–1527. https://doi.org/10.1016/j.cell.2012.11.034

Polo-Corrales, L., Latorre-Esteves, M., Ramirez-Vick, J.E., 2014. Scaffold Design for Bone Regeneration. J. Nanosci. Nanotechnol. 14, 15–56.

Pongkitwitoon, S., Uzer, G., Rubin, J., Judex, S., 2016. Cytoskeletal Configuration Modulates Mechanically Induced Changes in Mesenchymal Stem Cell Osteogenesis, Morphology, and Stiffness. Sci. Rep. 6, 34791. https://doi.org/10.1038/srep34791

Prestwich, G.D., Atzet, S., 2013. Chapter I.2.7 - Engineered Natural Materials, in: Ratner, B.D., Hoffman, A.S., Schoen, F.J., Lemons, J.E. (Eds.), Biomaterials Science (Third Edition). Academic Press, pp. 195–209. https://doi.org/10.1016/B978-0-08-087780-8.00022-X

Promkotra, S., Kangsadan, T., 2013. Characteristic Behaviors in Compressive Strength of Two-Dimensional Aggregates [WWW Document]. Adv. Mater. Res. https://doi.org/10.4028/www.scientific.net/AMR.746.293

Qi, T., Weng, J., Yu, F., Zhang, W., Li, G., Qin, H., Tan, Z., Zeng, H., 2021. Insights into the Role of Magnesium Ions in Affecting Osteogenic Differentiation of Mesenchymal Stem Cells. Biol. Trace Elem. Res. 199, 559–567. https://doi.org/10.1007/s12011-020-02183-y

Quantitative Imaging of Living Biological Samples Using PeakForce QNM [WWW Document], 2012. . AZoNano.com. URL https://www.azonano.com/article.aspx?ArticleID=3026 (accessed 3.2.21).

Ravindran, S., Song, Y., George, A., 2010. Development of three-dimensional biomimetic scaffold to study epithelial-mesenchymal interactions. Tissue Eng. Part A 16, 327–342. https://doi.org/10.1089/ten.TEA.2009.0110

Ravivarapu, H.B., Burton, K., DeLuca, P.P., 2000. Polymer and microsphere blending to alter the release of a peptide from PLGA microspheres. Eur. J. Pharm. Biopharm. 50, 263–270. https://doi.org/10.1016/S0939-6411(00)00099-0

Reddy, M.S.B., Ponnamma, D., Choudhary, R., Sadasivuni, K.K., 2021. A Comparative Review of Natural and Synthetic Biopolymer Composite Scaffolds. Polymers 13, 1105. https://doi.org/10.3390/polym13071105

Rodrigues, M.T., Leonor, I.B., Gröen, N., Viegas, C.A., Dias, I.R., Caridade, S.G., Mano, J.F., Gomes, M.E., Reis, R.L., 2014. Bone marrow stromal cells on a three-dimensional bioactive fiber mesh undergo osteogenic differentiation in the absence of osteogenic media supplements: the effect of silanol groups. Acta Biomater. 10, 4175–4185. https://doi.org/10.1016/j.actbio.2014.05.026

Rowlands, A.S., George, P.A., Cooper-White, J.J., 2008. Directing osteogenic and myogenic differentiation of MSCs: interplay of stiffness and adhesive ligand presentation. Am. J. Physiol.-Cell Physiol. 295, C1037–C1044. https://doi.org/10.1152/ajpcell.67.2008

Samanipour, R., Wang, Z., Ahmadi, A., Kim, K., 2016. Experimental and computational study of microfluidic flow-focusing generation of gelatin methacrylate hydrogel droplets. J. Appl. Polym. Sci. 133. https://doi.org/10.1002/app.43701

Santo, V.E., Gomes, M.E., Mano, J.F., Reis, R.L., 2013. Controlled Release Strategies for Bone, Cartilage, and Osteochondral Engineering—Part II: Challenges on the Evolution from Single to Multiple Bioactive Factor Delivery. Tissue Eng. Part B Rev. 19, 327–352. https://doi.org/10.1089/ten.teb.2012.0727

Scadden, D.T., 2006. The stem-cell niche as an entity of action. Nature 441, 1075–1079. https://doi.org/10.1038/nature04957

Schrader, J., Gordon-Walker, T.T., Aucott, R.L., Deemter, M. van, Quaas, A., Walsh, S., Benten, D., Forbes, S.J., Wells, R.G., Iredale, J.P., 2011. Matrix stiffness modulates proliferation, chemotherapeutic response, and dormancy in hepatocellular carcinoma cells. Hepatology 53, 1192–1205. https://doi.org/10.1002/hep.24108

Scuteri, A., Miloso, M., Foudah, D., Orciani, M., Cavaletti, G., Tredici, G., 2011. Mesenchymal stem cells neuronal differentiation ability: a real perspective for nervous system repair? Curr. Stem Cell Res. Ther. 6, 82–92. https://doi.org/10.2174/157488811795495486

Sekiya, I., Larson, B.L., Vuoristo, J.T., Cui, J.-G., Prockop, D.J., 2004. Adipogenic Differentiation of Human Adult Stem Cells From Bone Marrow Stroma (MSCs). J. Bone Miner. Res. 19, 256–264. https://doi.org/10.1359/JBMR.0301220

Sell, S.A., McClure, M.J., Garg, K., Wolfe, P.S., Bowlin, G.L., 2009. Electrospinning of collagen/biopolymers for regenerative medicine and cardiovascular tissue engineering. Adv. Drug Deliv. Rev. 61, 1007–1019. https://doi.org/10.1016/j.addr.2009.07.012

Sezer, U.A., Arslantunali, D., Aksoy, E.A., Hasirci, V., Hasirci, N., 2014. Poly(ε-caprolactone) composite scaffolds loaded with gentamicin-containing β-tricalcium phosphate/gelatin microspheres for bone tissue engineering applications. J. Appl. Polym. Sci. 131. https://doi.org/10.1002/app.40110

Shafrir, Y., Forgacs, G., 2002. Mechanotransduction through the cytoskeleton. Am. J. Physiol.-Cell Physiol. 282, C479–C486. https://doi.org/10.1152/ajpcell.00394.2001

Shalumon, K.T., Sheu, C., Fong, Y.T., Liao, H.-T., Chen, J.-P., 2016. Microsphere-Based Hierarchically Juxtapositioned Biphasic Scaffolds Prepared from Poly(Lactic-co-Glycolic Acid) and Nanohydroxyapatite for Osteochondral Tissue Engineering. Polymers 8, 429. https://doi.org/10.3390/polym8120429

Shi, Y., Dong, Y., Duan, Y., Jiang, X., Chen, C., Deng, L., 2013. Substrate stiffness influences TGF-β1-induced differentiation of bronchial fibroblasts into myofibroblasts in airway remodeling. Mol. Med. Rep. 7, 419–424. https://doi.org/10.3892/mmr.2012.1213

Shih, D.T., Lee, D.-C., Chen, S.-C., Tsai, R.-Y., Huang, C.-T., Tsai, C.-C., Shen, E.-Y., Chiu, W.-T., 2005. Isolation and characterization of neurogenic mesenchymal stem cells in human scalp tissue. Stem Cells Dayt. Ohio 23, 1012–1020. https://doi.org/10.1634/stemcells.2004-0125

Shih, Y.-R.V., Tseng, K.-F., Lai, H.-Y., Lin, C.-H., Lee, O.K., 2011. Matrix stiffness regulation of integrin-mediated mechanotransduction during osteogenic differentiation of human mesenchymal stem cells. J. Bone Miner. Res. Off. J. Am. Soc. Bone Miner. Res. 26, 730–738. https://doi.org/10.1002/jbmr.278

Shirahama, H., Lee, B.H., Tan, L.P., Cho, N.-J., 2016. Precise Tuning of Facile One-Pot Gelatin Methacryloyl (GelMA) Synthesis. Sci. Rep. 6, 31036. https://doi.org/10.1038/srep31036

Silich, L.M., Zayats, N.I., Chudakov, O.P., Shandyukova, M.A., Gailevich, S.A., 1992. Glass-ceramic bioimplants. Glass Ceram. 49, 197–200. https://doi.org/10.1007/BF00676999

Smith, D., Herman, C., Razdan, S., Abedin, M.R., Stoecker, W.V., Barua, S., 2019. Microparticles for Suspension Culture of Mammalian Cells. ACS Appl. Bio Mater. 2, 2791–2801. https://doi.org/10.1021/acsabm.9b00215

Solorio, L.D., Dhami, C.D., Dang, P.N., Vieregge, E.L., Alsberg, E., 2012. Spatiotemporal regulation of chondrogenic differentiation with controlled delivery of transforming growth factor-β1 from gelatin microspheres in mesenchymal stem cell aggregates. Stem Cells Transl. Med. 1, 632–639. https://doi.org/10.5966/sctm.2012-0039

Štefková, K., Procházková, J., Pacherník, J., 2015. Alkaline Phosphatase in Stem Cells [WWW Document]. Stem Cells Int. https://doi.org/10.1155/2015/628368

Sun, M., Chi, G., Xu, Juanjuan, Tan, Y., Xu, Jiayi, Lv, S., Xu, Z., Xia, Y., Li, L., Li, Y., 2018. Extracellular matrix stiffness controls osteogenic differentiation of mesenchymal stem cells mediated by integrin α5. Stem Cell Res. Ther. 9, 52. https://doi.org/10.1186/s13287-018-0798-0

Sung, H.W., Huang, R.N., Huang, L.L., Tsai, C.C., 1999. In vitro evaluation of cytotoxicity of a naturally occurring cross-linking reagent for biological tissue fixation. J. Biomater. Sci. Polym. Ed. 10, 63–78. https://doi.org/10.1163/156856299x00289

Suvarnapathaki, S., Ramos, R., Sawyer, S.W., McLoughlin, S., Ramos, A., Venn, S., Soman, P., 2018. Generation of cell-laden hydrogel microspheres using 3D printing-enabled microfluidics. J. Mater. Res. 33, 2012–2018. https://doi.org/10.1557/jmr.2018.77

Teh, S.-Y., Lin, R., Hung, L.-H., Lee, A.P., 2008. Droplet microfluidics. Lab. Chip 8, 198–220. https://doi.org/10.1039/B715524G

Tibbitt, M.W., Anseth, K.S., 2009. Hydrogels as Extracellular Matrix Mimics for 3D Cell Culture. Biotechnol. Bioeng. 103, 655–663. https://doi.org/10.1002/bit.22361

Toh, W.S., Loh, X.J., 2014. Advances in hydrogel delivery systems for tissue regeneration. Mater. Sci. Eng. C Mater. Biol. Appl. 45, 690–697. https://doi.org/10.1016/j.msec.2014.04.026

Tomihata, K., Ikada, Y., 1996. Cross-Linking of Gelatin with Carbodiimides. Tissue Eng. 2, 307–313. https://doi.org/10.1089/ten.1996.2.307

Torre, A.G., Shaw, J.E., Wood, A., Gilbert, H.T.J., Dobre, O., Genever, P., Brennan, K., Richardson, S.M., Swift, J., 2018. An immortalised mesenchymal stem cell line maintains mechano-responsive behaviour and can be used as a reporter of substrate stiffness. Sci. Rep. 8, 8981. https://doi.org/10.1038/s41598-018-27346-9

Trensz, F., Lucien, F., Couture, V., Söllrald, T., Drouin, G., Rouleau, A.-J., Grandbois, M., Lacraz, G., Grenier, G., 2015. Increased microenvironment stiffness in damaged myofibers promotes myogenic progenitor cell proliferation. Skelet. Muscle 5, 5. https://doi.org/10.1186/s13395-015-0030-1

Tse, J.R., Engler, A.J., 2011. Stiffness Gradients Mimicking In Vivo Tissue Variation Regulate Mesenchymal Stem Cell Fate. PLOS ONE 6, e15978. https://doi.org/10.1371/journal.pone.0015978

Tsimbouri, P.M., Murawski, K., Hamilton, G., Herzyk, P., Oreffo, R.O.C., Gadegaard, N., Dalby, M.J., 2013. A genomics approach in determining nanotopographical effects on MSC phenotype. Biomaterials 34, 2177–2184. https://doi.org/10.1016/j.biomaterials.2012.12.019

Underhill, G.H., Bhatia, S.N., 2007. High-throughput analysis of signals regulating stem cell fate and function. Curr. Opin. Chem. Biol. 11, 357–366. https://doi.org/10.1016/j.cbpa.2007.05.036

Utada, A.S., Lorenceau, E., Link, D.R., Kaplan, P.D., Stone, H.A., Weitz, D.A., 2005. Monodisperse double emulsions generated from a microcapillary device. Science 308, 537–541. https://doi.org/10.1126/science.1109164

Vakarelski, I.U., Edwards, S.A., Dagastine, R.R., Chan, D.Y.C., Stevens, G.W., Grieser, F., 2007. Atomic force microscopy: loading position dependence of cantilever spring constants and detector sensitivity. Rev. Sci. Instrum. 78, 116102. https://doi.org/10.1063/1.2805518

Van Den Bulcke, A.I., Bogdanov, B., De Rooze, N., Schacht, E.H., Cornelissen, M., Berghmans, H., 2000. Structural and rheological properties of methacrylamide modified gelatin hydrogels. Biomacromolecules 1, 31–38. https://doi.org/10.1021/bm990017d

Vining, K.H., Mooney, D.J., 2017. Mechanical forces direct stem cell behaviour in development and regeneration. Nat. Rev. Mol. Cell Biol. 18, 728–742. https://doi.org/10.1038/nrm.2017.108

Vladisavljević, G.T., Shahmohamadi, H., Das, D.B., Ekanem, E.E., Tauanov, Z., Sharma, L., 2014. Glass capillary microfluidics for production of monodispersed poly (dl-lactic acid) and polycaprolactone microparticles: Experiments and numerical simulations. J. Colloid Interface Sci. 418, 163–170. https://doi.org/10.1016/j.jcis.2013.12.002

Vogel, V., 2006. Mechanotransduction involving multimodular proteins: converting force into biochemical signals. Annu. Rev. Biophys. Biomol. Struct. 35, 459–488. https://doi.org/10.1146/annurev.biophys.35.040405.102013

Wang, H.-N., Huang, Y.-C., Ni, G.-X., 2020. Mechanotransduction of stem cells for tendon repair. World J. Stem Cells 12, 952–965. https://doi.org/10.4252/wjsc.v12.i9.952

Wang, Jianmei, Li, Y., Wang, X., Wang, Jianchun, Tian, H., Zhao, P., Tian, Y., Gu, Y., Wang, L., Wang, C., 2017. Droplet Microfluidics for the Production of Microparticles and Nanoparticles. Micromachines. https://doi.org/10.3390/mi8010022

Wang, M., Cui, C., Ibrahim, M.M., Han, B., Li, Q., Pacifici, M., Lawrence, J.T.R., Han, L., Han, L.-H., 2019. Regulating Mechanotransduction in Three Dimensions using Sub-Cellular Scale, Crosslinkable Fibers of Controlled Diameter, Stiffness, and Alignment. Adv. Funct. Mater. 29, 1808967. https://doi.org/10.1002/adfm.201808967

Wang, N., Tytell, J.D., Ingber, D.E., 2009. Mechanotransduction at a distance: mechanically coupling the extracellular matrix with the nucleus. Nat. Rev. Mol. Cell Biol. 10, 75–82. https://doi.org/10.1038/nrm2594

Wang, Y., Wang, G., Luo, X., Qiu, J., Tang, C., 2012. Substrate stiffness regulates the proliferation, migration, and differentiation of epidermal cells. Burns J. Int. Soc. Burn Inj. 38, 414–420. https://doi.org/10.1016/j.burns.2011.09.002

Wen, J.H., Vincent, L.G., Fuhrmann, A., Choi, Y.S., Hribar, K.C., Taylor-Weiner, H., Chen, S., Engler, A.J., 2014. Interplay of matrix stiffness and protein tethering in stem cell differentiation. Nat. Mater. 13, 979–987. https://doi.org/10.1038/nmat4051

West, J.L., 2011. Protein-patterned hydrogels: Customized cell microenvironments. Nat. Mater. 10, 727–729. https://doi.org/10.1038/nmat3132

White, L.J., Kirby, G.T.S., Cox, H.C., Qodratnama, R., Qutachi, O., Rose, F.R.A.J., Shakesheff, K.M., 2013. Accelerating protein release from microparticles for regenerative medicine applications. Mater. Sci. Eng. C Mater. Biol. Appl. 33, 2578–2583. https://doi.org/10.1016/j.msec.2013.02.020

Wilson, C.J., Clegg, R.E., Leavesley, D.I., Pearcy, M.J., 2005. Mediation of biomaterial-cell interactions by adsorbed proteins: a review. Tissue Eng. 11, 1–18. https://doi.org/10.1089/ten.2005.11.1

Xu, P., Jiang, F., Zhang, H., Yin, R., Cen, L., Zhang, W., 2020. Calcium Carbonate/Gelatin Methacrylate Microspheres for 3D Cell Culture in Bone Tissue Engineering. Tissue Eng. Part C Methods 26, 418–432. https://doi.org/10.1089/ten.tec.2020.0064

Xu, Q., Hashimoto, M., Dang, T.T., Hoare, T., Kohane, D.S., Whitesides, G.M., Langer, R., Anderson, D.G., 2009. Preparation of Monodisperse Biodegradable Polymer Microparticles Using a Microfluidic Flow-focusing Device for Controlled Drug Delivery. Small Weinh. Bergstr. Ger. 5, 1575–1581. https://doi.org/10.1002/smll.200801855

Yang, S., Leong, K.F., Du, Z., Chua, C.K., 2001. The design of scaffolds for use in tissue engineering. Part I. Traditional factors. Tissue Eng. 7, 679–689. https://doi.org/10.1089/107632701753337645

Yim, E.K.F., Darling, E.M., Kulangara, K., Guilak, F., Leong, K.W., 2010. Nanotopography-induced changes in focal adhesions, cytoskeletal organization, and mechanical properties of human mesenchymal stem cells. Biomaterials 31, 1299–1306. https://doi.org/10.1016/j.biomaterials.2009.10.037

Yoshizawa, S., Brown, A., Barchowsky, A., Sfeir, C., 2014. Magnesium ion stimulation of bone marrow stromal cells enhances osteogenic activity, simulating the effect of magnesium

alloy degradation. Acta Biomater. 10, 2834–2842. https://doi.org/10.1016/j.actbio.2014.02.002
Yue, K., Santiago, G.T., Alvarez, M.M., Tamayol, A., Annabi, N., Khademhosseini, A., 2015. Synthesis, properties, and biomedical applications of gelatin methacryloyl (GelMA) hydrogels. Biomaterials 73, 254–271. https://doi.org/10.1016/j.biomaterials.2015.08.045
Zhao, Y., Liu, Z., Pan, C., Li, Z., Zhou, J., Wang, J., Yin, Z., Wang, X., 2011. Preparation of gelatin microspheres encapsulated with bFGF for therapeutic angiogenesis in a canine ischemic hind limb. J. Biomater. Sci. Polym. Ed. 22, 665–682. https://doi.org/10.1163/092050610X489880
Zhao, Y., Sun, Z., 2017. Effects of gelatin-polyphenol and gelatin–genipin cross-linking on the structure of gelatin hydrogels. Int. J. Food Prop. 20, S2822–S2832. https://doi.org/10.1080/10942912.2017.1381111
Zhao, Z., Li, G., Ruan, H., Chen, K., Cai, Z., Lu, G., Li, R., Deng, L., Cai, M., Cui, W., 2021. Capturing Magnesium Ions via Microfluidic Hydrogel Microspheres for Promoting Cancellous Bone Regeneration. ACS Nano 15, 13041–13054. https://doi.org/10.1021/acsnano.1c02147
Zoldan, J., Karagiannis, E.D., Lee, C.Y., Anderson, D.G., Langer, R., Levenberg, S., 2011. The influence of scaffold elasticity on germ layer specification of human embryonic stem cells. Biomaterials 32, 9612–9621. https://doi.org/10.1016/j.biomaterials.2011.09.012

APPENDICES

Table S1 Diameter modelling fitting statistics

Source	Sum of Squares	Df	Mean Square	F-value	p-value	
Model	5.223E+05	4	1.306E+05	31.23	< 0.0001	significant
A - Disperse phase flow rate	3.247E+05	1	3.247E+05	77.66	< 0.0001	
B - Continuous phase flow rate	1.456E+05	1	1.456E+05	34.83	< 0.0001	
AB	0.1115	1	0.1115	0.0000	0.9960	
A^2	51953.13	1	51953.13	12.43	0.0042	
Residual	50169.59	12	4180.80			
Lack of Fit	28880.88	4	7220.22	2.71	0.1071	not significant
Pure Error	21288.71	8	2661.09			
Cor Total	5.724E+05	16				

Table S2 Regression statistics of Predicted vs. Actual diameter values

Std. Dev.	**64.66**	**R^2**	**0.9124**
Mean	510.49	Adjusted R^2	0.8831
C.V. %	12.67	Predicted R^2	0.8382
		Adeq Precision	17.1597

Table S3 Young's modulus modelling fitting statistics

Source	Sum of Squares	Df	Mean Square	F-value	p-value	
Model	5643.80	2	2821.90	7.83	0.0052	significant
A - Disperse phase flow rate	2828.45	1	2828.45	7.85	0.0141	
B - Continuous phase flow rate	2815.35	1	2815.35	7.81	0.0143	
Residual	5043.76	14	360.27			
Lack of Fit	1048.07	6	174.68	0.3497	0.8913	not significant
Pure Error	3995.68	8	499.46			
Cor Total	10687.55	16				

Table S4 Regression statistics of Predicted vs. Actual Young's modulus values

Std. Dev.	**18.98**	**R^2**	**0.5281**
Mean	65.52	Adjusted R^2	0.4607
C.V. %	28.97	Predicted R^2	0.2655
		Adeq Precision	8.4272

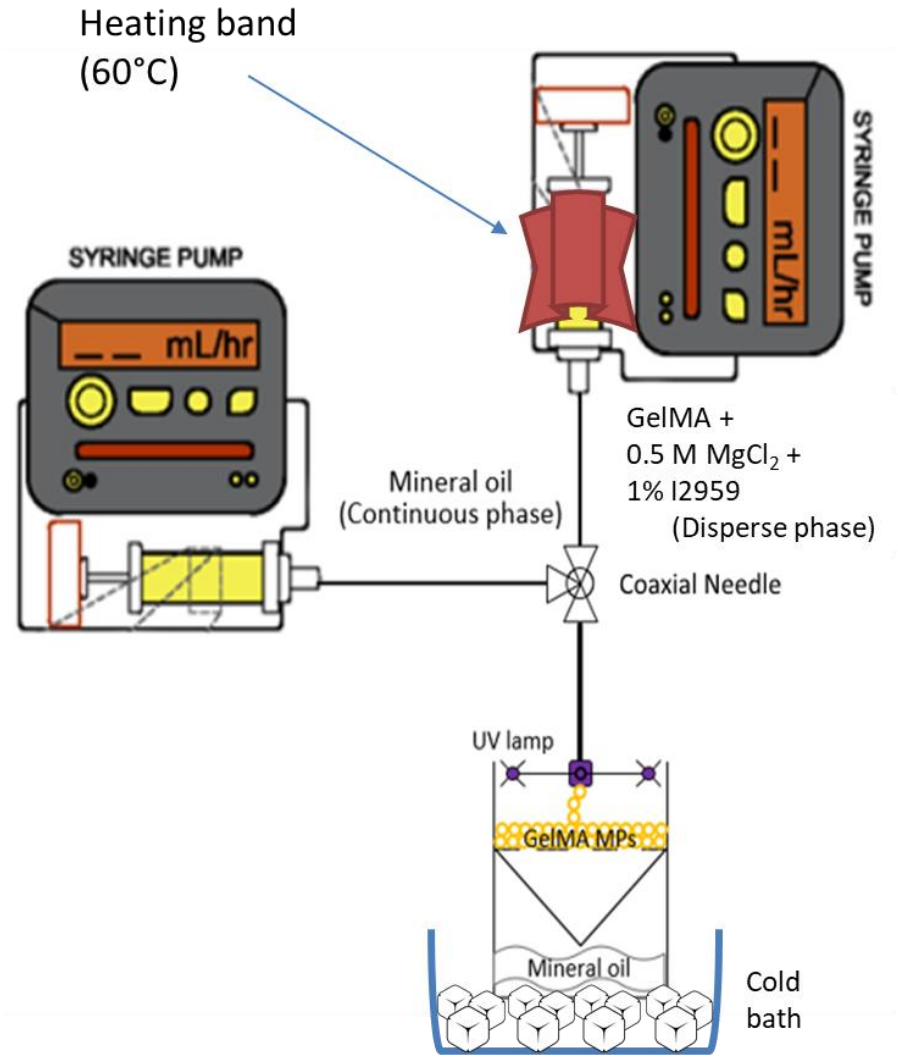


Figure S1 Setup for production of GelMA microparticles using the co-current flow system.

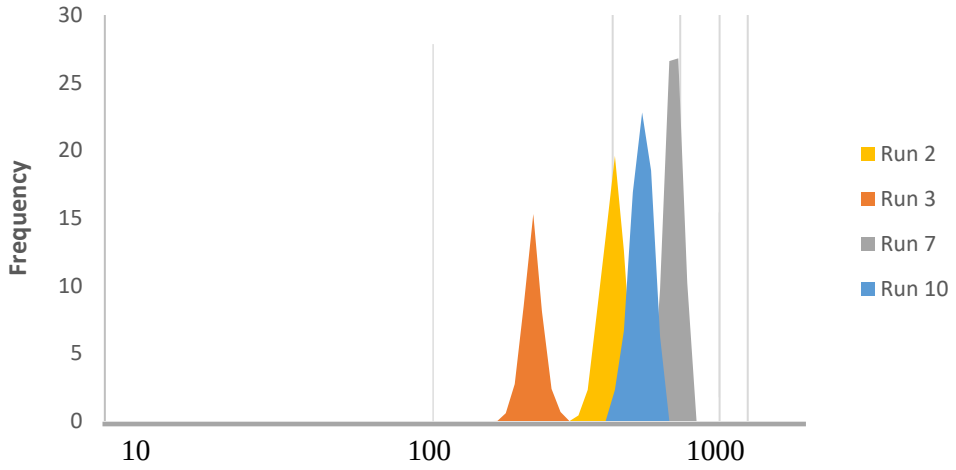


Figure S2 Size distribution of representative experimental runs at diameters of 404±45 µm, 203±30 µm, 650±33 µm and 532±102 µm respectively.

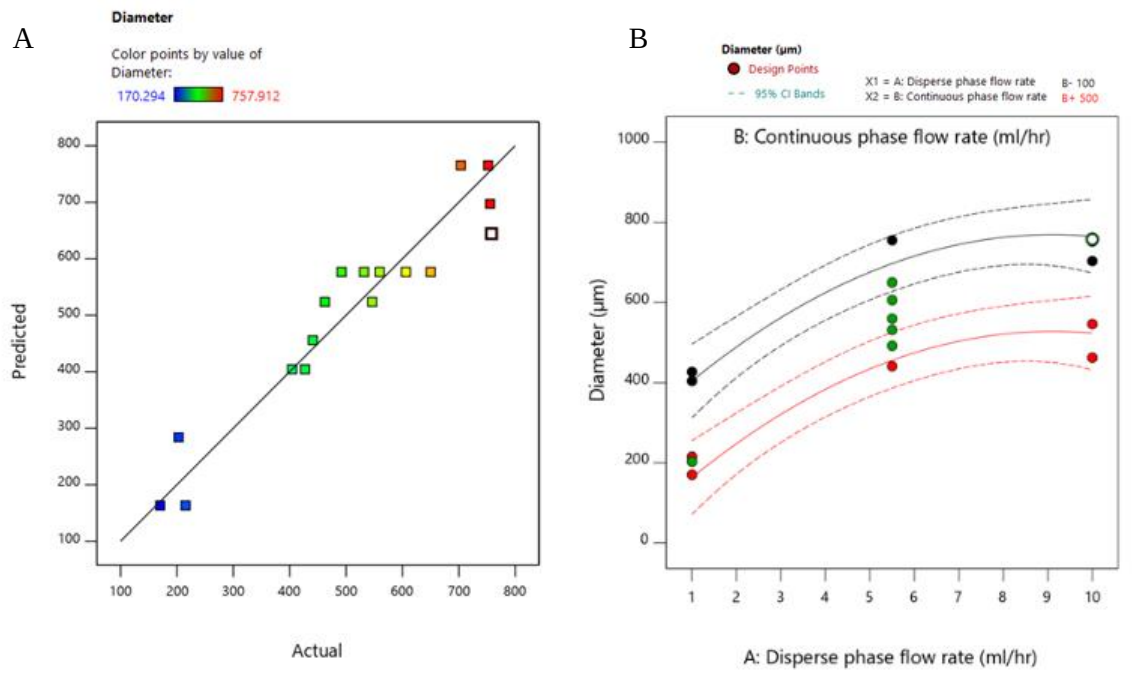


Figure S3 (A) Correlation between the Predicted values of the model versus the Actual experimental values; (B) First order interaction between the disperse phase flow rate and continuous flow rate in determining the microparticle diameter.

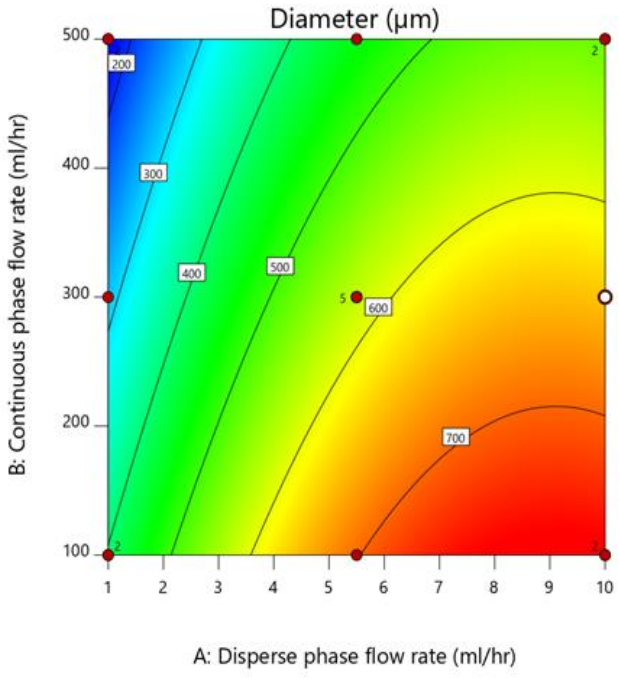


Figure S4 2D contour plot of the diameter response with respect to the disperse phase (DP) and continuous phase (CP) flow rates. The red areas define higher microparticle diameter, the blue ones smaller

microparticle diameter. The graph shows the direct proportionality between DP flow rate and diameter and the inverse proportionality between CP flow rate and diameter.

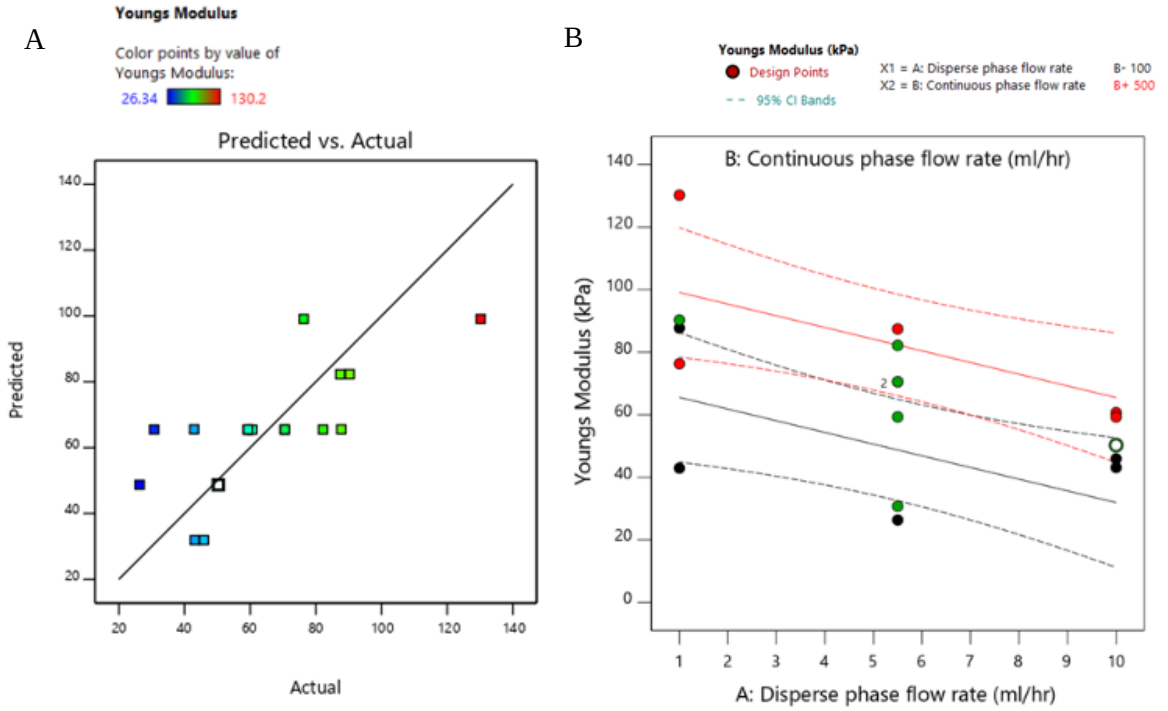


Figure S5 (A) Correlation between the Predicted values of the model versus the Actual experimental values; (B) First order interaction between the disperse phase flow rate and continuous flow rate in determining the microparticle Young's modulus.

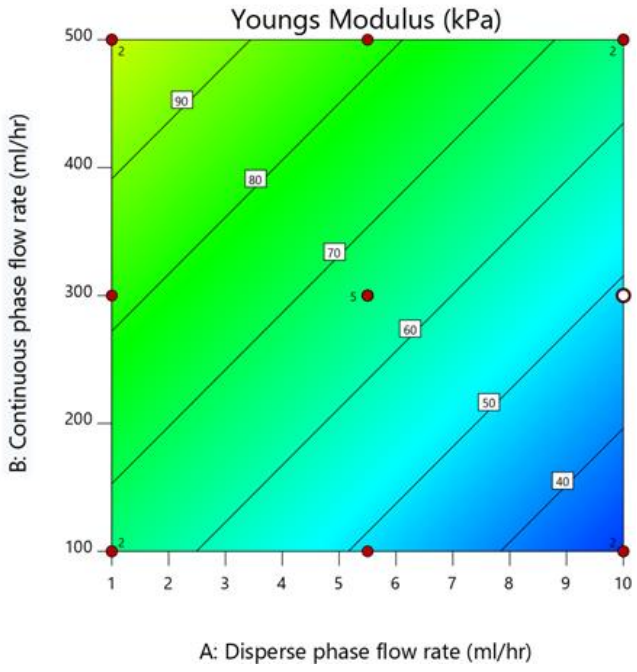


Figure S6 2D contour plot of surface Young's modulus response with respect to the disperse phase (DP) and continuous phase (CP) flow rates. Green areas show higher microparticle Young's modulus, blue areas

show lower microparticle Young's modulus. Considering the inverse proportionality between surface Young's modulus and the microparticle size, the effect of the DP flow rate is inversely proportional and the effect of CP flow rate is directly proportional.